

**USING HIGH THROUGHPUT SCREENS TO IDENTIFY LEAD COMPOUNDS  
FOR ALZHEIMER'S DISEASE THERAPEUTICS**

**Jermont Chen**

**A DISSERTATION  
PRESENTED TO THE FACULTY  
OF PRINCETON UNIVERSITY  
IN CANDIDACY FOR THE DEGREE  
OF DOCTOR OF PHILOSOPHY**

**RECOMMENDED FOR ACCEPTANCE  
BY THE DEPARTMENT OF CHEMISTRY**

**Adviser: Michael Hecht**

**November 2008**

Report Documentation Page			Form Approved OMB No. 0704-0188		
Public reporting burden for the collection of information is estimated to average 1 hour per response, including the time for reviewing instructions, searching existing data sources, gathering and maintaining the data needed, and completing and reviewing the collection of information. Send comments regarding this burden estimate or any other aspect of this collection of information, including suggestions for reducing this burden, to Washington Headquarters Services, Directorate for Information Operations and Reports, 1215 Jefferson Davis Highway, Suite 1204, Arlington VA 22202-4302. Respondents should be aware that notwithstanding any other provision of law, no person shall be subject to a penalty for failing to comply with a collection of information if it does not display a currently valid OMB control number.					
1. REPORT DATE <b>01 OCT 2008</b>		2. REPORT TYPE <b>N/A</b>		3. DATES COVERED <b>-</b>	
4. TITLE AND SUBTITLE <b>Using High Throughput Screens To Identify Lead Compounds For Alzheimers Disease Therapeutics</b>				5a. CONTRACT NUMBER	
				5b. GRANT NUMBER	
				5c. PROGRAM ELEMENT NUMBER	
6. AUTHOR(S)				5d. PROJECT NUMBER	
				5e. TASK NUMBER	
				5f. WORK UNIT NUMBER	
7. PERFORMING ORGANIZATION NAME(S) AND ADDRESS(ES) <b>Princeton University</b>				8. PERFORMING ORGANIZATION REPORT NUMBER	
9. SPONSORING/MONITORING AGENCY NAME(S) AND ADDRESS(ES) <b>AFIT Wright-Patterson AFB, OH 45433-7221</b>				10. SPONSOR/MONITOR'S ACRONYM(S)	
				11. SPONSOR/MONITOR'S REPORT NUMBER(S)	
12. DISTRIBUTION/AVAILABILITY STATEMENT <b>Approved for public release, distribution unlimited</b>					
13. SUPPLEMENTARY NOTES <b>The original document contains color images.</b>					
14. ABSTRACT					
15. SUBJECT TERMS					
16. SECURITY CLASSIFICATION OF:			17. LIMITATION OF ABSTRACT <b>SAR</b>	18. NUMBER OF PAGES <b>139</b>	19a. NAME OF RESPONSIBLE PERSON
a. REPORT <b>unclassified</b>	b. ABSTRACT <b>unclassified</b>	c. THIS PAGE <b>unclassified</b>			

**© Copyright by Jermont Chen, 2008. All rights reserved.**

**The views expressed in this thesis are those of the author and do not reflect the official policy or position of the United States Air Force, Department of Defense, or the U.S. Government.**

## Abstract

Alzheimer's disease (AD) is the leading cause for dementia, affecting over 4.6 million people in the United States. The current FDA approved drugs only provide temporary relief from memory loss symptoms, without treating the underlying root cause of the disease. The amyloid cascade hypothesis suggests that aggregation of the amyloid beta (AB) peptide into a neurotoxic oligomer initiates the disease. Small molecule compounds have been reported to inhibit AB peptide aggregation, as well as rescue AB induced toxicity. Screens to identify compounds are necessary to increase the chance of developing a therapeutic that prevents AB aggregation and the associated disease.

Chapter 1 reviews the possible mechanism for Alzheimer's disease and discusses methods to prevent the disease. Chapter 2 presents results from an *E coli* based GFP fusion anti-aggregation screen. A library of 65,000 compounds was screened, and potential hits were characterized for aggregation inhibition as well as for the ability to rescue toxicity of the AB peptide. Improvements to the screen are also discussed.

Chapter 3 presents the results from a screen designed to identify compounds that bind to the AB peptide. Small molecule microarrays (SMM) were used to identify compounds that bind to AB. Compounds that bind have the potential of becoming aggregation inhibitors. Over 20,000 compounds were screened, and several hits from the screen are shown to rescue AB induced toxicity.

Chapter 4 looks at the role of aromatic interactions in AB peptide aggregation. Pi-stacking has been suggested to play an important role in AB peptide aggregation. Disturbing the pi-stacking interaction has been proposed as the aggregation inhibition mechanism for aromatic compounds. Two AB mutant peptides lacking aromatic residues

were found to aggregate and form fibrils, suggesting that aromatic residues are not required for AB aggregation. Aromatic compounds were found to inhibit the aggregation of AB mutants lacking aromatic residues, suggesting that the mechanism for aggregation inhibition is not due to pi-stacking disruption.

For my dad, my favorite chemist

For Ollie, my favorite nephew

“In sooth, I know not why I am so sad.”

*The Merchant of Venice*

William Shakespeare

## Acknowledgements

I would like to thank my advisor, Michael Hecht, for his friendship, advice, and guidance throughout my time at Princeton. I would also like to extend thanks to my advisory committee of Martin Semmelhack, Jamie Link, and David Wood for providing valuable feedback on my research.

My time at Princeton has been funded by both the Air Force, and the Air Force Institute of Technology. Research funding was provided by the National Institutes of Health and the NJ Council on Science and Technology.

This thesis would not have been possible without the valuable collaboration with the Broad Institute of Harvard and MIT. The Broad Institute generously provided access to instruments, robotics, compound libraries, and data analysis. For the AB-GFP fusion assay, I would like to thank Dr Nicky Tolliday, Dr Frank An, and Stephanie Norton; for the SMM research, I would like to thank Dr Angela Koehler, Jason Fuller, Olivia McPherson, and Katie Doud.

Many thanks go to my family: my parents, my older brother, and my younger sister for their continued (and unending) support.

Finally, I would like to thank the members of the Hecht lab who made the time here infinitely more enjoyable: current lab members: Shona, Mike, Eaky, Emily, Angela, and Maria; previous lab members: Woojin and Abi, and undergraduates Debbie and Anne. Thanks also go to fellow fourth year graduate students, with special thanks to Emily and Bryson, (along with their lawyer spouses) for their friendship and, most importantly, for putting up with me for the past three years.

## Table of contents

Abstract .....	iv
Dedication .....	vi
Acknowledgements .....	vii
Table of contents .....	viii
List of Figures .....	xii
List of Tables.....	xvi
 Chapter 1. Background and introduction .....	 1
 1.1. Protein folding and aggregation .....	 1
1.2. Alzheimer's disease overview.....	3
1.3. Potential Alzheimer's disease therapies .....	5
1.3.1. Limiting production of AB .....	6
1.3.2. Reducing the amount of AB .....	7
1.3.3. Preventing the aggregation of AB .....	8
 1.4. Thesis outline .....	 13
1.5. References .....	15

Chapter 2. Characterizing amyloid beta peptide aggregation inhibitors selected by the AB-GFP fusion screen .....	20
2.1. Introduction .....	20
2.2. Results .....	23
2.2.1. AB-GFP fusion pre-screening .....	24
2.2.2. Fusion screen positive and negative controls .....	24
2.2.3. AB-GFP fusion data analysis .....	24
2.2.4. Thresholds for selection.....	26
2.2.5. Compounds selected by the AB-GFP fusion screen.....	27
2.2.6. Characterization of compound 737.....	30
2.2.7. Toxicity studies.....	32
2.2.8. Structure activity relationship (SAR) studies of compound 737 .....	33
2.2.9. Toxicity rescue by compound 737 analogs .....	37
2.2.10. Compound efficacy.....	39
2.2.11. Testing 737 analogs into the AB-GFP fusion system.....	41
2.3. Discussion .....	44
2.3.1. Potential rescue mechanism of 737 and analogs .....	46
2.3.2. Why was 737 selected by the AB-GFP fusion screen? .....	46
2.4. Summary .....	49
2.5. Materials and methods .....	50
2.6. References .....	53

Chapter 3. Amyloid beta binding as a primary screen for identifying aggregation inhibitors .....	55
3.1. Introduction .....	55
3.2. Results .....	58
3.2.1. Developing conditions for the SMM screen.....	58
3.2.2. SMM results: Identifying compound binding to AB40.....	60
3.2.3. Toxicity experiments of hits identified by SMM .....	66
3.2.4. Biophysical characterization of D1 .....	68
3.3. Discussion .....	81
3.3.1. SMM screening effectiveness.....	81
3.3.2. Rescue ability of D1 .....	82
3.3.3. Does D1 cause aggregation of AB?.....	83
3.3.4. Possible mechanisms of D1 rescue.....	84
3.3.5. D1 SAR study.....	85
3.3.6. SMM screening questions .....	85
3.4. Summary .....	87
3.5. Materials and methods: .....	88
3.6. References .....	91

Chapter 4. Identifying the role of aromaticity in AB aggregation, fibrilization, toxicity, and aggregation inhibition .....	95
4.1. Introduction to aromatic interactions .....	95
4.2. Investigating the role of aromatic residues and $\pi$ -stacking in Alzheimer's disease .....	98
4.3. Results .....	101
4.3.1. Aggregation and fibrilization propensity of AB mutant peptides lacking Phe 19 and Phe 20.....	101
4.3.2. Electron microscopy images of 42 Ile Ile and 42 Leu Leu mutant AB peptides.....	107
4.3.3. Inhibiting AB Ile Ile and Leu Leu mutants with aromatic inhibitors	108
4.3.4. Toxicity of AB Ile Ile and Leu Leu mutants .....	111
4.4. Discussion .....	114
4.5. Summary .....	118
4.6. Materials and methods .....	120
4.7. References .....	122

## List of Figures

### Chapter 1

<b>Figure 1.1.</b> Fibrils from Alzheimer's disease.....	1
<b>Figure 1.2.</b> Model of Alzheimer's AB fibril.. .....	2
<b>Figure 1.3.</b> General aggregation pathway for amyloid peptides and proteins .....	2
<b>Figure 1.4.</b> PET image of levels of Alzheimer's plaque in diseased and control patients brains. ....	4
<b>Figure 1.5.</b> Potential targets for inhibition of Alzheimer's disease .....	6
<b>Figure 1.6.</b> Structures of Congo Red and triazine inhibitors. ....	10
<b>Figure 1.7.</b> Structure of polyphenol AB aggregation inhibitors .....	11
<b>Figure 1.8.</b> Structure of melatonin, curcumin, and nicotine .....	12

### Chapter 2

<b>Figure 2.1.</b> Top: AB-GFP fusion protein layout. Left: Cartoon representation of AB-GFP fusion assay. Right: Compound inhibitor (E2) and ineffective compound (D2) found by the AB GFP fusion assay.....	22
<b>Figure 2.2.</b> Determining if a compound is fluorescently active at the GFP wavelength. ....	26
<b>Figure 2.3.</b> Selection rules to identify compounds hits in the AB-GFP fusion assay.....	27
<b>Figure 2.4.</b> Structures of compounds selected by the AB-GFP fusion screen for addition testing.....	28

<b>Figure 2.5.</b> Aggregation inhibition of compounds found by AB-GFP fusion with AB42.....	30
<b>Figure 2.6.</b> Dose dependence aggregation inhibition of AB42 with different concentrations of 737.....	31
<b>Figure 2.7.</b> Time course inhibition plot of AB42 with varying concentrations of 737.....	32
<b>Figure 2.8.</b> Ability of 737 to rescue AB induced toxicity in PC12 cells.. .....	33
<b>Figure 2.9.</b> Compound analogs of 737 selected for additional tests .....	34
<b>Figure 2.10.</b> Inhibition of AB42 aggregation by 737 and analogs.....	36
<b>Figure 2.11.</b> Toxicity of 737 analogs in PC12 cells.....	38
<b>Figure 2.12.</b> Ability of 737 and analogs to rescue AB42 induced toxicity in PC12 cells.. .....	40
<b>Figure 2.13.</b> Fluorescence of 737 analogs in LB media and in fusion system. .	42
<b>Figure 2.14.</b> Compound fluorescence in LB and compound fluorescence in <i>E. coli</i> without fusion plasmid vector after incubation. ....	44

### Chapter 3

<b>Figure 3.1.</b> Cartoon representation of a SMM binding screen.....	57
<b>Figure 3.2.</b> SDS gel image of N-terminally labeled Anaspec Hilyte 647 fluorescent-AB40 (lanes 2, 3 and 4) and N-terminally labeled Anaspec Hilyte 488 fluorescent-AB42 (lanes 5, 6 and 7) at listed concentrations.. .....	59
<b>Figure 3.3.</b> SDS gel image of N-terminally labeled Anaspec 647 fluorescent-AB40 after 60 minute room temperature incubation at labeled concentrations.. .....	60

<b>Figure 3.4.</b> An enlarged view of the DIV compound microarray slide after scanning..	62
<b>Figure 3.5.</b> Histogram plot of compound (blue) and DMSO control (red) composite Z-scores from DIV and NPC slides.....	63
<b>Figure 3.6.</b> An expanded view of 225 compound spots on the NPC small molecule microarray..	65
<b>Figure 3.7.</b> An expanded view of 15 compound spots on each NPC small molecule microarray replica slide.....	65
<b>Figure 3.8.</b> SMM selected compound initial toxicity study.....	67
<b>Figure 3.9.</b> Structure of D1 (left) and thioflavin T (right) .....	69
<b>Figure 3.10.</b> Ability of D1 to rescue AB42 induced toxicity in PC12 cells.....	70
<b>Figure 3.11.</b> Toxicity study of D1 in PC12 cells..	71
<b>Figure 3.12.</b> D1 parent scaffold and analogs .....	72
<b>Figure 3.13.</b> Toxicity of D1 analogs..	75
<b>Figure 3.14.</b> Rescue ability of D1 analogs at 100 uM.....	76
<b>Figure 3.15.</b> Rescue ability of D1 analogs at 50 uM.....	77
<b>Figure 3.16.</b> Thioflavin T timecourse of AB42 with and without compound D1.. .....	79
<b>Figure 3.17.</b> EM images of AB42 and AB42 with D1.....	80
<b>Figure 3.18.</b> Structure of compound 1216 (left) and frentizole (right). .....	82

## Chapter 4

<b>Figure 4.1.</b> Illustration of $\pi$ -stacking structures..	96
---	----

<b>Figure 4.2.</b> Potential mechanism for aggregation inhibition by disturbing aromatic $\pi$ interactions.....	97
<b>Figure 4.3.</b> Model structure of AB 10 – 40 fibril based on solid state NMR studies..	99
<b>Figure 4.4.</b> Amino acid sequences of AB42 and mutants used in this study. .	102
<b>Figure 4.5.</b> Aggregation profile in hours of AB42 and mutants as determined by thioflavin T fluorescence..	104
<b>Figure 4.6.</b> Aggregation profile in days of AB42 and mutants as determined by thioflavin T fluorescence..	105
<b>Figure 4.7.</b> Aggregation profile in days of AB40 and mutants as determined by thioflavin T fluorescence..	106
<b>Figure 4.8.</b> Electron microscopy images of AB42, 42 Ile Ile, and 42 Leu Leu mutants.....	108
<b>Figure 4.9.</b> Structure of aromatic and non-aromatic inhibitors.....	109
<b>Figure 4.10.</b> Aggregation reduction by aromatic compounds of AB42 and Ile Ile mutants, as measured by thioflavin T fluorescence.....	110
<b>Figure 4.11.</b> Aggregation reduction by non-aromatic MTMA of AB42 and Ile Ile mutants, as measured by thioflavin T fluorescence.....	111
<b>Figure 4.12.</b> Viability of PC12 cells when treated with AB and mutants.....	113
<b>Figure 4.13.</b> Viability of PC12 cells when treated with 40 Ile Ile and 42 Ile Ile. PC12 cells with concentration of 20 $\mu$ M, and incubated for 24 hours.....	114

## List of Tables

### Chapter 3

<b>Table 3.1.</b> Ability of SMM compounds to rescue AB42 induced toxicity in PC12 cells. ....	68
--	----

<b>Table 3.2.</b> Summary of D1 analog toxicity and rescue ability summary. ....	74
--	----

### Chapter 4

<b>Table 4.1.</b> Functional amyloid related sequences that contain aromatic residues... ..	97
---	----

<b>Table 4.2.</b> Hydrophobicity and $\beta$ sheet propensity of Phe, Ile and Leu. ....	101
---	-----

# Chapter 1. Background and introduction

## 1.1. Protein folding and aggregation

Proper polypeptide folding is a necessary and complex step in creating a functional protein. Proteins predominantly fold into their final conformation based on their amino acid sequence (1). However, proteins can misfold and aggregate, resulting in a gain or loss of protein function (2). A large number of proteins have been shown to have the intrinsic ability to fold (or misfold) and self aggregate into highly ordered structures based on the peptide backbone (3-6). These ordered structures are long and unbranched fibers, as shown in Figure 1.1.

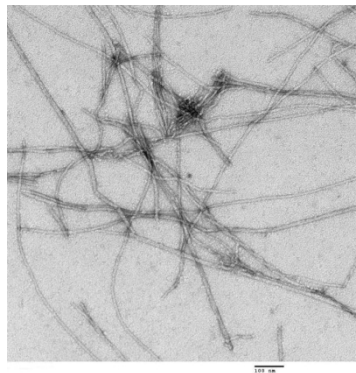


**Figure 1.1.** Fibrils from Alzheimer's disease. Scale bar is 100 nm.

The fibrils are formed by the aggregation of monomeric  $\beta$ -strands which form multiple  $\beta$ -sheets, as shown in Figure 1.2. These fibrils then aggregate to form extracellular protein deposits called amyloid plaques. They were named amyloid because early investigators thought that the plaques were comprised of starch. It was not until 1971 that Glenner *et al* reported that they were made from proteins (7).

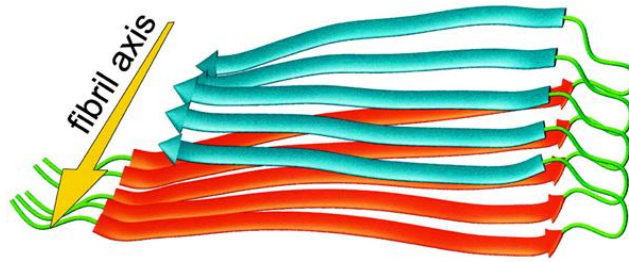


**Figure 1.2.** Model of Alzheimer's AB fibril. The yellow arrow represents the direction of the fibril axis. The cross  $\beta$  unit seen here is comprised of five individual  $\beta$  strands. Hydrogen bonding between the peptide backbones from separate peptides form the two  $\beta$ -sheets in blue and orange. Figure from Petkova (8).

The transition from the native state conformation to amyloid fibril is a complicated process. The peptide transitions from its native, unfolded state, passing through different conformations and oligomeric intermediates, which may be toxic, before making the final transition to the fibril, as shown in Figure 1.3.

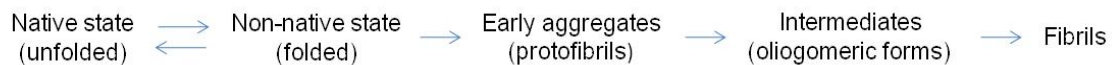


**Figure 1.3.** General aggregation pathway for amyloid peptides and proteins

Over 100 human diseases are associated with amyloid like protein aggregation in various tissues and organs (9-11). The location of the protein aggregation and deposits determines the disease and symptoms. For example, the 37 residue amylin protein self-aggregates and forms amyloid fibers and plaques in the islets of Langerhans, which results in type II diabetes. Similarly, protein accumulation in the brain results in neurodegenerative diseases. Examples (and their protein or peptide component) include

Creutzfeldt-Jakob disease (prion peptide), Parkinson's disease ( $\alpha$ -synuclein protein), and Alzheimer's disease (amyloid beta peptide).

## 1.2. Alzheimer's disease overview

Alzheimer's disease is a fatal neurodegenerative disease inflicting approximately 4.5 million Americans, and is the leading cause of dementia in the elderly (12).

Increasing age is the greatest risk factor for the disease – 10% of the American population over 65 years and 50% over 85 years are affected by the disease. These statistics, in addition to the cost associated with current treatment of the disease (estimated at \$100 billion a year), indicate that this disease may “soon become the most prevalent and socially disruptive illness in the aging populations of all developed nations” (13).

Alzheimer's disease (AD) is associated with the accumulation of amyloid plaques in specific memory centers of the brain, as shown in Figure 1.4. The main protein component of the plaques is the amyloid beta (AB42) peptide. AB is produced by the cleavage of the amyloid beta precursor protein (APP), a transmembrane protein 770 amino acids in length. APP is first cleaved by  $\beta$  secretase to form the N-terminal of AB, and then by  $\gamma$  secretase to form the C-terminal end of AB.  $\gamma$  secretase cleaves the C-terminal end in varying lengths, with the most prominent lengths of AB being 40 and 42 residues long with sequence as shown below using the single letter abbreviations for amino acids.

DAEFRHDSGY<sup>10</sup> EVHHQKLVFF<sup>20</sup> AEDVGSNKGA<sup>30</sup> IIGLMVGGVV<sup>40</sup> IA<sup>42</sup>

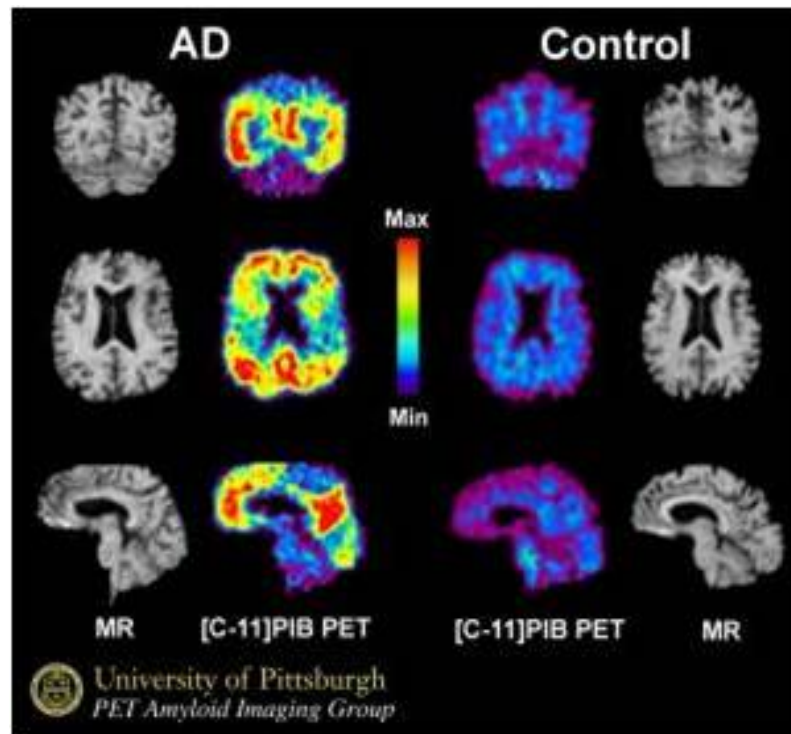


**Figure 1.4.** PET image of levels of Alzheimer's plaque in diseased and control patients brains. Alzheimer's patient, second from left, non-diseased patient, third from left. Stained used is specific for Alzheimer's plaques (Pittsburg B compound). Colors indicate amount of plaque. Figure from University of Pittsburgh Medical Center website.

Genetic and biochemical studies have indicated that AB plays a causal role in the development of AD (14-16). Evidence for this can be seen in both the early onset and late onset forms of the disease. Mutations in the sequence of both APP and  $\gamma$  secretases are linked to the early onset form of the disease. These early onset forms have mutations that result in increased production of AB, or alter AB so that it is more fibrillogenic (17, 18). Additional evidence that AB was causative was found when overexpression of mutant APP and mutant secretases genes in the brains of transgenic mice led to AB deposition and other disease-like symptoms (19). Also, in humans, the APP gene is

located on chromosome 21. Down's syndrome patients have a third copy of chromosome 21, which results in increased AB42 production with the formation of plaques as early as 12 years old (20, 21). Biochemical research indicates that AB can aggregate *in vitro*, and that these aggregates are directly and indirectly toxic (22). Finally, the amount of apolipoprotein E4, a lipid binding protein, is a genetic risk factor in late onset AD, which results in increased AB deposition (23). All of these data indicate that AB is responsible for the disease.

The amyloid cascade hypothesis for Alzheimer's disease suggests that a neurotoxic species exists on the AB aggregation pathway (24-26). The toxic species has yet to be identified, but evidence for the toxic species has shifted from the plaques and fibrils to the soluble oligomers, which have shown to be better correlated with disease symptoms (27-31). More recently, soluble AB dodecamers and dimers have been reported as the toxic species (32, 33).

### **1.3. Potential Alzheimer's disease therapies**

Based on the amyloid cascade theory, methods that reduce the amount of AB should be effective at treating the disease. As shown in Figure 1.5, there are three targets for treating AD. These include controlling or limiting AB production, preventing AB aggregation or increasing AB clearance (34). By reducing the amount of AB, or preventing AB aggregation, these treatments will prevent the formation of the putative toxic species.

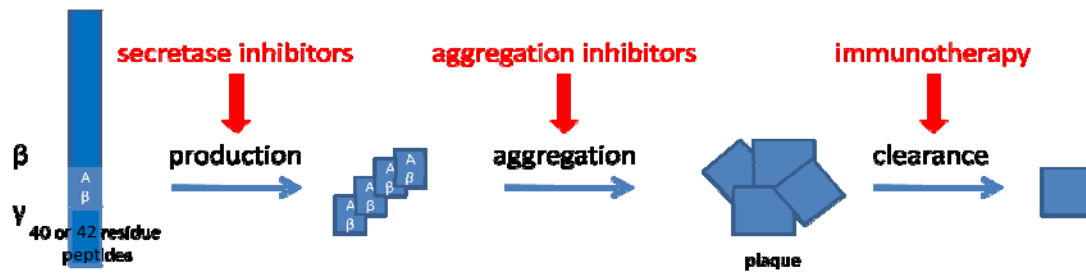


**Figure 1.5.** Potential targets for inhibition of Alzheimer's disease

### 1.3.1. Limiting production of AB

Controlling AB production can be done by inhibiting either of the two secretases that cleave APP to form AB. However, there are concerns with blocking secretases, as they may be involved in vital biological functions. For example,  $\gamma$  secretase is critical for Notch signaling in embryological development, so completely inhibiting this secretase may have undesirable side effects, as mice lacking  $\gamma$  secretase die *in utero* (35). A  $\gamma$  secretase inhibitor has been discovered that does not inhibit Notch signaling. Tarenflurbil binds  $\gamma$  secretase at a different location than the active site, and alters the conformation of  $\gamma$  secretase (36, 37). The overall effect is the production of a shorter, non-toxic form of AB (AB38) (36, 37). AD mice treated with tarenflurbil resulted in reduced plaque load and a slowing of learning and behavioral deterioration (38). Despite the fact that tarenflurbil was well tolerated in humans, and Phase II clinical trials showed some benefits to mild Alzheimer's disease patients (39), the Phase III study of tarenflurbil showed no benefit over placebo, and studies were ultimately discontinued by the company (40).

### **1.3.2. Reducing the amount of AB**

Another possible therapy is to increase the clearance rate of AB so the total amount of AB is reduced. One method is to activate the body's immune response to clear AB from the brain. Active immunization of young (6 months) and older (11 months) transgenic AD mice with AB42 prevented or reduced the development of amyloid-plaque formation, neuritic dystrophy and astrogliosis (41-45). Active immunization in humans also reduced plaque levels, but included a dangerous side effect. During the Phase II human clinical trial with active immunization by a synthetic AB peptide (Elan Pharmaceuticals, AN-1792), 6% of the patients developed meningitis. This event halted the Phase II clinical trial (46).

In 2008, the long term follow up of the patients involved in the Phase I AN-1792 clinical trial was reported. The follow up report revealed that AB immunization resulted in effective plaque removal, but there was no evidence of improved survival rates, or an increase in time before reaching severe dementia versus the unimmunized control group (47).

Passive immunization can also be used to reduce AB levels. Instead of injecting AB and having the host develop antibodies, antibodies raised against the AB peptide can be injected. Immunization of transgenic mice with AB42 antibodies was shown to decrease the levels of AB plaques without any meningitis-like side effects (48). Elan and Wyeth used a humanized monoclonal antibody, bapineuzumab, in a clinical trial to study passive AB immunization therapy. The Phase II clinical trial data of bapineuzumab showed that passive immunization was not effective, and had a significant side effect of

vasogenic edema (excess fluid in the brain) (49). Immunization therapy, while promising at plaque removal, can have unwanted side effects, as well as questions of effectiveness.

### **1.3.3. Preventing the aggregation of AB**

The third focus area is targeted at preventing the aggregation and subsequent toxicity of AB. Peptide fragments and small molecule compounds are effective at reducing AB aggregation, fibrilization, as well as reducing AB induced toxicity. If a small molecule is capable of preventing aggregation prior to the toxic species, the small molecule may become a therapeutic or a scaffold for drug development. Numerous AB aggregation inhibitors have been reported and can be separated into peptide fragments or small molecule compounds.

Peptide fragments of AB are designed to prevent aggregation and subsequent fibril formation. A popular inhibitor strategy has been designing peptides to cap the edges of  $\beta$ -sheets to prevent fibril extension. Soto *et al* designed a pentapeptide fragment, LPFFD (residues 17 – 21), based on the core AB sequence known to form fibrils (KLVFFAE, residues 16 - 22) (50). The designed pentapeptide included a proline residue, known to disturb  $\beta$ -sheets, and a charged amino acid, asparagine. This pentapeptide was able to reduce AB aggregation and reduce toxicity. Sciarretta *et al* used a shorter peptide fragment, KLVFF (residues 16 – 20) with alternating N-methylation of the amide residues (51). One side of the extended  $\beta$ -strand of the inhibitor can form a  $\beta$ -sheet with the AB peptide, while the methylated amide side cannot donate a hydrogen bond to extend the sheet, effectively capping the edge of the fibril. Despite the effectiveness at aggregation inhibition, small peptide inhibitors are not good as drug

compounds for three reasons: inefficient delivery mechanisms, low metabolic stability, and high cost (52). Oral delivery of small peptides will suffer from degradation by enzymes, requiring an increased dosage requirement. In addition, these small peptides have short metabolic stability, with half lives on the order of minutes to hours. Finally, there are the high costs of synthesis and purification of peptides, with estimated costs of \$1600/gram for a 40 residue peptide.

A set of small molecules have been shown to disrupt AB aggregation and/or fibrilization. I will discuss a small number of compounds that have been identified to inhibit AB aggregation. Interestingly, many of these inhibitor compounds have aromatic groups or are antioxidants.

Congo Red, as shown in Figure 1.6, is a histological staining dye used to identify generic amyloid plaques. Congo Red has been shown to bind to AB, and block fibrilization and toxicity in AB42 (53, 54). In AB40, Congo Red only shows the ability to block AB toxicity (54).

Triazine compounds have a broad range of biological activities to include anti-angiogenesis, herbicidal, and anti-microbial activities (55). Nakagami *et al* identified a triazine, RS-0466 (shown in Figure 1.6), which prevents fibril formation and inhibits AB induced toxicity (56). Walsh *et al* identified that RS-0466 inhibits the formation of cellular secreted oligomers of AB (57). In addition, Kim and Hecht identified a different triazine, E2, shown in Figure 1.6, as an aggregation inhibitor found by an *E. coli* based AB-GFP fusion screen for AB aggregation inhibitors (58).

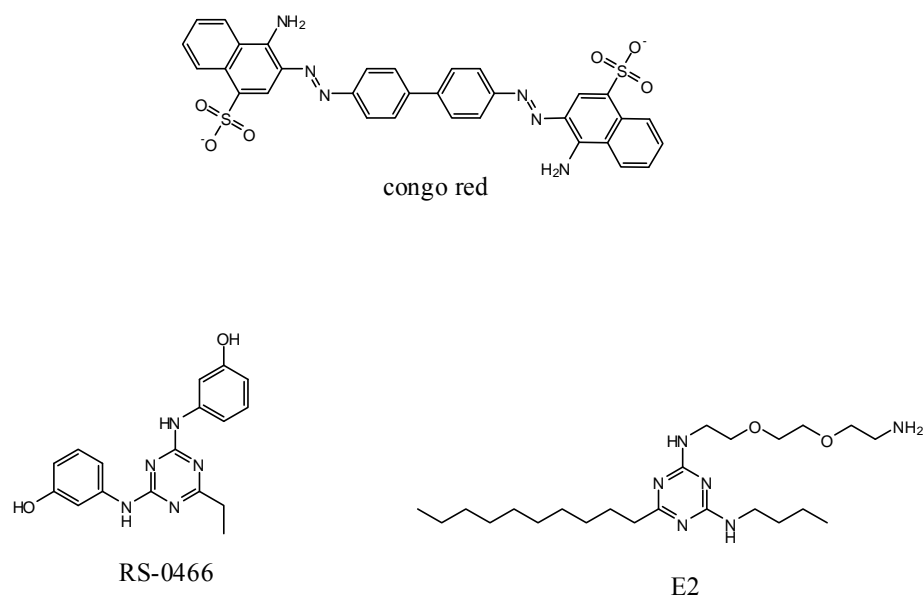
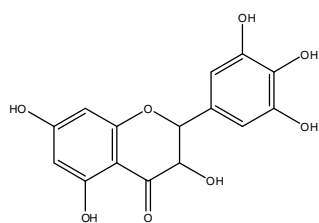


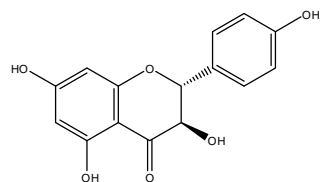
**Figure 1.6.** Structures of Congo Red and triazine inhibitors.

Ono *et al* showed that six red wine polyphenols, myricetin, morin, quercetin, kaempferol, catechin and epicatechin were able to dose dependently inhibit formation of fibrillar AB 40 and 42 (59). Ono suggested that more hydroxyl groups attached to a compound were associated with higher anti-amyloidogenic activity (59). Resveratrol, the polyphenol associated with extending life, was shown to lower AB peptide level through intracellular degradation of AB via a mechanism that involves the proteasome (60). However, in our experiments, resveratrol was shown to inhibit AB aggregation (discussed in Chapter 4).

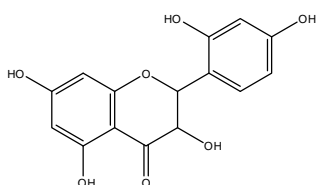
Recently, Ehrnhoefer *et al* show that the green tea polyphenol epigallocatechin gallate (EGCG) is effective at inhibiting AB by directly binding to the natively unfolded polypeptide (61). They suggest that EGCG shifts the normal aggregation pathway from toxic to non-toxic by acting as a chemical chaperone by modulating the folding pathway of AB to prevent the assembly of the toxic species.



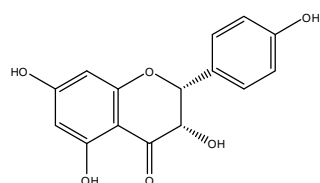
myricetin



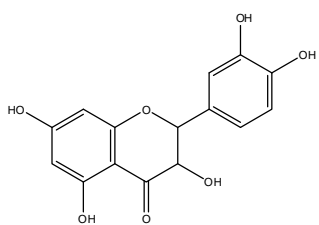
(+)-catechin



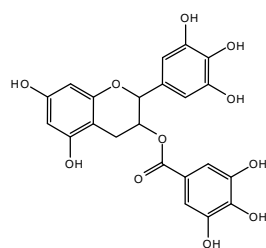
morin



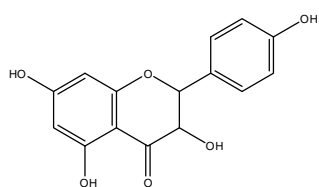
(-)-epicatechin



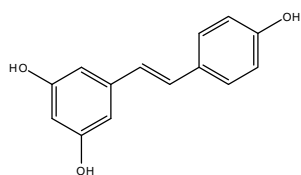
quercetin



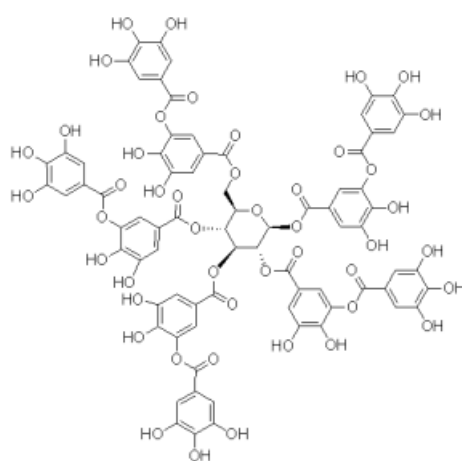
EGCG



kaempferol



resveratrol



tannic acid

**Figure 1.7.** Structure of polyphenol AB aggregation inhibitors

Tannic acid is a water soluble polyphenol that is used in tanning leather. Ono *et al* show that tannic acid inhibits fibril formation of AB, and destabilizes existing fibrils at a level higher than wine related polyphenols (62).

Other small molecules that have been identified to inhibit aggregation include nicotine, melatonin, and curcumin. Nicotine is suggested to bind to the small, soluble  $\beta$ -sheet aggregate (63). The hormone melatonin has been shown to prevent  $\beta$ -sheet formation, and has increased the survival rate of transgenic AD mice (64). Curcumin is a spice found in yellow curry, and has been shown to inhibit AB oligomerization and fibrilization (65).

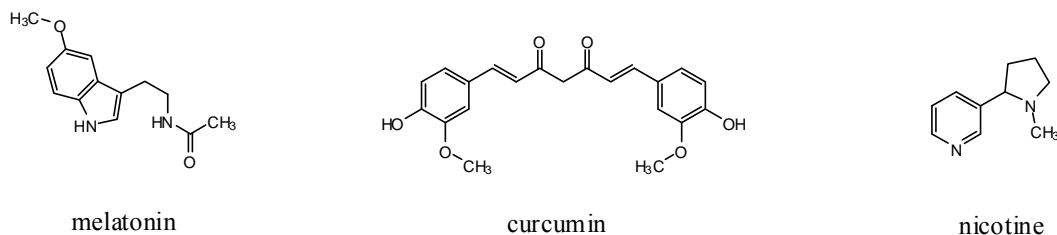


**Figure 1.8.** Structure of melatonin, curcumin, and nicotine

An aggregation inhibitor that inhibits by a different mechanism is tramiprosate, (3-amino-1-propane sulfonic acid). Tramiprosate is a small molecule glycosaminoglycan mimetic. Glycosaminoglycans have been shown to bind to soluble AB and initiate fibril formation as well as stabilize amyloid fibrils once formed (66, 67). Tramiprosate, competes for glycosaminoglycan binding sites on AB which prevents fibril formation and reduces soluble AB levels. In the AD mice model, tramiprosate was able to reduce plaque burden and lower cerebral spinal fluid concentrations of AB (68). However, the

FDA recently ruled that the data from the Phase III clinical trial were inconclusive and problematic and did support a claim for clinical efficacy (69).

In summary, all three potential mechanisms to inhibit AB production, aggregation, or reduce the AB concentration have compounds in development or in a clinical trial. However, initial success in animal tests or human Phase I/II clinical trials do not indicate Phase III success or FDA approval. Because of this low success rate, a larger number of potential inhibitors need to be identified to increase the number of compounds that reach clinical trials in order to find an effective aggregation inhibitor.

#### **1.4. Thesis outline**

This thesis will focus on identifying small molecule inhibitors of AB aggregation as well as investigating the role of aromaticity in AB aggregation and inhibition. In Chapter 2, I characterize a compound selected from an AB-GFP fusion aggregation screen for its ability to inhibit aggregation and reduce AB induced toxicity. This compound was also chosen as a scaffold for additional structure activity studies. In Chapter 3, I describe the development and implementation of a high throughput binding screen to identify compounds that bind to monomeric or low molecular weight AB oligomers as a pre-screen to identify aggregation inhibitors. Compounds that bind to monomeric AB have the potential to prevent the subsequent AB aggregation and toxicity. Compounds identified from these screens were similar to known motifs that bind to AB, and were also able to rescue AB induced toxicity. A compound selected by the binding screen was characterized for its ability to inhibit aggregation and reduce AB induced toxicity. In Chapter 4, I describe the role of aromaticity in AB aggregation. It has been

suggested that aromatic residues play an important role in amyloid aggregation. I identify two AB mutants without aromatic residues are still able to aggregate and form fibrils. I also show that aromatic inhibitors do not inhibit aggregation by disturbing the pi stacking process.

## 1.5. References

1. Anfinsen, C. B. (1973) Principles that govern the folding of protein chains, *Science* 181, 223-230.
2. Cohen, F. E., and Kelly, J. W. (2003) Therapeutic approaches to protein-misfolding diseases, *Nature* 426, 905-909.
3. Calamai, M., Chiti, F., and Dobson, C. M. (2005) Amyloid Fibril Formation Can Proceed from Different Conformations of a Partially Unfolded Protein, *Biophys. J.* 89, 4201-4210.
4. Hamada, D., and Dobson, C. M. (2002) A kinetic study of beta-lactoglobulin amyloid fibril formation promoted by urea, *Protein Sci* 11, 2417-2426.
5. Dobson, C. M. (1999) Protein misfolding, evolution and disease, *Trends in Biochemical Sciences* 24, 329-332.
6. Sipe, J. D., and Cohen, A. S. (2000) Review: History of the Amyloid Fibril, *Journal of Structural Biology* 130, 88-98.
7. Glenner, G. G., Terry, W., Harada, M., Isersky, C., and Page, D. (1971) Amyloid Fibril Proteins: Proof of Homology with Immunoglobulin Light Chains by Sequence Analyses, *Science* 172, 1150-1151.
8. Petkova, A. T., Ishii, Y., Balbach, J. J., Antzutkin, O. N., Leapman, R. D., Delaglio, F., and Tycko, R. (2002) A structural model for Alzheimer's beta - amyloid fibrils based on experimental constraints from solid state NMR, *Proc Natl Acad Sci U S A* 99, 16742-16747.
9. Kelly, J. W. (2002) Towards an understanding of amyloidogenesis, *Nat Struct Mol Biol* 9, 323-325.
10. Hoshino, M., Katou, H., Hagihara, Y., Hasegawa, K., Naiki, H., and Goto, Y. (2002) Mapping the core of the beta2-microglobulin amyloid fibril by H/D exchange, *Nat Struct Mol Biol* 9, 332-336.
11. Kelly, J. W. (1996) Alternative conformations of amyloidogenic proteins govern their behavior, *Current Opinion in Structural Biology* 6, 11-17.
12. [www.alz.org/AboutAD/statistics.asp](http://www.alz.org/AboutAD/statistics.asp).
13. Dobson, C. M. (2002) Getting out of shape, *Nature* 418, 729-730.
14. Hardy, J. (1997) Amyloid, the presenilins and Alzheimer's disease, *Trends in Neurosciences* 20, 154-159.
15. Younkin, S. G. (1998) The role of Amyloid Beta 42 in Alzheimer's disease, *Journal of Physiology-Paris* 92, 289-292.
16. Selkoe, D. J. (2001) Alzheimer's Disease: Genes, Proteins, and Therapy, *Physiol. Rev.* 81, 741-766.
17. Nilsberth, C., Westlind-Danielsson, A., Eckman, C. B., Condron, M. M., Axelman, K., Forsell, C., Stenh, C., Luthman, J., Teplow, D. B., Younkin, S. G., Naslund, J., and Lannfelt, L. (2001) The 'Arctic' APP mutation (E693G) causes Alzheimer's disease by enhanced Amyloid beta protofibril formation, *Nat Neurosci* 4, 887-893.
18. Scheuner, D., Eckman, C., Jensen, M., Song, X., Citron, M., Suzuki, N., Bird, T. D., Hardy, J., Hutton, M., Kukull, W., Larson, E., Levy-Lahad, L., Viitanen, M., Peskind, E., Poorkaj, P., Schellenberg, G., Tanzi, R., Wasco, W., Lannfelt, L.,

- Selkoe, D., and Younkin, S. (1996) Secreted amyloid beta protein similar to that in the senile plaques of Alzheimer's disease is increased in vivo by the presenilin 1 and 2 and APP mutations linked to familial Alzheimer's disease, *Nat Med* 2, 864-870.
19. Price, D. L., and Sisodia, S. S. (1998) Mutant genes in familial Alzheimer's disease and transgenic models, *Annual Review of Neuroscience* 21, 479-505.
  20. Mann, D. M. (1989) Cerebral amyloidosis, aging and Alzheimer's disease; a contribution from studies on Down's syndrome, *Neurobiol Aging* 10, 397-399; discussion 412-394.
  21. Lemere, C. A., Blusztajn, J. K., Yamaguchi, H., Wisniewski, T., Saido, T. C., and Selkoe, D. J. (1996) Sequence of Deposition of Heterogeneous Amyloid beta-Peptides and APOE in Down Syndrome: Implications for Initial Events in Amyloid Plaque Formation, *Neurobiology of Disease* 3, 16-32.
  22. Yankner, B. A. (1996) Mechanisms of Neuronal Degeneration in Alzheimer's Disease, *Neuron* 16, 921-932.
  23. Strittmatter, W. J., Saunders, A. M., Schmechel, D., Pericak-Vance, M., Enghild, J., Salvesen, G. S., and Roses, A. D. (1993) Apolipoprotein E: high-avidity binding to beta-amyloid and increased frequency of type 4 allele in late-onset familial Alzheimer disease, *Proceedings of the National Academy of Sciences of the United States of America* 90, 1977-1981.
  24. Hardy, J. (2006) Alzheimer's disease: The amyloid cascade hypothesis: An update and reappraisal, *J Alzheimers Dis* 9, 151-153.
  25. Hardy, J., and Selkoe, D. J. (2002) The amyloid hypothesis of Alzheimer's disease: progress and problems on the road to therapeutics, *Science* 297, 353-356.
  26. Hardy, J. A., and Higgins, G. A. (1992) Alzheimer's disease: the amyloid cascade hypothesis, *Science* 256, 184-185.
  27. Haass, C., and Steiner, H. (2001) Protofibrils, the unifying toxic molecule of neurodegenerative disorders?, *Nat Neurosci* 4, 859-860.
  28. Kirkitadze, M. D., Bitan, G., and Teplow, D. B. (2002) Paradigm shifts in Alzheimer's disease and other neurodegenerative disorders: the emerging role of oligomeric assemblies, *J Neurosci Res* 69, 567-577.
  29. Klein, W. L., Krafft, G. A., and Finch, C. E. (2001) Targeting small Amyloid beta oligomers: the solution to an Alzheimer's disease conundrum?, *Trends Neurosci* 24, 219-224.
  30. Klein, W. L., Stine, W. B., Jr., and Teplow, D. B. (2004) Small assemblies of unmodified amyloid beta-protein are the proximate neurotoxin in Alzheimer's disease, *Neurobiol Aging* 25, 569-580.
  31. Walsh, D. M., and Selkoe, D. J. (2004) Deciphering the molecular basis of memory failure in Alzheimer's disease, *Neuron* 44, 181-193.
  32. Shankar, G. M., Li, S., Mehta, T. H., Garcia-Munoz, A., Shepardson, N. E., Smith, I., Brett, F. M., Farrell, M. A., Rowan, M. J., Lemere, C. A., Regan, C. M., Walsh, D. M., Sabatini, B. L., and Selkoe, D. J. (2008) Amyloid-beta protein dimers isolated directly from Alzheimer's brains impair synaptic plasticity and memory, *Nat Med advanced online publication*.

33. Lesne, S., Koh, M. T., Kotilinek, L., Kaye, R., Glabe, C. G., Yang, A., Gallagher, M., and Ashe, K. H. (2006) A specific amyloid-beta protein assembly in the brain impairs memory, *Nature* 440, 352-357.
34. Cohen, F. E., and Kelly, J. W. (2003) Therapeutic approaches to protein-misfolding diseases, *Nature* 426, 905-909.
35. Selkoe, D. J. (2001) Alzheimer's disease: genes, proteins, and therapy, *Physiol Rev* 81, 741-766.
36. Beher, D., Clarke, E. E., Wrigley, J. D., Martin, A. C., Nadin, A., Churcher, I., and Shearman, M. S. (2004) Selected non-steroidal anti-inflammatory drugs and their derivatives target gamma-secretase at a novel site. Evidence for an allosteric mechanism, *J Biol Chem* 279, 43419-43426.
37. Lleo, A., Berezovska, O., Herl, L., Raju, S., Deng, A., Bacskai, B. J., Frosch, M. P., Irizarry, M., and Hyman, B. T. (2004) Nonsteroidal anti-inflammatory drugs lower Abeta42 and change presenilin 1 conformation, *Nat Med* 10, 1065-1066.
38. Kukar, T., Prescott, S., Eriksen, J. L., Holloway, V., Murphy, M. P., Koo, E. H., Golde, T. E., and Nicolle, M. M. (2007) Chronic administration of R-flurbiprofen attenuates learning impairments in transgenic amyloid precursor protein mice, *BMC Neurosci* 8, 54.
39. Wilcock, G. K., Black, S. E., Hendrix, S. B., Zavitz, K. H., Swabb, E. A., and Laughlin, M. A. (2008) Efficacy and safety of tarenflurbil in mild to moderate Alzheimer's disease: a randomised phase II trial, *The Lancet Neurology* 7, 483-493.
40. <http://www.myriad.com/news/release/1170283>.
41. Morgan, D., Diamond, D. M., Gottschall, P. E., Ugen, K. E., Dickey, C., Hardy, J., Duff, K., Jantzen, P., DiCarlo, G., Wilcock, D., Connor, K., Hatcher, J., Hope, C., Gordon, M., and Arendash, G. W. (2000) A[beta] peptide vaccination prevents memory loss in an animal model of Alzheimer's disease, *Nature* 408, 982-985.
42. Schenk, D., Barbour, R., Dunn, W., Gordon, G., Grajeda, H., Guido, T., Hu, K., Huang, J., Johnson-Wood, K., Khan, K., Kholodenko, D., Lee, M., Liao, Z., Lieberburg, I., Motter, R., Mutter, L., Soriano, F., Shopp, G., Vasquez, N., Vandever, C., Walker, S., Wogulis, M., Yednock, T., Games, D., and Seubert, P. (1999) Immunization with amyloid-beta attenuates Alzheimer-disease-like pathology in the PDAPP mouse, *Nature* 400, 173-177.
43. Janus, C., Pearson, J., McLaurin, J., Mathews, P. M., Jiang, Y., Schmidt, S. D., Chishti, M. A., Horne, P., Heslin, D., French, J., Mount, H. T. J., Nixon, R. A., Mercken, M., Bergeron, C., Fraser, P. E., St George-Hyslop, P., and Westaway, D. (2000) Amyloid beta peptide immunization reduces behavioural impairment and plaques in a model of Alzheimer's disease, *Nature* 408, 979-982.
44. Bacskai, B. J., Kajdasz, S. T., Christie, R. H., Carter, C., Games, D., Seubert, P., Schenk, D., and Hyman, B. T. (2001) Imaging of amyloid-beta deposits in brains of living mice permits direct observation of clearance of plaques with immunotherapy, *Nat Med* 7, 369-372.
45. Bard, F., Cannon, C., Barbour, R., Burke, R.-L., Games, D., Grajeda, H., Guido, T., Hu, K., Huang, J., Johnson-Wood, K., Khan, K., Kholodenko, D., Lee, M., Lieberburg, I., Motter, R., Nguyen, M., Soriano, F., Vasquez, N., Weiss, K., Welch, B., Seubert, P., Schenk, D., and Yednock, T. (2000) Peripherally

- administered antibodies against amyloid beta peptide enter the central nervous system and reduce pathology in a mouse model of Alzheimer disease, *Nat Med* 6, 916-919.
46. Nicoll, J. A., Wilkinson, D., Holmes, C., Steart, P., Markham, H., and Weller, R. O. (2003) Neuropathology of human Alzheimer disease after immunization with amyloid-beta peptide: a case report, *Nat Med* 9, 448-452.
  47. Holmes, C., Boche, D., Wilkinson, D., Yadegarfar, G., Hopkins, V., Bayer, A., Jones, R. W., Bullock, R., Love, S., Neal, J. W., Zotova, E., and Nicoll, J. A. R. (2008) Long-term effects of Amyloid beta 42 immunisation in Alzheimer's disease: follow-up of a randomised, placebo-controlled phase I trial, *The Lancet* 372, 216-223.
  48. Spooner, E. T., Desai, R. V., Mori, C., Leverone, J. F., and Lemere, C. A. (2002) The generation and characterization of potentially therapeutic amyloid beta antibodies in mice: differences according to strain and immunization protocol, *Vaccine* 21, 290-297.
  49. <http://www.scripnews.com/news/elan-and-wyeths-alzheimers-hope-fails-to-impress-129>.
  50. Soto, C., Sigurdsson, E. M., Morelli, L., Asok Kumar, R., Castano, E. M., and Frangione, B. (1998) Beta-sheet breaker peptides inhibit fibrillogenesis in a rat brain model of amyloidosis: Implications for Alzheimer's therapy, *Nat Med* 4, 822-826.
  51. Sciarretta, K. L., Gordon, D. J., Meredith, S. C., Indu, K., and Ronald, W. (2006) Peptide Based Inhibitors of Amyloid Assembly, in *Methods in Enzymology*, pp 273-312, Academic Press.
  52. Latham, P. W. (1999) Therapeutic peptides revisited, *Nat Biotech* 17, 755-757.
  53. Lee, V. M. (2002) Amyloid binding ligands as Alzheimer's disease therapies, *Neurobiol Aging* 23, 1039-1042.
  54. Lorenzo, A., and Yankner, B. A. (1994) Beta-amyloid neurotoxicity requires fibril formation and is inhibited by congo red, *Proc Natl Acad Sci U S A* 91, 12243-12247.
  55. Bork, J. T., Lee, J. W., Khersonsky, S. M., Moon, H. S., and Chang, Y. T. (2003) Novel Orthogonal Strategy toward Solid-Phase Synthesis of 1,3,5-Substituted Triazines, *Org. Lett.* 5, 117-120.
  56. Nakagami, Y., Nishimura, S., Murasugi, T., Kubo, T., Kaneko, I., Meguro, M., Marumoto, S., Kogen, H., Koyama, K., and Oda, T. (2002) A novel compound RS-0466 reverses beta-amyloid-induced cytotoxicity through the Akt signaling pathway in vitro, *Eur J Pharmacol* 457, 11-17.
  57. Walsh, D. M., Townsend, M., Podlisny, M. B., Shankar, G. M., Fadeeva, J. V., El Agnaf, O., Hartley, D. M., and Selkoe, D. J. (2005) Certain inhibitors of synthetic amyloid beta-peptide fibrillogenesis block oligomerization of natural Abeta and thereby rescue long-term potentiation, *J Neurosci* 25, 2455-2462.
  58. Kim, W., Kim, Y., Min, J., Kim, D., Chang, Y.-T., and Hecht, M. (2006) A High-Throughput Screen for Compounds That Inhibit Aggregation of the Alzheimer's Peptide, *ACS Chem. Biol.* 1, 461-469.
  59. Ono, K., Naiki, H., and Yamada, M. (2006) The development of preventives and therapeutics for Alzheimer's disease that inhibit the formation of beta-amyloid

- fibrils (fA $\beta$ ), as well as destabilize preformed fA $\beta$ , *Curr Pharm Des* 12, 4357-4375.
60. Marambaud, P., Zhao, H., and Davies, P. (2005) Resveratrol Promotes Clearance of Alzheimer's Disease Amyloid-beta Peptides, *J. Biol. Chem.* 280, 37377-37382.
  61. Ehrnhoefer, D. E., Bieschke, J., Boeddrich, A., Herbst, M., Masino, L., Lurz, R., Engemann, S., Pastore, A., and Wanker, E. E. (2008) EGCG redirects amyloidogenic polypeptides into unstructured, off-pathway oligomers, *Nat Struct Mol Biol* 15, 558-566.
  62. Ono, K., Hasegawa, K., Naiki, H., and Yamada, M. (2004) Anti-amyloidogenic activity of tannic acid and its activity to destabilize Alzheimer's beta-amyloid fibrils in vitro, *Biochim Biophys Acta* 1690, 193-202.
  63. Ono, K., Hasegawa, K., Yamada, M., and Naiki, H. (2002) Nicotine breaks down preformed Alzheimer's beta-amyloid fibrils in vitro, *Biological Psychiatry* 52, 880-886.
  64. Pappolla, M., Bozner, P., Soto, C., Shao, H., Robakis, N. K., Zagorski, M., Frangione, B., and Ghiso, J. (1998) Inhibition of Alzheimer beta -Fibrillogenesis by Melatonin, *J. Biol. Chem.* 273, 7185-7188.
  65. Yang, F., Lim, G. P., Begum, A. N., Ubeda, O. J., Simmons, M. R., Ambegaokar, S. S., Chen, P. P., Kaye, R., Glabe, C. G., Frautschy, S. A., and Cole, G. M. (2005) Curcumin Inhibits Formation of Amyloid Beta Oligomers and Fibrils, Binds Plaques, and Reduces Amyloid in Vivo, *J. Biol. Chem.* 280, 5892-5901.
  66. Castillo, G. M., Lukito, W., Wight, T. N., and Snow, A. D. (1999) The sulfate moieties of glycosaminoglycans are critical for the enhancement of beta-amyloid protein fibril formation, *J Neurochem* 72, 1681-1687.
  67. Díaz-Nido, J., Wandosell, F., and Avila, J. (2002) Glycosaminoglycans and beta amyloid, prion and tau peptides in neurodegenerative diseases, *Peptides* 23, 1323-1332.
  68. Geerts, H. (2004) NC-531 (Neurochem), *Curr Opin Investig Drugs* 5, 95-100.
  69. <http://www.alzforum.org/new/detail.asp?id=1647>.

## **Chapter 2. Characterizing amyloid beta peptide aggregation inhibitors selected by the AB-GFP fusion screen**

### **2.1. Introduction**

Currently, over 4.5 million people in the US have been diagnosed with Alzheimer's disease (AD) (1). AD is linked to aging, so as the population gets older, the number of people diagnosed with AD will also increase. Because of this trend, there is an increased need for Alzheimer's therapeutics to either ease symptoms, or prevent the disease. The current FDA approved drugs for Alzheimer's disease only temporarily slow the memory loss symptoms and do not treat underlying root cause of Alzheimer's disease.

The root cause of the disease is still unknown, but focus has been centered on the accumulation of the Alzheimer's amyloid beta (AB) peptide. The amyloid cascade theory suggests that a toxic species exists on the aggregation pathway of AB, as it aggregates from monomer to oligomer to fibril and to plaque (2-4). Preventing AB formation, increasing AB clearance, and inhibiting AB aggregation are three possible methods to treat the disease (5). Preventing formation of AB can be accomplished by inhibiting the secretases that cleave the precursor protein, and increasing the AB clearance rate has been demonstrated with immunization against AB (6, 7). However, there are questions about effectiveness and unwanted side effects in both of these treatment methods (8). The third treatment path is to identify compounds that inhibit the aggregation of AB into the putative toxic species. Compounds that have this ability can be used as potential

drugs for AD treatment. In order to search the numerous compound libraries available, high throughput screens to identify aggregation inhibitors are necessary.

Our lab has previously developed an *E. coli* based high throughput screen to identify compounds that inhibit AB aggregation (9). The screen is based on a GFP fusion protein expressed in *E. coli*. As shown in Figure 2.1, the sequence for AB is located at the N-terminal of the fusion protein, followed by a linker sequence, and GFP. The 12 amino acid linker sequence was shown to correlate the solubility of the inserted protein to GFP fluorescence (10).

Kim *et al* showed that the AB-GFP fusion protein was able to identify compounds that inhibited AB aggregation (9). These inhibitor compounds prevent the AB portion of the fusion from aggregating which allows the GFP portion of the fusion to effectively fold and fluoresce. Ineffective compounds, or compounds that do not get past the membranes of *E. coli*, do not prevent the aggregation of the AB fusion, and therefore do not fluoresce. In a pilot study of 1000 triazine compounds, Kim *et al* identified compound E2 as an aggregation inhibitor and D2 as an ineffective compound (9). The structures are shown below, in Figure 2.1.

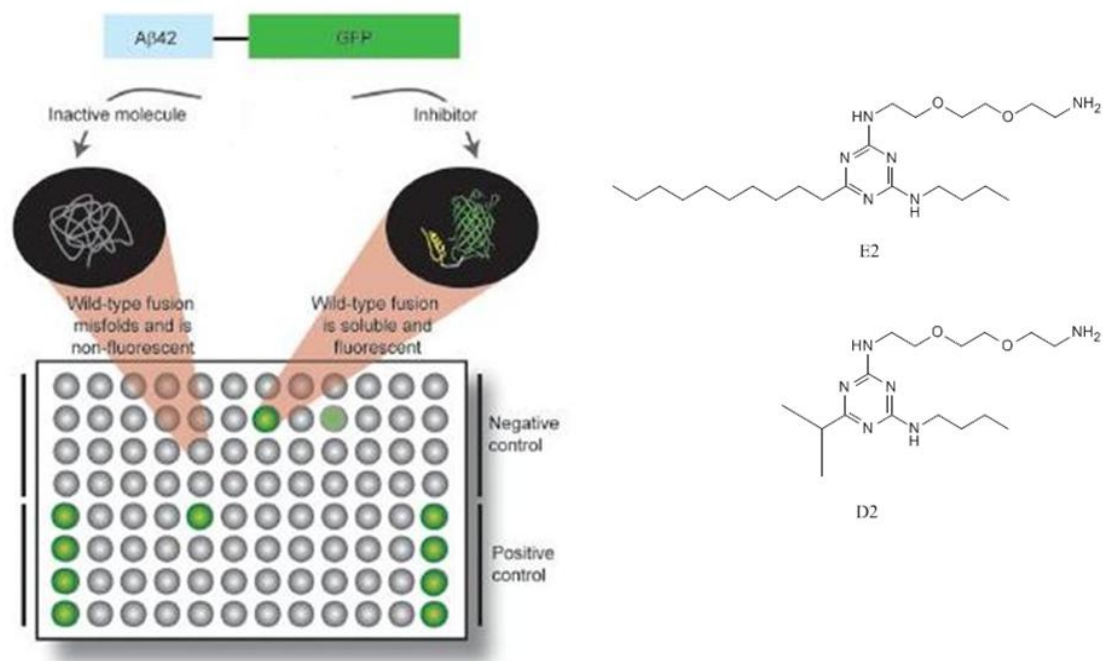


**Figure 2.1.** Top: AB-GFP fusion protein layout. Left: Cartoon representation of AB-GFP fusion assay. Right: Compound inhibitor (E2) and ineffective compound (D2) found by the AB GFP fusion assay. Figure from Kim *et al* (9).

In this chapter, I will discuss the implementation of the AB-GFP fusion screen on a library of 65,000 compounds. Compound 737 was a compound identified by the AB GFP screen as a possible AB aggregation inhibitor. Secondary studies indicated that compound 737 was able to reduce AB aggregation as determined by the thioflavin T fluorescence assay. Subsequent toxicity studies in a neuronal cell culture model showed that compound 737 rescued AB induced toxicity. Several compound analogs to 737 were chosen for a structure activity study. Several 737 analogs also reduced AB aggregation as well as rescued AB induced toxicity. These results indicate that compound 737 is a good scaffold for development of AB aggregation inhibitors. Further studies indicated

that although compound 737 was indeed active in both thioflavin T and cell toxicity assays, its initial selection in the AB-GFP fusion screen was due to an artifact.

## 2.2. Results

Compounds that inhibit the aggregation of AB42 are useful as potential therapeutics for Alzheimer's disease as well as for providing additional information about the process of aggregation inhibition. I used our lab's *E. coli* based AB-GFP fusion assay to screen the compound collection at the Broad Institute of Harvard and MIT. Their collection contains libraries of commercially developed compounds, natural product extracts, as well as university synthesized compounds. Over 65,000 compounds were assayed, and after data analysis, the screen reduced the number of compounds for follow on testing. Compounds from the selection were selected based on availability for additional aggregation and toxicity tests.

Briefly, LB media with IPTG was added to 384 well plates. IPTG was added to LB media without *E. coli* present to prevent AB-GFP expression prior to compound addition. Compounds and/or DMSO were added to the LB and IPTG plates by a 384 well drug dispensing machine. After compound dispensing, plates containing LB, IPTG, and compounds were read for fluorescence on a plate reader at the GFP wavelength to identify fluorescently active compounds. After the fluorescent pre-screen, *E. coli* with AB-GFP fusion plasmid was added to the 384 well plates and incubated at 37°C for 5 hours. A final post incubation fluorescent measurement was taken and the data were analyzed.

### **2.2.1. AB-GFP fusion pre-screening**

The AB-GFP fusion assay is based on the fluorescence of the GFP fusion protein. During preliminary assay development, I discovered that compounds may also be fluorescently active at the same excitation and emission wavelengths as used for the AB-GFP fusion, with riboflavin being a notable example. Because it would be difficult or impossible to separate the fraction of fluorescence attributed to the fusion protein and the fraction due to the fluorescence of the compound, I decided eliminate these compounds during data analysis. A pre-read of the compounds was implemented to identify fluorescently active compounds in an attempt to reduce the number of false positives.

### **2.2.2. Fusion screen positive and negative controls**

The GFP fusion system negative control consists of the AB-GFP fusion protein without any test compound added. The positive control is another GFP fusion protein, where a soluble mutant of AB is located at the N-terminal. GM6 is a double mutant of AB42 (F19P L34S), and was shown by Wurth *et al* to be soluble and aggregate less than AB42 (11). The GM6 fusion was chosen as the positive control for the upper fluorescence limit on the assay because it has the same length peptide as AB, and it is unlikely that a small molecule compound would have the ability to inhibition aggregation to the level of fluorescence as GM6.

### **2.2.3. AB-GFP fusion data analysis**

Fluorescence readings after incubation of *E. coli* with compound were collected for each test compound in duplicate. Z-scores, or standard scores, were calculated for

each compound using a standard pipeline calculation for high throughput screening as developed by Seiler *et al* (12, 13). Z-scores indicate how many standard deviations a fluorescence compound measurement is above or below the control value mean. Since each screen involved duplicates, the Z-score was combined to form a composite Z-score. Composite Z-scores were calculated for both fluorescence pre-read and after incubation measurements.

To remove the compounds that are fluorescently active at the GFP wavelength, the pre-read composite Z was plotted on the X axis, and the after incubation measurement was plotted on the Y axis, as shown in Figure 2.2. Compounds that are fluorescently active will show up on the  $x = y$  diagonal. As shown in Figure 2.2, several compounds in blue are fluorescently active at the same wavelength as GFP.

### Data analysis: removing fluorescently active compounds

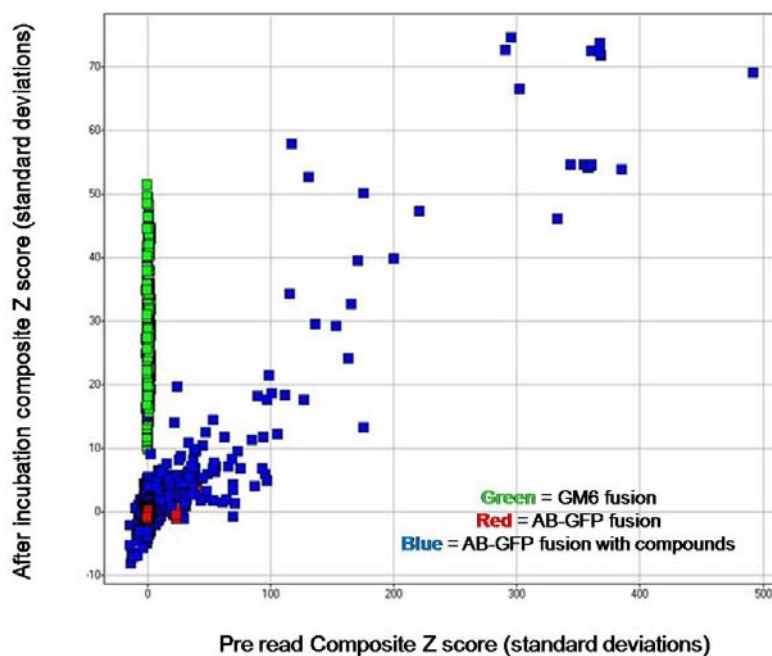


**Figure 2.2.** Determining if a compound is fluorescently active at the GFP wavelength. Compound pre-read composite Z-scores are plotted on X axis, with post incubation GFP fluorescence Z-scores plotted on Y axis. Red squares represent negative control (AB-GFP fusion without compounds), green squares represent positive control (GM6 fusion), and blue squares represent AB-GFP fusion with compounds. Compounds on the  $x = y$  diagonal indicate compounds that are fluorescently active at the GFP wavelength.

#### 2.2.4. Thresholds for selection

Fluorescently active compounds were identified by the pre-screening data were eliminated by removing compounds that had a pre-read Z score of 3 or greater (3 standard deviations above the control AB42 with DMSO) as shown by the blue vertical line in Figure 2.3. 3 standard deviations was used as the criteria as it was the highest

value reached by the AB-GFP pre read control wells with no compound. Compounds were considered as hits if their post-incubation fluorescence Z-score (as plotted on the Y axis on Figure 2.3) was greater than 3 (black horizontal line). These selection rules identify compounds that are not fluorescently active at the GFP wavelength and have post incubation GFP fluorescence, which are the hits from the screen, and are highlighted by the red box in Figure 2.3.

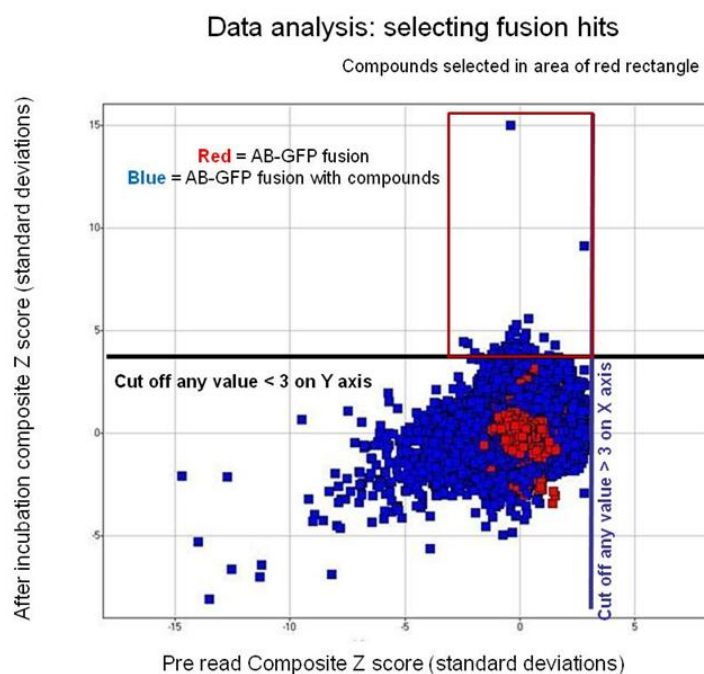


**Figure 2.3.** Selection rules to identify compounds hits in the AB-GFP fusion assay.

### 2.2.5. Compounds selected by the AB-GFP fusion screen

A total of 269 compounds were selected by the AB-GFP screen. 9 compounds from this group were selected for additional testing based on availability, as shown in Figure 2.4.

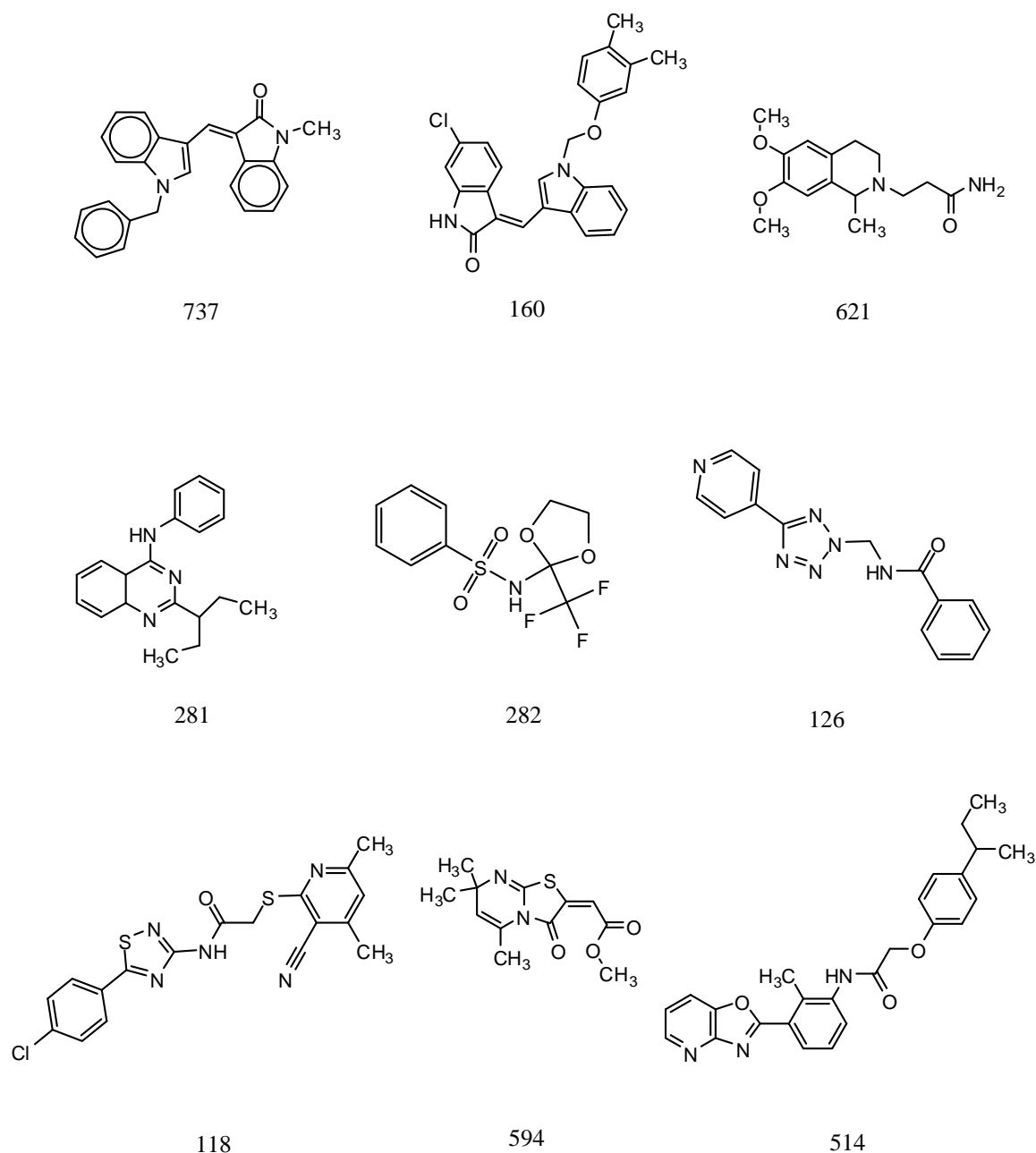


**Figure 2.4.** Structures of compounds selected by the AB-GFP fusion screen for addition testing.

These compounds were then tested for their ability to inhibit aggregation with the thioflavin T assay. Thioflavin T is a dye that is negligibly fluorescent in solution but

experiences a significant increase in fluorescence after binding to amyloid fibrils (14). An aggregation inhibitor added to a sample of AB would show reduced thioflavin T fluorescence when compared to an untreated sample. In this assay, AB peptide is incubated at 37°C for 5 hours with and without aggregation inhibitor. The aggregation inhibition ability of selected screening compounds is shown in Figure 2.5. (Compound 160 was not tested because it was not soluble in DMSO). Compound 737 has a clear dose dependent inhibition and compound 594 has a slight aggregation inhibition. Compounds 621, 282, 126, and 118 were not effective at inhibiting aggregation. Interestingly, compounds 281 and 514 show a very large increase in AB aggregation.

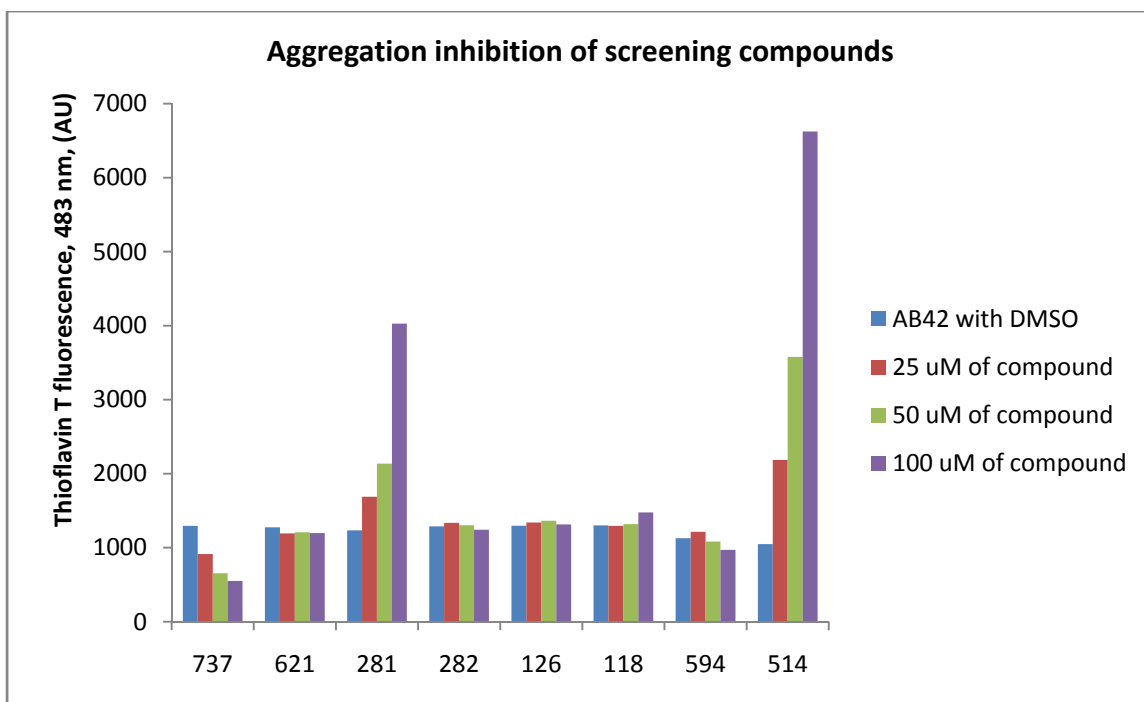


**Figure 2.5.** Aggregation inhibition of compounds found by AB-GFP fusion with AB42. AB42 concentration of 20 uM, with 5 hour incubation at 37°C. Single measurements.

#### 2.2.6. Characterization of compound 737

Compound 737 was selected for additional testing, as it was identified as a potential inhibitor by the AB-GFP fusion screen and was able to reduce AB aggregation (Figure 2.5). Compound 737, shown in Figure 2.4, is aromatic and has a relatively flat structure, which are characteristic of previously identified AB aggregation inhibitors.

Subsequent thioflavin T studies of compound 737 show a similar dose dependence aggregation inhibition. As shown in Figure 2.6, the IC<sub>50</sub> of 737, or concentration of compound necessary to reduce the thioflavin T fluorescence value by half, is approximately 9 uM. In comparison, the triazine E2, from Kim *et al* had a reported IC<sub>50</sub> of approximately 30 uM (9).

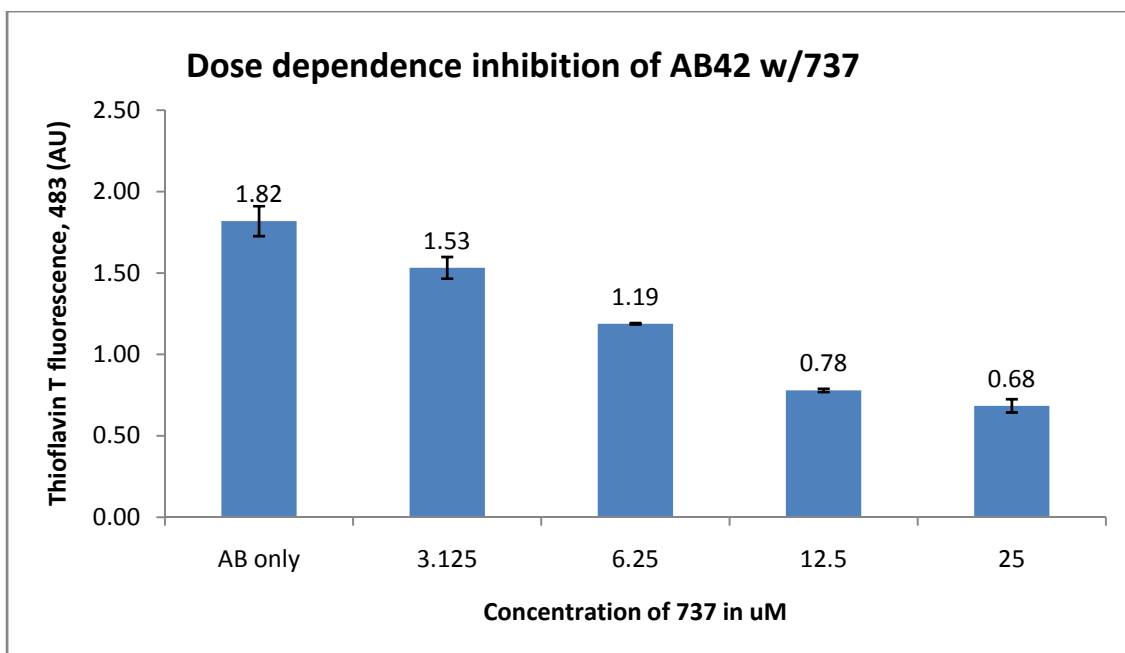


**Figure 2.6.** Dose dependence aggregation inhibition of AB42 with different concentrations of 737. AB42 concentration of 20 uM, with 24 hours incubation at 37°C. In triplicate, standard error reported.

The thioflavin T time course of AB42 with and without compound 737 at varying concentrations is shown in Figure 2.7. As increasing amounts of 737 are added to the AB42, the fluorescence of thioflavin T decreases, indicating less aggregation.

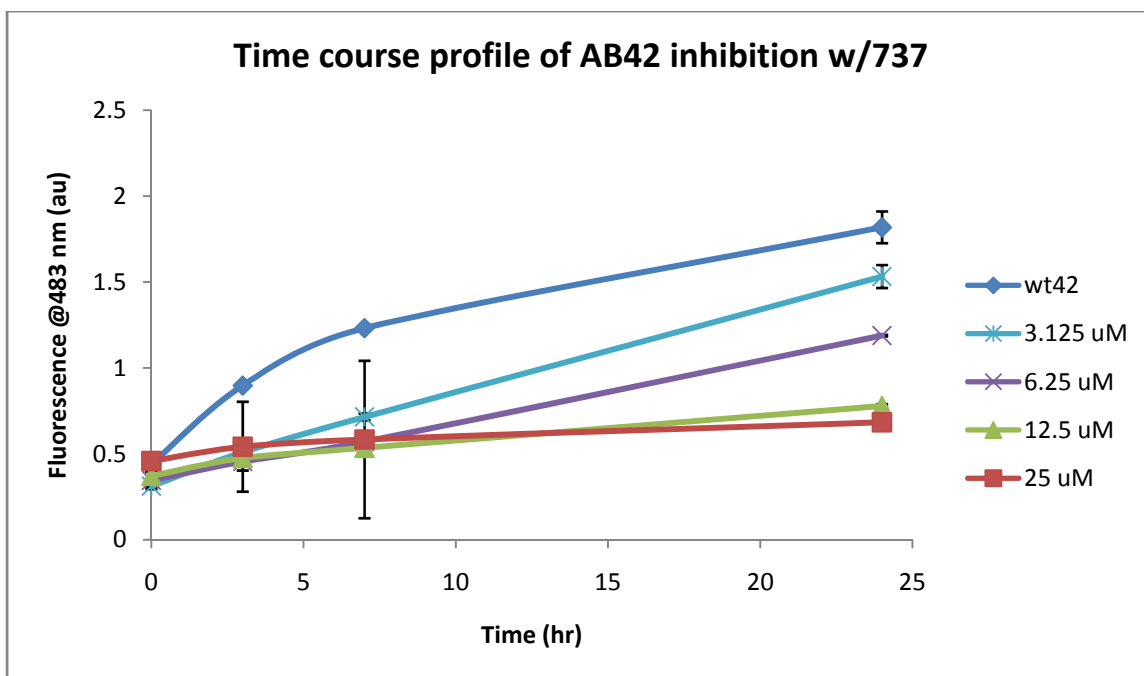


**Figure 2.7.** Time course inhibition plot of AB42 with varying concentrations of 737.

AB42 concentration of 20 uM. Values are an average of two wells with standard deviation reported as error.

### 2.2.7. Toxicity studies

The previous data indicate that compound 737 effectively inhibits AB aggregation. The next step was to determine the ability of compound 737 to rescue AB induced toxicity in a neuronal cell culture model. PC12 cells are a neuronal cells line extracted from the brains of rats, and have been used as a model system for AB rescue. As shown in Figure 2.8, compound 737 is able to rescue AB42 induced toxicity. PC12 cells treated with 737 and AB42 had a viability of 73%, while cells with AB without any compound had a viability of 51%.

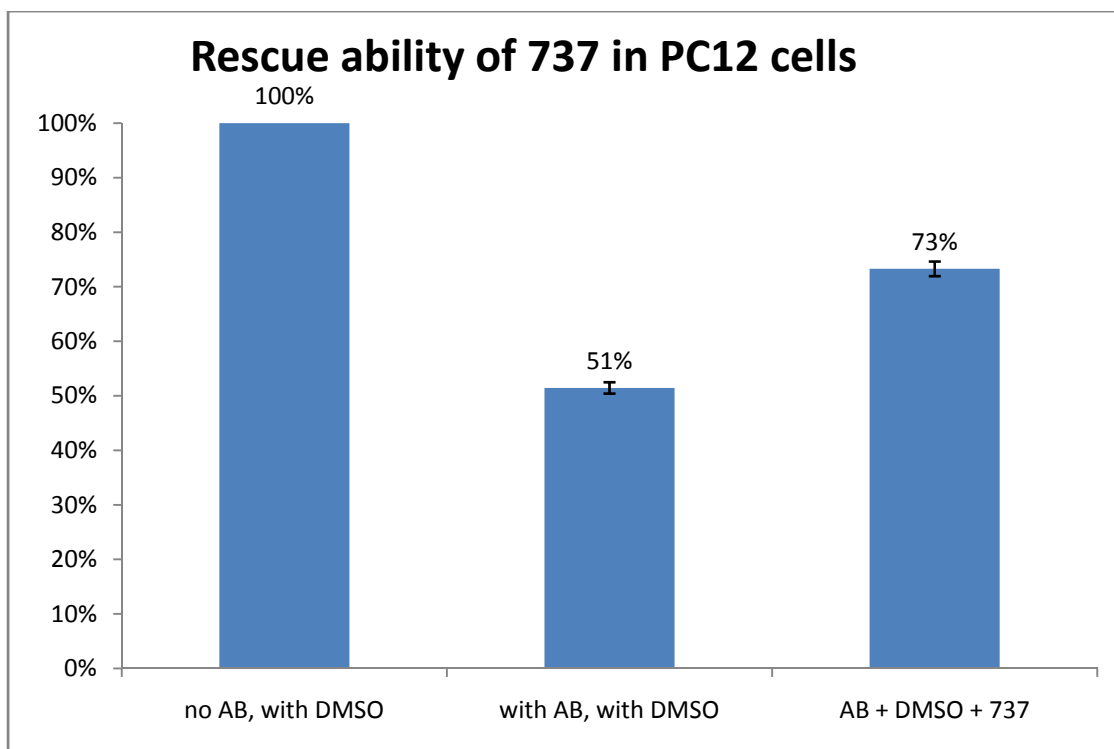


**Figure 2.8.** Ability of 737 to rescue AB induced toxicity in PC12 cells. AB42 concentration of 20  $\mu$ M with 737 concentration of 100  $\mu$ M. Data normalized to PC12 cells with no AB. Average of triplicate samples with standard error reported. DMSO used to dissolve compound 737. Rescue by 737 is statistically significant at rescue, with  $p < 0.05$  as determined by the Student's TTest.

### 2.2.8. Structure activity relationship (SAR) studies of compound 737

Because compound 737 was able to inhibit AB aggregation and rescue AB induced toxicity, I used the structure as a scaffold to identify other AB inhibitors. In addition, structure activity relationship studies can provide information on motifs necessary for aggregation inhibition and toxicity rescue. 13 analogs to 737 were selected for additional studies, as shown in Figure 2.9.

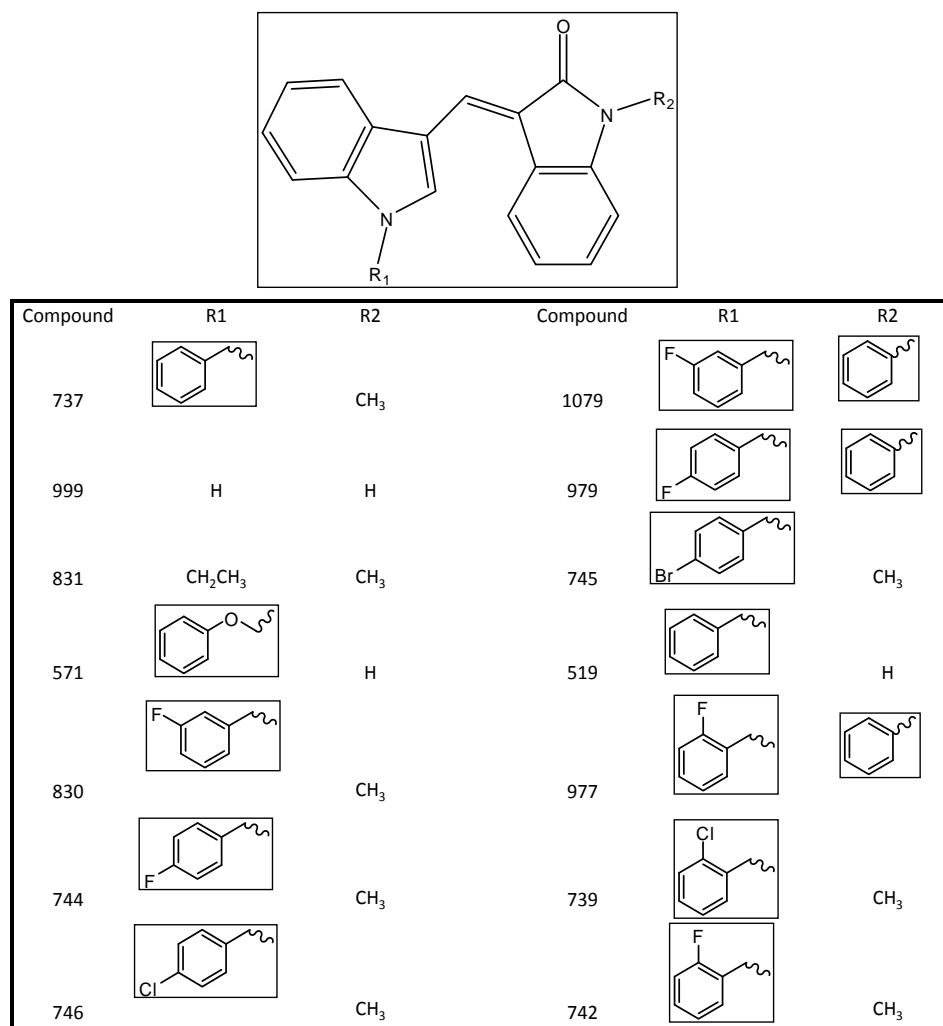


**Figure 2.9.** Compound analogs of 737 selected for additional tests

The analogs were tested for their ability to inhibit AB aggregation with the thioflavin T assay, as shown in Figure 2.10. All but one compound analog (compound 742) was able to reduce AB aggregation. As shown in Figure 2.10, two analogs, 999 and 831, are better aggregation inhibitors than compound 737. Both of these compounds have smaller substituents at both the R<sub>1</sub> and R<sub>2</sub> position. Compound 999 has a hydrogen

at both positions  $R_1$  and  $R_2$ , while compound 831 has methyl groups at both  $R_1$  and  $R_2$  positions. Both of these substituents are smaller than the  $R_1$  group on compound 737, which suggests that a smaller substituent group at  $R_1$  makes a difference in aggregation inhibition. This trend is also shown when comparing 999 and 831 to 519 and 571. 519 has a  $R_1$  of  $\sim\text{CH}_2\text{-Ph}$ , and 571 had a  $R_1$  of  $\sim\text{CH}_2\text{-O-Ph}$ , and both are worse at aggregation inhibition. Position  $R_1$  has steric issues associated with aggregation inhibition, with smaller substituents being better than larger ones.

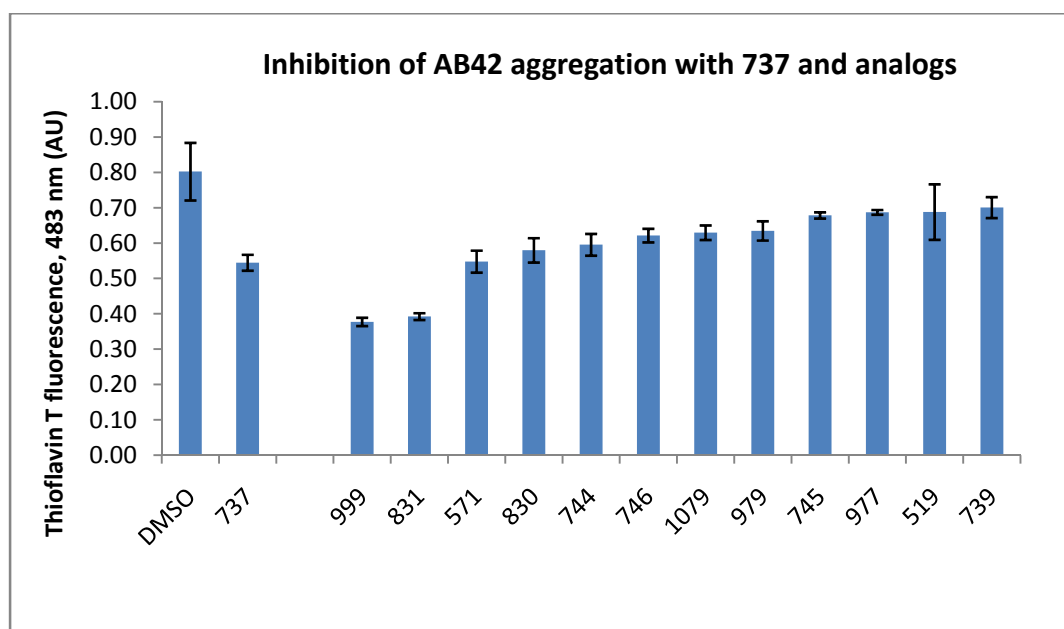
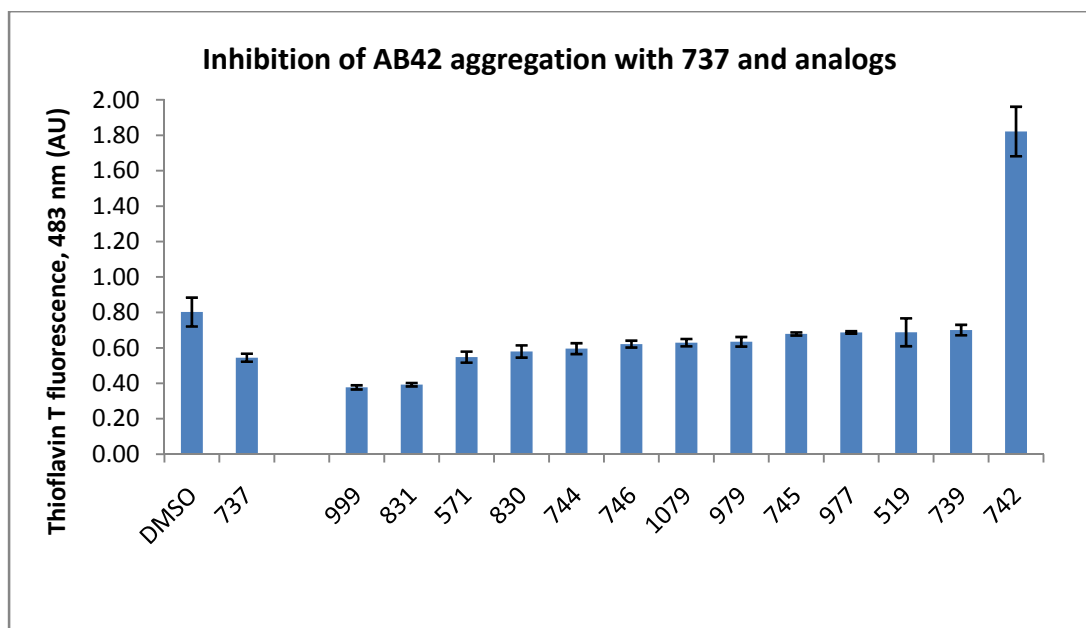


**Figure 2.10.** Inhibition of AB42 aggregation by 737 and analogs. Top: 737 and analog compounds. Bottom: Without compound 742 and scaled Y axis. AB42 concentration at 20  $\mu$ M with compound concentration at 100  $\mu$ M. 5 hour incubation at 37°C. Average value of three wells, with standard deviation reported as error.

Large substitutions at position R<sub>2</sub> also reduce the compound's aggregation inhibition. Compounds 977, 1079 and 979 all have a phenyl substitution at position R<sub>2</sub> and do not inhibit as well as 999, 831, and 737, which have smaller substituents. This also suggests that sterics play a role at the R<sub>2</sub> position.

Halogenations of the phenyl ring at R<sub>1</sub> in general did not lower aggregation inhibition, as 737, without any halogenations of the ring was better than any analog with a halogenated R<sub>1</sub> substituent. However, a trend was identified with halogens located at the *para* position on the phenyl ring at R<sub>1</sub> based on halogen size. The *para* fluoro phenyl substituent was slightly better than the *para* chloro, which was better than the *para* bromo compound, 744, 746, and 745 respectively. This trend reinforces the R<sub>1</sub> steric interaction as described above, as the smallest halogen had the best aggregation inhibition. It is also possible that electronic interaction has a role in aggregation inhibition.

The final trend identified that any *ortho* halogen substitution on the phenyl ring at position R<sub>1</sub> would prevent aggregation inhibition by the compound. Compounds 977, 739, and 742 are either *ortho* fluoro or *ortho* chloro and were the least effective analogs. Compound 742 had an increased thioflavin T fluorescence value, suggesting that this compound could increase AB aggregation.

#### **2.2.9. Toxicity rescue by compound 737 analogs**

The compound analogs were also tested for their ability to rescue AB42 induced toxicity. Before rescue experiments were attempted, the toxicity of the compound alone was determined by adding compounds to PC12 cells without AB. Compound toxicity is

shown in Figure 2.11, with cell viability was normalized to untreated PC cells. Three out of the 13 compound analogs were clearly toxic to the PC12 cells. These three compounds share a common structure of a  $\sim\text{H}$  as the substituent at the  $\text{R}_2$  position. All the other compound analogs had either a methyl or phenyl group located at the  $\text{R}_2$  position, and were not toxic. Some analogs seemed to increase the viability of the PC12 cells. These compounds may increase viability, but can also be attributed to several factors, including an increased starting number of PC12 cells prior to compound addition, incubator hotspots, or plate edge effects, all of which would increase cell viability.

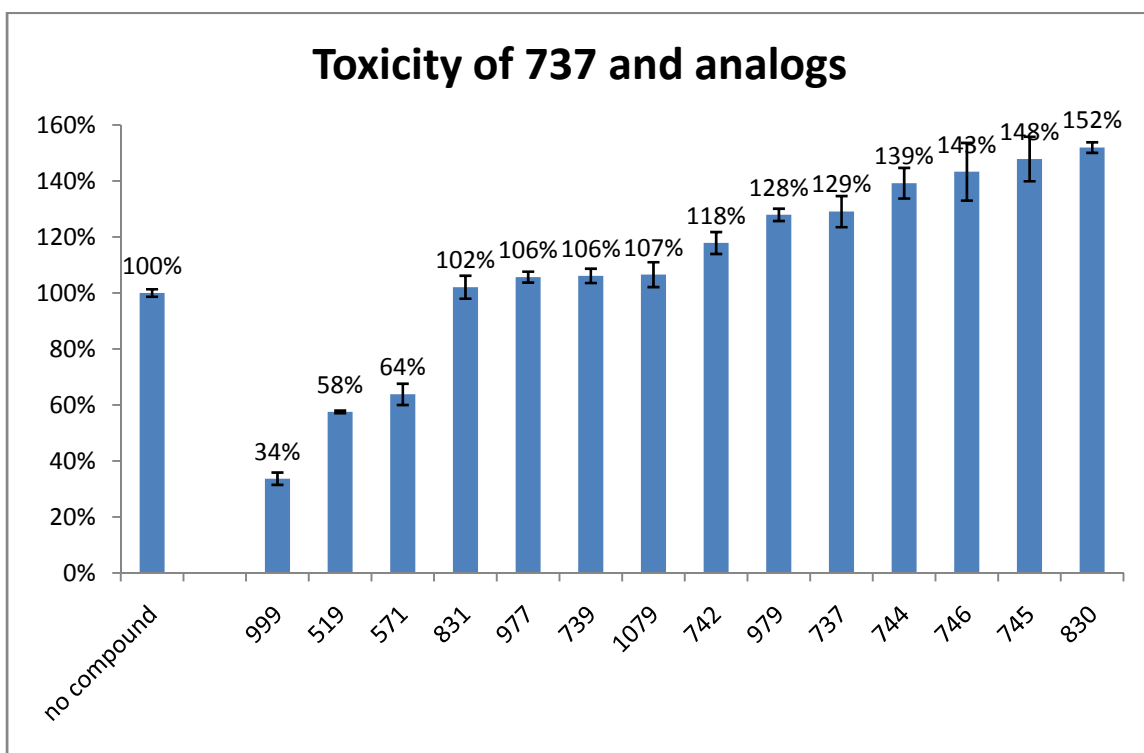


**Figure 2.11.** Toxicity of 737 analogs in PC12 cells. Values are average of triplicate samples. Data normalized to PC12 cells with no compounds added. Standard errors are reported.

### 2.2.10. Compound efficacy

As shown in Figure 2.12, eight out of the 13 analogs were able to significantly rescue AB induced toxicity. The compounds that were identified as toxic to PC12 cells (Figure 2.11, compounds 999, 519, and 571) were not significantly effective at rescue.

The top 5 analogs for rescue all had a methyl group at R<sub>2</sub>. Compound 744 was the best at rescue, and has a *para* fluoro phenyl R<sub>1</sub> group; next was compound 830, with the *meta* fluoro phenyl R<sub>1</sub> group; third was compound 746 with the *para* chloro phenyl R<sub>1</sub> group; followed by compound 742 with the *meta* fluoro phenyl R<sub>1</sub> group. In comparing the *para* fluoro (744), *para* chloro (746), and *para* bromo (745), the smaller the halogen, the better the rescue ability of the compound. Halogenation on the phenyl ring at the R<sub>1</sub> position is responsible for the difference in viability. For rescue, the *para* fluoro position was better at rescue than the *meta*, which was better than the *ortho* for the R<sub>1</sub> position. The same trend was shown when the halogen was changed from fluoro to chloro; the *para* chloro was better than the *ortho* chloro position for rescue.

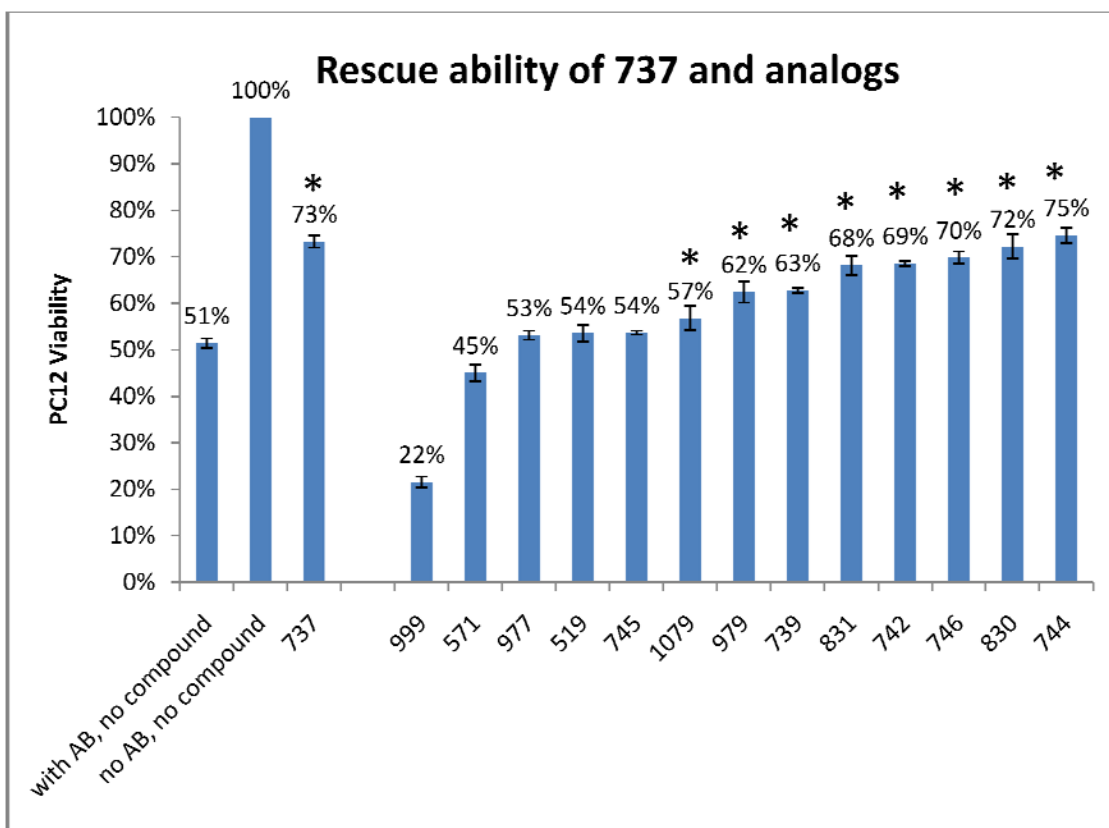


**Figure 2.12.** Ability of 737 and analogs to rescue AB42 induced toxicity in PC12 cells. Values are averages of triplicate samples. Data normalized to PC12 cells with no AB average wells, with standard error reported. \* indicates that the compound is statistically significant.  $p < 0.05$ . with Student's TTest.

There did not seem to be a correlation between compound aggregation inhibition ability and toxicity rescue among the compounds that were not toxic. For example, compound 831 was a compound that had the second lowest thioflavin T fluorescence value (less aggregation), but was 5<sup>th</sup> best at rescuing AB induced toxicity. Additionally, compound 742 had an extremely high thioflavin T fluorescence value (more aggregation) but yet was able to rescue AB induced toxicity to 69% (4<sup>th</sup> best at rescue). Because both of these compounds have different substituents at R<sub>1</sub> and R<sub>2</sub>, it is possible that they

inhibit at different timepoints on the aggregation pathway (monomeric or oligomeric forms). Since these compounds rescue AB induced toxicity, these compounds also shift the aggregation pathway from the normally toxic to a different non-toxic pathway.

#### **2.2.11. Testing 737 analogs into the AB-GFP fusion system**

Compound analogs of 737 were also tested in the GFP fusion system to identify the effects of the different substituent on the fusion screen. Analogs were first checked for fluorescence at the GFP wavelength, as shown in the top of Figure 2.13. After incubation with *E. coli* and expression of the AB-GFP fusion protein, it was noted that some compounds had abnormally high GFP fluorescence values (742). These values were even higher than the GM6 fusion control, which was used as the upper fluorescence limit. The pre-read of the compounds indicated that some analogs were slightly fluorescently active, but not as high as the post-incubation levels. These abnormally high fluorescence reading suggested the possibility that *E. coli* was metabolizing the compounds into a fluorescently active compound, or that the compounds become fluorescent upon binding to the *E. coli* membrane or other cellular component.

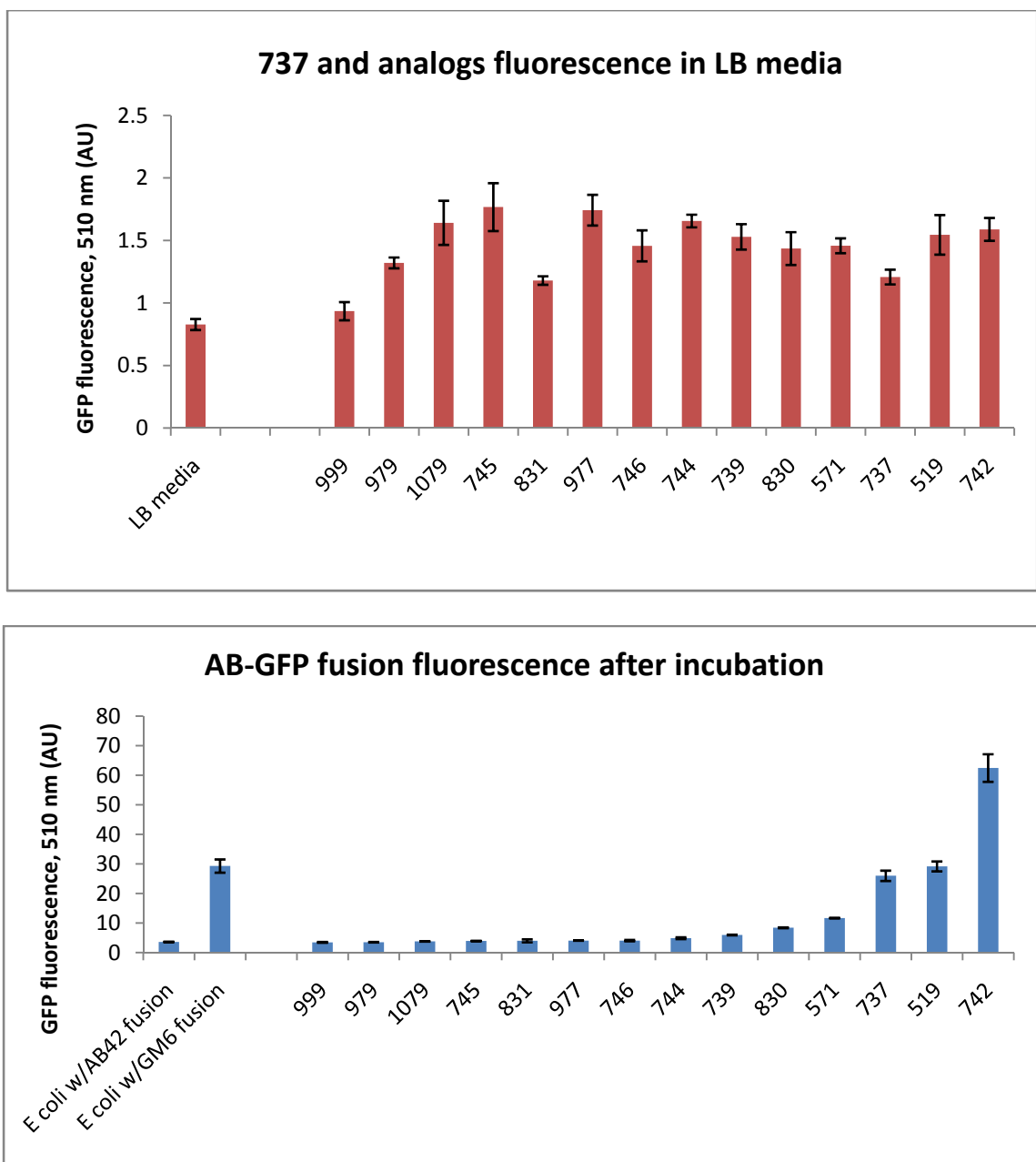


**Figure 2.13.** Fluorescence of 737 analogs in LB media and in fusion system. Top. Pre read of compound in LB media. Bottom. GFP fluorescence after addition of *E. coli*, induction and incubation at 37°C for 5 hours. Values are averages of three wells, with standard error reported. Final compound concentration at 100  $\mu$ M. Y-axis scales are comparable.

In order to identify if *E. coli* was processing compounds, *E. coli* without the AB-GFP fusion plasmid vector was incubated with the compounds. According to Figure 2.14, the fluorescence of the compounds in LB media (compound pre-read, in blue) is nominal, with 742 being slightly high. After 5 hour incubation with *E. coli* (after incubation, in red), it is clear that the addition of *E. coli* is responsible for the increase in fluorescence. Compounds 519, 571, 737, 739, 742, and 830 all exhibited very large increases in fluorescence at the GFP wavelength. Since there is no plasmid present in this *E. coli*, there is no GFP fusion protein being produced. This indicates that *E. coli* is processing the compound into a fluorescent active compound, or compound binding to the *E. coli* membrane is causing the fluorescent activity. Thus it appears that the selection of compound 737 from the GFP fusion screen was because it became fluorescent upon the interaction with *E. coli*. Thus it was a false positive and not due to its effect on the AB-GFP fusion.

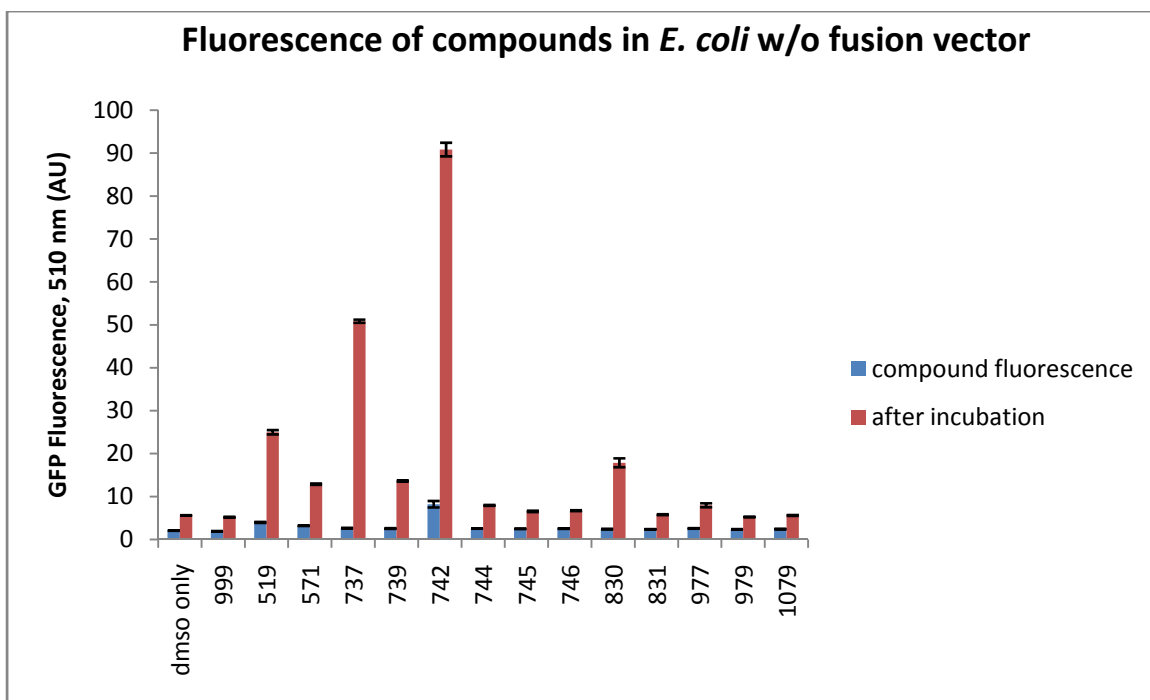


**Figure 2.14.** Compound fluorescence in LB and compound fluorescence in *E. coli* without fusion plasmid vector after incubation. Fluorescence of compounds in LB media is shown in blue, and the compound and *E. coli* fluorescence after 5 hour incubation at 37°C is shown in red. Final compound concentration is 100 uM. Values are averages of three wells, with standard error reported.

## 2.3. Discussion

Screens to identify AB aggregation inhibitors are necessary in order to select compounds with the potential to become Alzheimer's therapeutics. The AB-GFP fusion assay was previously shown to be successful at identifying aggregation inhibitors in a pilot library. The next step was to screen larger compound libraries. I screened a 65,000 compound library with the AB-GFP fusion screen. Data analysis of the fusion screen narrowed the potential compounds, and after revalidation of the selected compounds,

compound 737 was selected for additional characterization. Subsequent test indicated that the compound 737 was able to reduce AB aggregation and rescue AB induced toxicity.

Based on both results from aggregation and toxicity studies, compound 737 was an effective AB aggregation inhibitor, and used to identify compound analogs for a structure activity study (SAR). 13 analogs were selected and tested for their ability to reduce aggregation and rescue toxicity. Most of the analogs were able to reduce aggregation, with some compounds being more effective. The main trend identified was that the size of the R<sub>1</sub> and R<sub>2</sub> groups were linked to the aggregation inhibition ability. Smaller sized R<sub>1</sub> substituents, such as ~H and ~CH<sub>2</sub>-CH<sub>3</sub> were better than ~Ph and ~CH<sub>2</sub>-Ph at reducing AB aggregation. Of note, the most effective compounds at reducing aggregation did not have the ~CH<sub>2</sub>-Ph group attached at position R<sub>1</sub>. This is interesting as compounds that can disturb aromatic-aromatic interactions have been suggested as a mechanism in how compounds inhibit amyloid aggregation (15). This is investigated further in Chapter 4 of this thesis. These results can also be explained by compound solubility in the final assay solution. The compounds with the smaller R<sub>1</sub> and R<sub>2</sub> substituents will be more soluble than the compounds with a ~CH<sub>2</sub>-Ph group. An increased solubility of a compound provides more compound to bind to AB.

The toxicity studies indicated that the analogs were able to rescue AB42 induced toxicity. Only one compound, 744, had a viability score higher than compound 737. The difference was a *para* fluoro substituted phenyl ring at position R<sub>1</sub>. Changing the halogen from fluoro to chloro or bromo significantly decreased PC12 cell viability, suggesting that the overall size of the R<sub>1</sub> group is critical, or that the fluorine is making a

critical hydrogen bond. In contrast to the trend found in aggregation inhibition, the phenyl substituent on R<sub>1</sub> significantly increases viability. This can be shown when comparing compound 737 to 831. Toxicity studies also show that when the R<sub>2</sub> substituent is an H, the compound is toxic to PC12 cells, regardless of what substituent is at R<sub>1</sub>. Finally, at position R<sub>1</sub>, methyl substituents are better than aromatic substituents.

### **2.3.1. Potential rescue mechanism of 737 and analogs**

The thioflavin T data indicate that less aggregation occurs when AB42 is treated with 737 and analogs. In the toxicity study, 737 and analogs were also able to rescue AB induced toxicity. The toxic species has been suggested to be an oligomer and recently, dimers and dodecamers have been identified as the toxic species (*16, 17*). Because the exact toxic species is unknown, it is extremely difficult to determine where the compound interferes with the normal aggregation process. Thioflavin studies indicate that less aggregation is occurring, and that the compound can rescue AB induced toxicity. This suggests that the compounds are preventing the formation of the toxic species.

### **2.3.2. Why was 737 selected by the AB-GFP fusion screen?**

False positives from high throughput screening are not desirable but expected. Therefore, screening processes have to be in place to minimize false positives. Since the fusion screen uses fluorescence to determine compound effectiveness, compounds that are active at the emission wavelengths of GFP will be selected as hits. In addition, false positives can arise from mutations in the AB-GFP fusion sequence that make the AB portion of the fusion more soluble as demonstrated by the GM6-fusion protein.

However, this false positive scenario is an unlikely to happen because of plasmid sequencing, and that all the wells would be fluorescent, as the mutation would be in every well.

In the pilot study of the AB-GFP fusion assay with the triazine library, mechanisms for generating false positive hits were not discussed. However, during assay development to move the screen from 96 to 384 well plates, I identified that several compounds were fluorescently active at the GFP wavelength. To account for these fluorescently active compounds, a step was added to pre-screen the compounds after they were dispensed into the plates. This pre-read data was used in to identify and remove compounds that were inherently fluorescent. However, this pre-screen step does not account for the possibility of *E. coli* processing or membrane interactions altering the fluorescence of the compounds. This was exactly the reason why compound 737 was selected as a false hit from the fusion screen. I did not take into account that *E. coli* would process a non-fluorescent compound into one that was fluorescent at the screening wavelength.

For this AB-GFP aggregation screen, false positives from compound fluorescence as well as *E. coli* processing and membrane interaction will always be an issue. From this study and from the small molecule microarray screening results (Chapter 3) many compounds fluoresce at the green wavelength. Because of this, a shift in the color of the fluorescent fusion protein may reduce the number of false positives. There are a variety of different fluorescent proteins, so a change to a wavelength that has less compound activity would reduce the number of fluorescently active compounds that have to be eliminated (18). The shift to red to a RFP (mCherry; monomeric) is likely to reduce the

number of fluorescently active compounds, because not as many small molecule compounds fluoresce at the red wavelength (personal observation, Chapter 3). For example, if compound 737 was screened in an AB-RFP fusion, compound 737 would still be processed into an active green compound, but it would have been scanned for aggregation inhibition at the red wavelength.

While considering fluorescent protein replacements for the fusion system, other characteristics have to be considered. The folding time of the potential fluorescent protein replacement is a critical component, because a very rapidly folding fluorescent protein may not report the aggregation inhibition of the compound effectively (19). The AB-GFP fusion currently has a 5 hour incubation time, which was sufficient to identify aggregation inhibitors (9). Other fluorescent proteins have a range of folding times: mCherry has a folding time of 15 minutes, while the orange variant, mOrange, has a folding time of 2.5 hours (18). Another important consideration is the brightness, or quantum efficiency of the fluorescent protein replacement. A higher quantum efficiency is a critical factor because fluorescence of the fusion protein is measured, and higher quantum efficiency would provide better sensitivity. mCherry has a quantum efficiency of 0.22, while mOrange has a significantly higher quantum efficiency at 0.69 (18), which is also slightly higher than the 0.60 quantum efficiency of the GFP currently used in the fusion system.

In addition to changing the fluorescence wavelength to reduce false positives, the AB-GFP screen can be moved to a cell free system for transcription and translation, where the cell membranes are eliminated by containers having necessary components for

protein expression. This cell free system would virtually eliminate any processing or membrane interaction effects.

Despite the fact that compound 737 was found fortuitously in the AB-GFP fusion screen through an artifact, it is an effective inhibitor of AB aggregation, and has the ability to rescue AB induced toxicity. Analogs based on the 737 scaffold were also able to inhibit aggregation and rescue AB induced toxicity. The next step is to determine the effectiveness in animal models of Alzheimer's disease – fruit flies, nematodes, and eventually mice.

## **2.4. Summary**

I screened 65,000 compounds with the AB-GFP fusion to identify compounds that could inhibit AB aggregation inhibition and identified compound 737 as a potential inhibitor. Aggregation and toxicity experiments indicated that it was a good compound and scaffold for identifying other inhibitors of AB aggregation. SAR studies of analogs identified trends for aggregation inhibition and toxicity rescue. However, compound 737 was a false positive result from the AB-GFP screen, due to *E. coli* processing or membrane interaction into a fluorescently active compound. Solutions in order to prevent future false positives include prescreening compounds at the observation wavelength, in addition to shifting fluorescent protein from the green wavelength to one where compounds are not fluorescent, such as red or orange, as well as moving the AB GFP fusion screen to a cell free system.

## 2.5. Materials and methods

**AB GFP Fusion assay:** IPTG (1 mM final concentration) was added to LB media and 20 uL of induced media was dispensed into each well of a 384 well plates (Corning, black with clear and flat bottom) using a Multidrop Combi microplate dispenser (Thermo). 300 nL of compounds was transferred from the stock compound library plates by the CyBi-Well 96- and 384- Channel Simultaneous Pipettor (Cybio), with the 384 tip/300nL dispensing pin head installed. All stock compounds were dissolved in DMSO. Each library drug plate was screened in duplicate. A DMSO stock drug plate was included as the no compound control. After drug addition, screening plates were read at the GFP wavelength (485 nm excitation, 510 nm emission) on an EnVision plate reader (Perkin Elmer).

*E. coli* BL21 containing the AB42 GFP or GM6 fusion plasmid were grown overnight at 37°C, at 250 RPM. A larger volume (depending on the number of plates to be screened) of LB was inoculated and grown at 37°C at 250 RPM to an OD<sub>600</sub> of 0.5. After pre screening of drug compounds, 20 uL of AB42-GFP *E. coli* was added using a Multidrop Combi microplate dispenser (Thermo) to each compound and DMSO control well for a final volume of 40 uL. Final compound concentration was approximately 75 uM. 20 uL of GM6-GFP *E. coli* was added to each positive control well. Plates were incubated in a warm room at 37°C for 5 hours, without shaking or plate covers. After incubation, screening plates were read at the GFP wavelength (485 nm excitation, 510 nm emission) on an EnVision plate reader (Perkin Elmer).

**Compounds:** Compound 737 and analogs were purchased from ChemDiv (San Diego, CA).

**Peptide purification.** Crude peptides from Fmoc synthesis were purchased from the Keck Institute at Yale University, and purified using a C4 reverse phase column. Solvent gradients were run at 65°C using solvent A (95% water, 5% acetonitrile, 0.1% TFA); and Solvent B (50% acetonitrile, 50% water, 0.1% TFA).

**Thioflavin T Assay.** 0.5 mg of AB peptide was dissolved in 300 uL DMSO and diluted with 5 mL of 8 mM NaOH for a final peptide concentration of 20 uM. Concentrated PBS buffer was added to the solution to adjust the pH (final concentration: 50 mM NaH<sub>2</sub>PO<sub>4</sub>, 100 mM NaCl, pH 7.10 – 7.20). Samples were incubated with and without compound at 37°C under quiescent conditions for the indicated time period. At various timepoints, 100 uL aliquot of peptide sample was mixed with 100 uL of a solution of thioflavin T (7 uM ThT, 50 mM glycerol-NaOH, pH 7.10) and fluorescence was measured at 483 nm (excitation at 450 nm) on a Varioskan plate reader (Thermo Scientific).

**Toxicity experiments:** Rat pheochromocytoma (PC12) cells (ATCC, Rockville, MD) were grown on collagen coated (BD Biosciences), tissue treated petrie dishes (Falcon 3003) in complete growth media (82.5% F12K 15% horse serum, 2.5% fetal bovine serum, ATCC Rockville, MD) in a humidified incubator at 37°C and 5% CO<sub>2</sub> (Herra, Thermo Scientific). Cells were grown to confluence, and harvested by spraying through an 18.5 gauge needle, resuspended in fresh media and plated onto tissue treated flat bottom 96 well plates (Costar) at a density of 10, 000 cells per well (100 uL/well). Plates were incubated at 37°C for 24 hours to allow cells to attach. Lyophilized AB42 (1 mg) was dissolved in 100 uL of cell culture grade DMSO (ATCC), sonicated and diluted with 1.0 mL of sterile 1 x PBS buffer (Invitrogen) for a final stock concentration of 200

uM. 10 uL of the AB42 peptide solution was added to each well (100 uL) for a final peptide concentration of 20 uM. 1 uL of 10 mM inhibitor compound dissolved in DMSO was added to each well (in triplicate) for a final drug concentration of 100 uM. Plates with AB peptide and inhibitor compound were incubated for 24 hours. Cell viability was determined with the MTT assay (Roche,(20, 21)). Briefly, 10 uL of MTT was added to each well. After incubation for 4 hr at 37°C, 100 uL of solubilization solution (10% SDS in 0.01 M HCl) was added and incubated overnight at 37°C. The absorbance at 570 nm was measured using a Varioskan microplate reader (Thermo Scientific), with background subtraction at 670 nm. Statistical significance was calculated with the two tailed (uncorrelated) TTEST function in Microsoft Excel.

## 2.6. References

1. [www.alz.org/AboutAD/statistics.asp](http://www.alz.org/AboutAD/statistics.asp).
2. Hardy, J. (2006) Alzheimer's disease: The amyloid cascade hypothesis: An update and reappraisal, *J Alzheimers Dis* 9, 151-153.
3. Hardy, J., and Selkoe, D. J. (2002) The amyloid hypothesis of Alzheimer's disease: progress and problems on the road to therapeutics, *Science* 297, 353-356.
4. Hardy, J. A., and Higgins, G. A. (1992) Alzheimer's disease: the amyloid cascade hypothesis, *Science* 256, 184-185.
5. Cohen, F. E., and Kelly, J. W. (2003) Therapeutic approaches to protein-misfolding diseases, *Nature* 426, 905-909.
6. Selkoe, D. J. (2001) Alzheimer's Disease: Genes, Proteins, and Therapy, *Physiol. Rev.* 81, 741-766.
7. Spooner, E. T., Desai, R. V., Mori, C., Leverone, J. F., and Lemere, C. A. (2002) The generation and characterization of potentially therapeutic amyloid beta antibodies in mice: differences according to strain and immunization protocol, *Vaccine* 21, 290-297.
8. Holmes, C., Boche, D., Wilkinson, D., Yadegarfar, G., Hopkins, V., Bayer, A., Jones, R. W., Bullock, R., Love, S., Neal, J. W., Zotova, E., and Nicoll, J. A. R. (2008) Long-term effects of Amyloid beta 42 immunisation in Alzheimer's disease: follow-up of a randomised, placebo-controlled phase I trial, *The Lancet* 372, 216-223.
9. Kim, W., Kim, Y., Min, J., Kim, D., Chang, Y.-T., and Hecht, M. (2006) A High-Throughput Screen for Compounds That Inhibit Aggregation of the Alzheimer's Peptide, *ACS Chem. Biol.* 1, 461-469.
10. Waldo, G. S., Standish, B. M., Berendzen, J., and Terwilliger, T. C. (1999) Rapid protein-folding assay using green fluorescent protein, *Nat Biotechnol* 17, 691-695.
11. Wurth, C., Guimard, N. K., and Hecht, M. H. (2002) Mutations that reduce aggregation of the Alzheimer's amyloid beta 42 peptide: an unbiased search for the sequence determinants of Abeta amyloidogenesis, *J Mol Biol* 319, 1279-1290.
12. Seiler, K. P., George, G. A., Happ, M. P., Bodycombe, N. E., Carrinski, H. A., Norton, S., Brudz, S., Sullivan, J. P., Muhlich, J., Serrano, M., Ferraiolo, P., Tolliday, N. J., Schreiber, S. L., and Clemons, P. A. (2008) ChemBank: a small-molecule screening and cheminformatics resource database, *Nucl. Acids Res.* 36, D351-359.
13. Vegas, A. J., Fuller, J. H., and Koehler, A. N. (2008) Small-molecule microarrays as tools in ligand discovery, *Chem Soc Rev* 37, 1385-1394.
14. LeVine, I., H. (1995) Thioflavine T Interaction with Amyloid Beta-Sheet Structures., *Amyloid: The International Journal of Experimental and Clinical Investigation* 2, 1-6.
15. Gazit, E. (2002) A possible role for pi-stacking in the self-assembly of amyloid fibrils, *FAESB J* 16, 77-83.
16. Lesne, S., Koh, M. T., Kotilinek, L., Kaye, R., Glabe, C. G., Yang, A., Gallagher, M., and Ashe, K. H. (2006) A specific amyloid-beta protein assembly in the brain impairs memory, *Nature* 440, 352-357.

17. Shankar, G. M., Li, S., Mehta, T. H., Garcia-Munoz, A., Shepardson, N. E., Smith, I., Brett, F. M., Farrell, M. A., Rowan, M. J., Lemere, C. A., Regan, C. M., Walsh, D. M., Sabatini, B. L., and Selkoe, D. J. (2008) Amyloid-beta protein dimers isolated directly from Alzheimer's brains impair synaptic plasticity and memory, *Nat Med advanced online publication*.
18. Shaner, N. C., Campbell, R. E., Steinbach, P. A., Giepmans, B. N. G., Palmer, A. E., and Tsien, R. Y. (2004) Improved monomeric red, orange and yellow fluorescent proteins derived from *Discosoma* sp. red fluorescent protein, *Nat Biotech* 22, 1567-1572.
19. Kim, W., and Hecht, M. H. (2005) Sequence determinants of enhanced amyloidogenicity of Alzheimer Amyloid beta 42 peptide relative to Amyloid beta 40, *J Biol Chem* 280, 35069-35076.
20. Vistica, D. T., Skehan, P., Scudiero, D., Monks, A., Pittman, A., and Boyd, M. R. (1991) Tetrazolium-based assays for cellular viability: a critical examination of selected parameters affecting formazan production, *Cancer Res* 51, 2515-2520.
21. Maehara, Y., Anai, H., Tamada, R., and Sugimachi, K. (1987) The ATP assay is more sensitive than the succinate dehydrogenase inhibition test for predicting cell viability, *European Journal of Cancer and Clinical Oncology* 23, 273-276.

## **Chapter 3. Amyloid beta binding as a primary screen for identifying aggregation inhibitors**

### **3.1. Introduction**

Aberrant protein aggregation is responsible for many human diseases (1, 2). The location of the aggregated proteins determines the disease symptoms. For example, protein aggregation in the brain results in neurological diseases; examples include Parkinson's and Alzheimer's disease (AD). In AD, the peptide responsible for the aggregation is 40 – 42 residues long, named amyloid beta (AB). After production, monomeric AB self-aggregates to eventually form the characteristic plaques that are found in specific memory centers of the brain, leading to the physical symptoms of memory loss, dementia, and eventual death.

The mechanism leading to Alzheimer's disease can be explained by the updated amyloid cascade theory, which suggests that a neurotoxic oligomer forms as AB aggregates from monomer to fibril (3, 4). The nature of the toxic species is still unknown, but studies have indicated that the presence of soluble AB oligomers is better correlated with dementia than plaque load (5-10). Recently, Lesne *et al* identified that a dodecamer oligomer form of AB42 was toxic in mice (11) and Shankar *et al* identified that soluble dimers isolated from confirmed AD patients were disruptive to a learned task when injected in rat brains (12).

Current drugs used to treat Alzheimer's disease only treat the symptoms of memory loss, and not the root cause of the disease. Currently, there are no FDA

approved drugs that interfere with the aggregation pathway to prevent the toxic species in Alzheimer's disease. Therefore, identifying small molecule aggregation inhibitors is important for the development of AD therapeutics.

Aggregation inhibitors must first bind to AB. Compounds that bind to AB are critical because binding is a necessary first step for any interaction, inhibition or enzymatic action. If these compounds can bind to the early stages of AB aggregation, they can potentially inhibit further aggregation into toxic species. These compounds would be useful to slow down disease progression, and provide additional insight into the toxic species. Currently, there are no high throughput screens to identify compounds that bind to monomeric or low molecular weight AB oligomers.

I wanted to identify compounds that bound to monomeric or early oligomers of AB to see if these compounds could be used as inhibitors or scaffolds for leads. To do this, I probed small molecule microarrays (SMMs) with fluorescently labeled AB. SMMs have libraries of diverse small compounds covalently attached to the surface of a glass slide. Compounds that bind to AB are identified by the fluorescent tag, as shown in Figure 3.1.

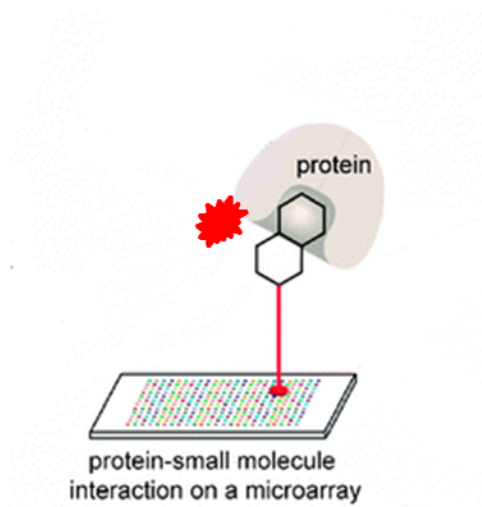


**Figure 3.1.** Cartoon representation of a SMM binding screen. Compounds are covalently attached to the slide surface and are probed by incubating with fluorescently labeled peptide (or protein). Compounds that bind are identified by the fluorescent tag after several wash steps. Figure modified from Vegas *et al* (13).

SMMs are high throughput parallel binding assays which have been effective at identifying several specific protein-ligand interactions, including transcriptional regulators uretupamine A and haptamine A, ligands to human IgG, calmodulin ligands, and histone deacetylase inhibitors (14-20). This technique also does not require knowledge of the exact protein structure or binding pocket information, which is also critical in the case of AB, since the exact structure of AB is not known, and a traditional enzymatic binding pocket does not exist.

In this chapter, I will describe a screen to identify compounds that bind to monomeric or low molecular weight AB oligomers with SMMs. The screen was successful at identifying compounds that bound to monomeric or LMW AB, and several compounds were able to prevent AB induced toxicity in PC12 cells. One compound that

rescued AB induced toxicity was selected for structure activity studies to identify motifs necessary for rescue.

## **3.2. Results**

### **3.2.1. Developing conditions for the SMM screen**

Because AB aggregates quickly in solution, I needed to identify conditions where the majority of the peptide would exist as monomer or low molecular weight oligomers. It is known that AB42 aggregates faster than AB40 (21), with the critical concentration of AB42 reported at 25  $\mu$ M (22), and AB40 at 32  $\mu$ M (23). As shown in the SDS gel in Figure 3.2, fluorescently labeled AB40 has less aggregation than fluorescently labeled AB42. At 9.35  $\mu$ M fluorescently labeled AB42 (lane 5) shows monomer (4 kD), dimer (8 kD), trimer (12 kD) and tetramer (16kD) while AB40 shows monomer (4kD) and dimer (8kD). 185 nM peptide concentrations were initially tested, because it was the recommended concentration for SMM screening (24). 185 nM fluorescently labeled AB42 (lanes 6 and 7) show a faint monomer band, while fluorescently labeled AB40 is not detected by staining.

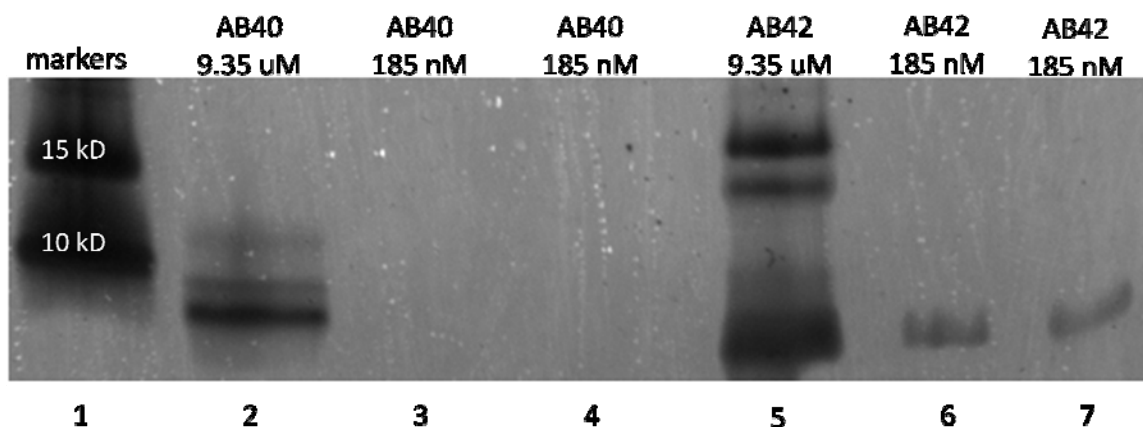


**Figure 3.2.** SDS gel image of N-terminally labeled Anaspec Hilyte 647 fluorescent-AB40 (lanes 2, 3 and 4) and N-terminally labeled Anaspec Hilyte 488 fluorescent-AB42 (lanes 5, 6 and 7) at listed concentrations. Both AB40 and AB42 have a size of 4kD. SDS 8-25% gel with silver staining.

In order to show that labeled AB40 did not aggregate during the SMM incubation times, SDS gels of labeled AB40 were run at concentrations higher than 185 nM and longer incubation times (60 minutes) than those conditions used for the SMM experiments (30 minutes) as shown in Figure 3.3. Fluorescently labeled AB40 at micromolar concentrations (lanes 2 – 5) show monomer and dimer bands, while nanomolar concentrations (lanes 6 – 9) are not detected by silver staining.

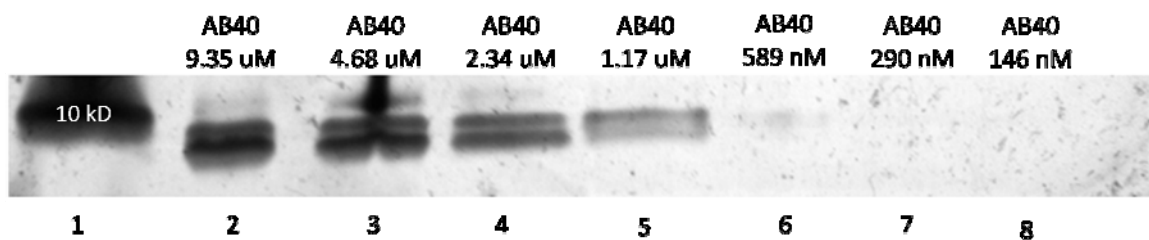


**Figure 3.3.** SDS gel image of N-terminally labeled Anaspec 647 fluorescent-AB40 after 60 minute room temperature incubation at labeled concentrations. SDS gel with silver staining.

These two gels show that the labeled AB40 exists as an equilibrium between monomer and dimer forms at uM concentrations. Labeled AB40 was chosen for the SMM experiment because it aggregates less than AB42 and the core residues of AB40 are the same as AB42, so if a compound binds to AB40, it is likely to bind to AB42. 185 nM concentration was used as it is well below the critical concentration, and is presumed to be monomeric.

### 3.2.2. SMM results: Identifying compound binding to AB40

Each SMM slide has 10,800 spots for compounds, DMSO controls, or grid alignment spots. Two different SMM slide sets, natural products compounds (NPC) and diversity oriented synthesis compounds (DIV) were screened in triplicate, for a total of 17,905 compounds.

The DIV SMM slide is shown in Figure 3.4. Red (632 nm) colored spots indicate compounds that bind to fluorescently labeled AB40, while green (532 nm) colored spots are control spots used for grid alignment, or compounds that were excited and emit at the same wavelength as that used for grid alignment.

Fluorescent images as shown in Figure 3.4 were collected for each replica slide using standard microarray scanner software. Fluorescence intensity scores of the three replica slides were background subtracted and converted to a Z-score, or standard score. A Z-score was calculated for each array feature using a standard analysis program for SMM data developed by Seiler *et al* (25). The Z-score represents how many standard deviations a spot (or observation) is above or below the mean value (13, 25, 26). Since the screen was accomplished in triplicate, the replicates were combined to produce a composite Z-score for each compound.

The composite Z-score for compounds and controls were plotted onto a histogram, as shown in Figure 3.5. The resulting shape of the compound histogram (in blue) is normal with a small shoulder on the right and centered on zero. The DMSO control histogram (in red) was also normal, and centered on zero.

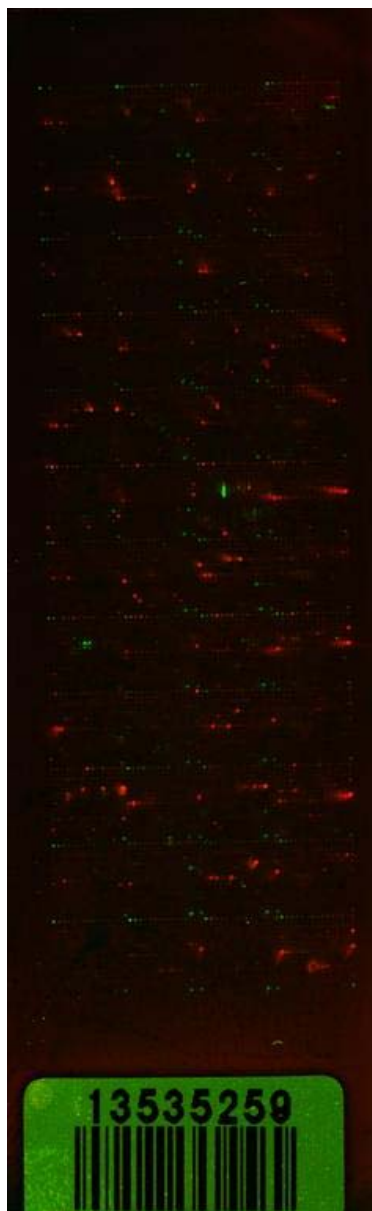


**Figure 3.4.** An enlarged view of the DIV compound microarray slide after scanning. Each slide is an array of 48 15 x 15 grids, for a total of 10,800 compound locations. Fluorescent-AB40 was passed over the microarray slide and the resulting slide was washed and scanned for fluorescence. Red color indicates binding of AB to compound, green color represents grid alignment spots. Actual slide dimensions are 1 inch x 3 inch.

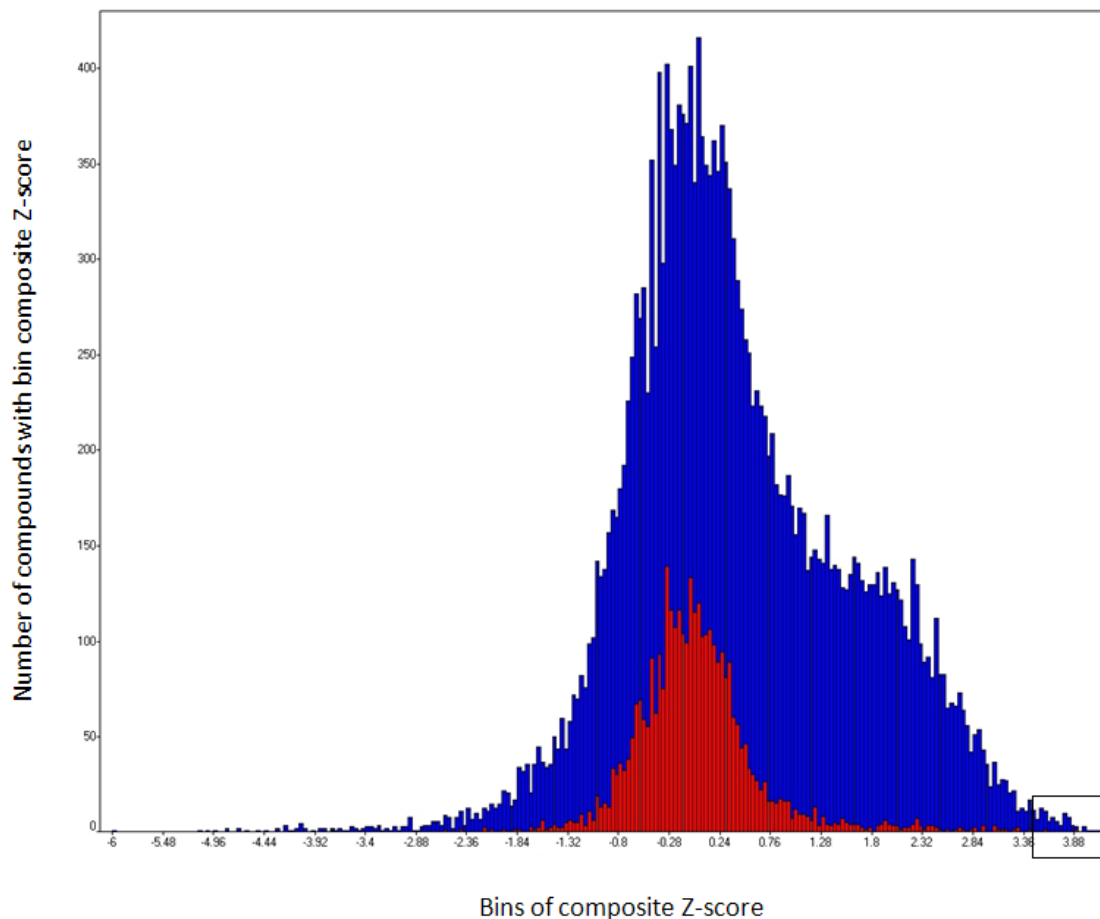


**Figure 3.5.** Histogram plot of compound (blue) and DMSO control (red) composite Z-scores from DIV and NPC slides. 254 bins.

Since the shape of the histogram is normal, standard values were used (99.73% of all the distribution lies within 3 standard deviations) for statistical calculations.

Compounds that had a composite Z, or standard deviation, of 3.4 or greater were identified as hits in the screen (compounds that bind to AB), as highlighted by the square on Figure 3.5, were selected for additional testing. A total of 79 compounds were selected for toxicity tests.

D1 was a compounds identified by the SMM screen that bound to AB40. As shown in Figure 3.6, D1 has a bright and uniform red fluorescence, in contrast to the six DMSO control wells. This clearly indicates that labeled AB40 binds to D1, even after the protocol wash steps. The six (6) DMSO control wells do not show any red fluorescence, and do not bind to AB40. Figure 3.7 shows the expanded scans of the D1 row (total of 15 compounds) from each NPC replica slide. The three scans indicate that the binding of AB40 to D1 is consistent and repeatable. These data illustrate that the AB40-SMM system can reliably and consistently identify compound that bind to monomeric or low molecular weight oligomers of AB40.

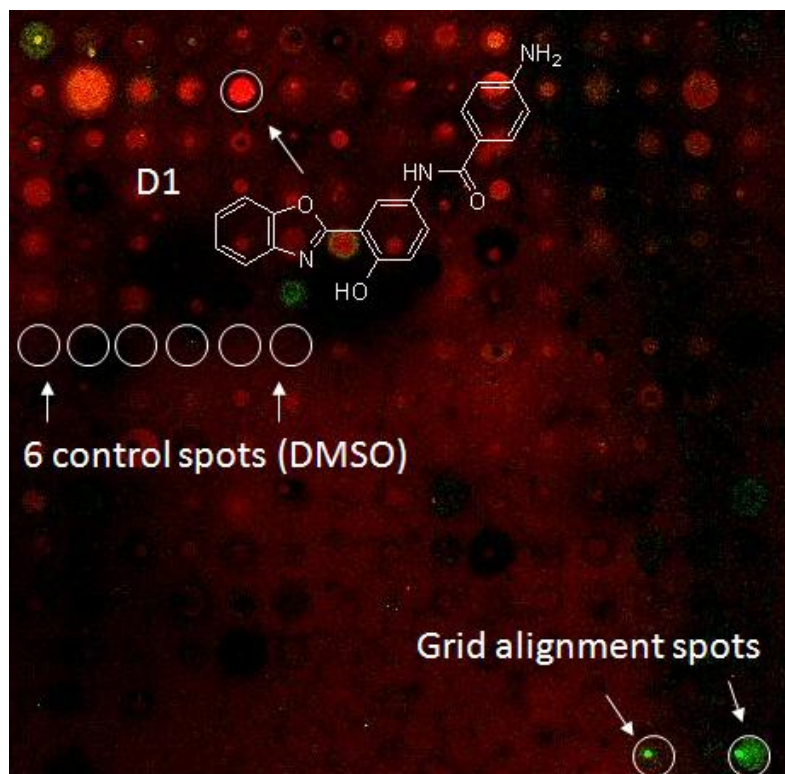


**Figure 3.6.** An expanded view of 225 compound spots on the NPC small molecule microarray. The spot corresponding to D1, DMSO controls, and grid alignment spots are shown.

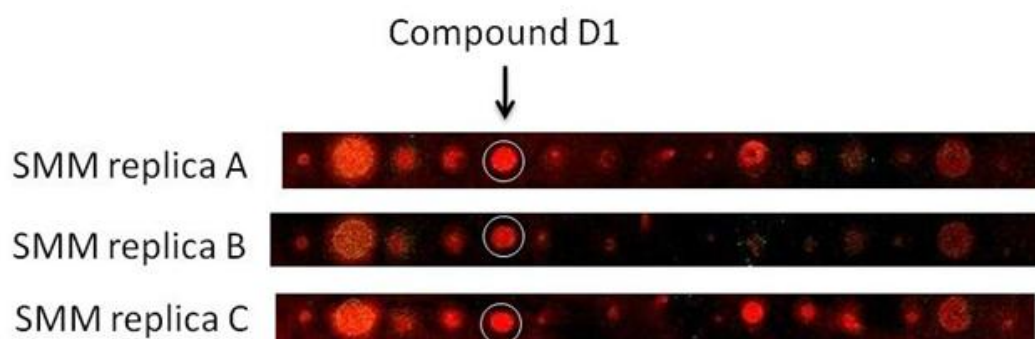


**Figure 3.7.** An expanded view of 15 compound spots on each NPC small molecule microarray replica slide. The Compound D1 spot is circled.

### 3.2.3. Toxicity experiments of hits identified by SMM

After data analysis of the SMM screening results, 79 compounds were selected for toxicity tests. These compounds were tested for their ability to rescue AB42 induced toxicity in a cultured neuronal cell line from rat adrenal medulla cells, or PC12 cells. The AB42 peptide was used for toxicity studies as it is the principal component found in AD plaques.

The toxicity assay is based on the reduction of the yellow tetrazolium salt, MTT, (3-(4,5-dimethylthiazol-2yl)-2,5-diphenyltetrazolium bromide) to the purple formazan crystals by mitochondria. Reduction of MTT occurs when the mitochondrial reductase enzymes are active, and can be used to measure the viability of cells. The formazan crystals are solublized, and the absorbance is measured photometrically.

Briefly, PC12 cells are grown and dispensed into tissue treated 96 well plates. AB42 and compounds are added to the PC12 cells and incubated overnight. After the overnight incubation, MTT is added to the wells and incubated for an additional 4 hours. The formazan crystals then are solublized overnight, and absorbance is quantified photometrically with a plate reader. Data is normalized to the 100% viable control wells of untreated PC12 cells,

Initial toxicity tests of the 79 compounds selected by the SMM assay identified several compounds that rescued AB42 induced toxicity. Figure 3.8 shows the results of the initial toxicity test of compounds able to rescue viability to 80%. PC12 cells incubated with AB42 have a viability of 69%. As shown in Table 3.1, three compounds were able to rescue AB toxicity above 90%, with the AB42 treated control cells at 69%.

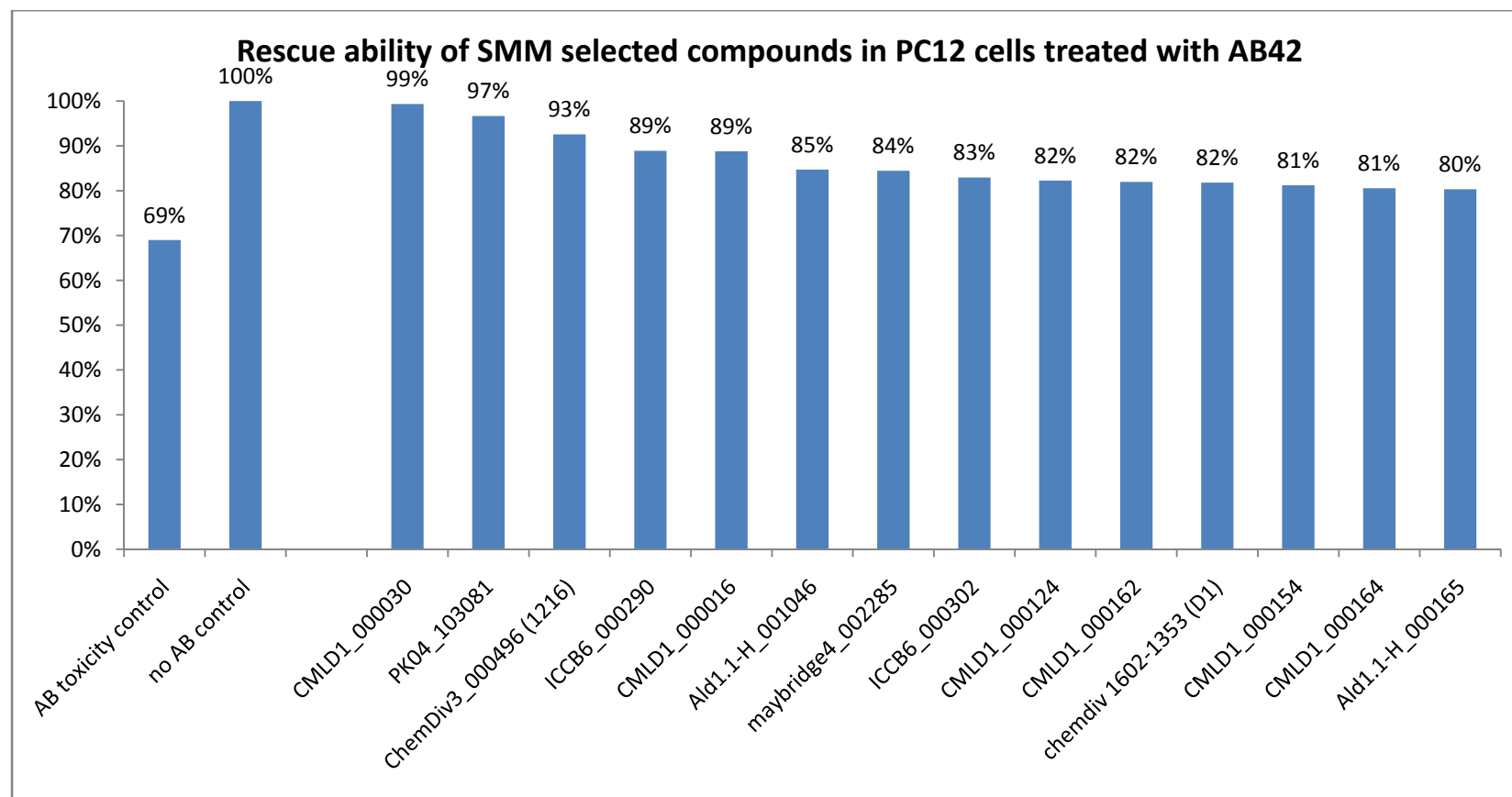


**Figure 3.8.** SMM selected compound initial toxicity study. Top 15 viability scores of compounds shown. AB42 concentration of 20 uM. Single measurement.

**Table 3.1.** Ability of SMM compounds to rescue AB42 induced toxicity in PC12 cells

AB42 treated PC12 cells had a viability of 69%.

viability	number of compounds
90 - 100	3
80 - 90	12
70 - 80	29
60 - 70	24
50 - 60	8
40 - 50	1
0 - 10	2

Compound D1 binds to AB40, (Figure 3.6), and rescues AB42 induced toxicity (Figure 3.8). Untreated PC12 cells with AB42 had a viability of 69%. D1 treated PC12 cells with AB increased viability to 82%. Based on these data, and because compound D1 was commercially available, it was selected for additional characterization.

### **3.2.4. Biophysical characterization of D1**

#### **3.2.4.1. Structure**

The structure of compound D1 is shown in Figure 3.9. It is an aromatic compound, flat, and has several locations for hydrogen bonding, which are consistent with other Alzheimer's and amyloid aggregation inhibitors. D1 shares some structural similarities with thioflavin T, a dye used to detect amyloid fibrils. Both compounds share a central phenyl ring, with either a benzothiazole or benzoxazol substituent attached.

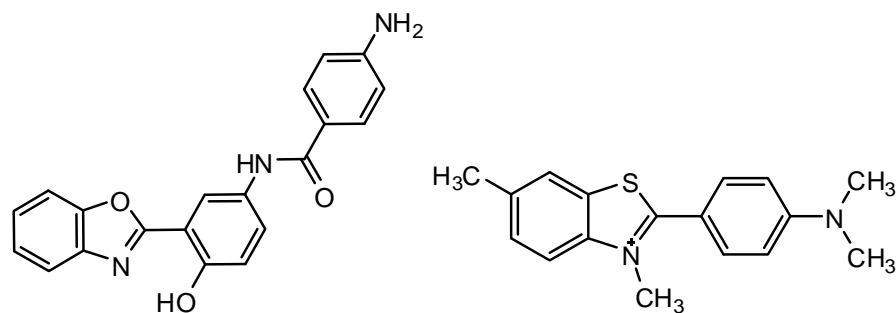


**Figure 3.9.** Structure of D1 (left) and thioflavin T (right)

#### 3.2.4.2. Toxicity rescue by D1

The initial test indicated that D1 was able to rescue AB42 induced toxicity (Figure 3.8). Subsequent toxicity studies show that D1 is effective at rescuing AB42 induced toxicity at several concentrations. PC12 cells incubated with AB42 without D1 had a viability of 37% (Figure 3.10). D1 concentrations of less than 6  $\mu$ M were not effective at rescue. However, D1 was statistically significant at increasing PC12 viability at concentrations above 6  $\mu$ M. From 6.25  $\mu$ M to 50  $\mu$ M, there is a dose dependence increase in PC12 viability. The highest PC12 cell viability of 75% occurred with a D1 concentration of 50  $\mu$ M.

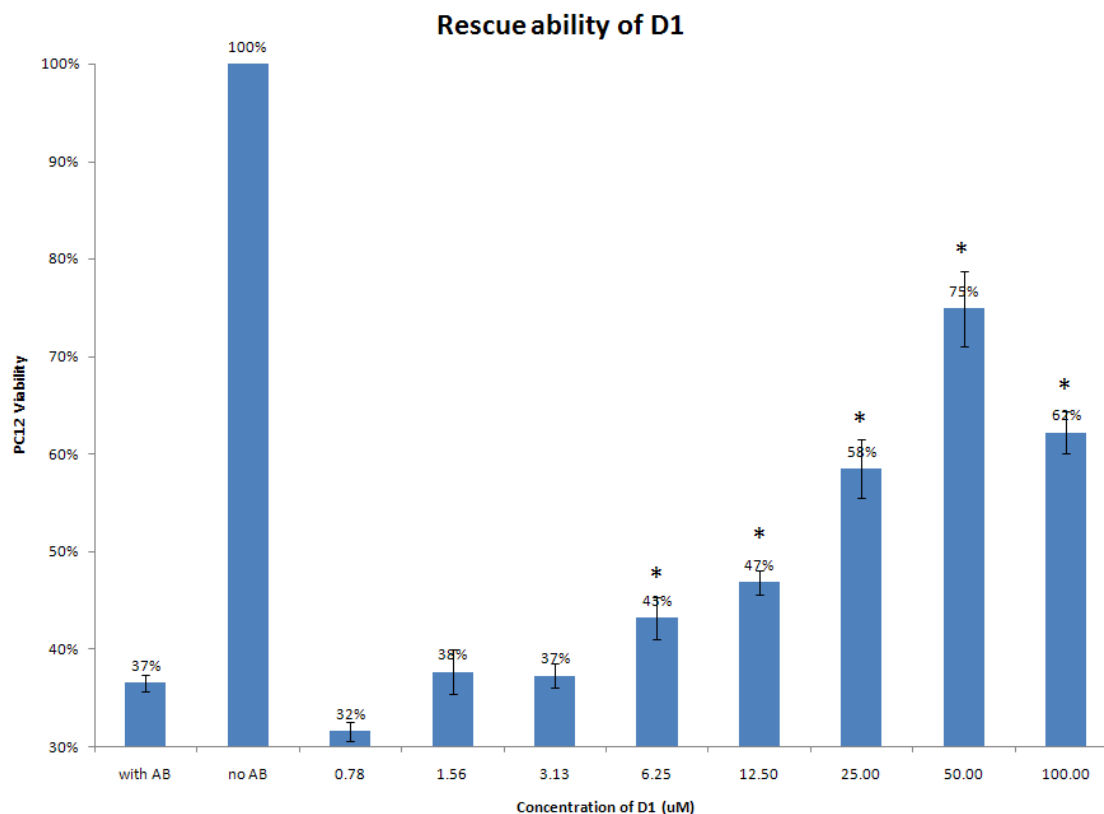


**Figure 3.10.** Ability of D1 to rescue AB42 induced toxicity in PC12 cells. AB42 was used at a concentration of 20 uM, with varying amounts of D1. Values reported are the average viability scores of three wells with standard error reported. Cells were incubated for 24 hours with AB42 and D1. (\*) An asterisk indicates statistical significance as determined the two tailed Student's T-test ( $p < 0.05$ ).

### 3.2.4.3. Toxicity of D1

PC12 cells treated with D1 only show some concentration dependent toxicity, as shown in Figure 3.11. Low concentrations (0.78 and 1.56 uM) were toxic, but higher concentrations (3.13, 6.25, and 12.5 uM) were not. The two highest concentrations tested

(50  $\mu$ M and 100  $\mu$ M) were both toxic to PC12 cells, with 100  $\mu$ M concentration being the most toxic.

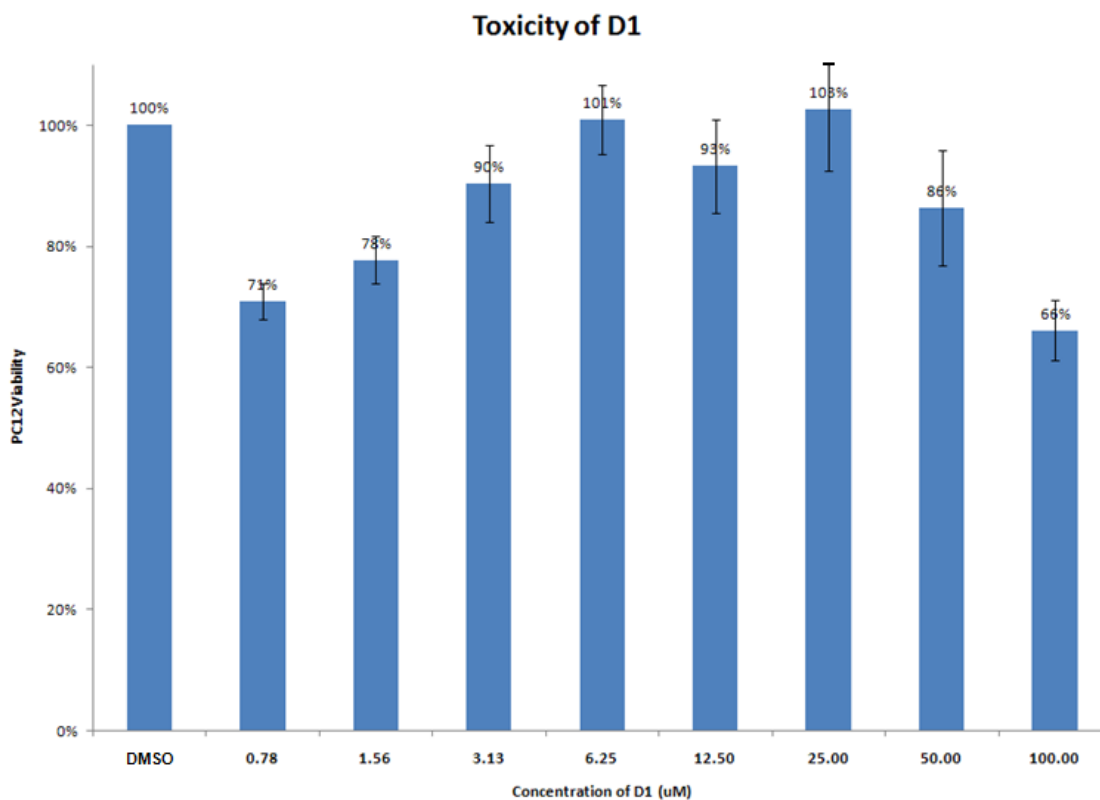
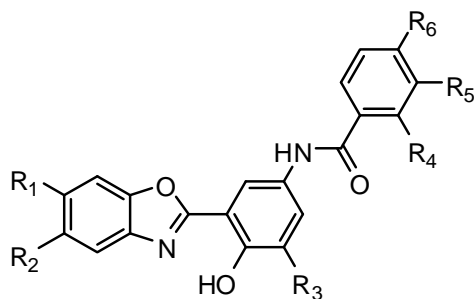


**Figure 3.11.** Toxicity study of D1 in PC12 cells. Varying concentrations of D1 were used. Values reported are the average viability scores of three wells with standard error reported. Cells were incubated for 24 hours with D1.

#### 3.4.4. Is the D1 scaffold good at rescue?

The SMM screen identified D1 as a compound that bound to AB40, and subsequent experiments with D1 indicate that it can rescue AB42 induced toxicity. Structure activity relationship studies of the D1 analogs can provide additional

information as to what motifs on D1 are effective at rescue. Compound analogs are based off of substitutions at six (6) positions as shown on the scaffold in Figure 3.12.



ChemDiv	R <sub>1</sub>	R <sub>2</sub>	R <sub>3</sub>	R <sub>4</sub>	R <sub>5</sub>	R <sub>6</sub>
1602-1352 (D1)	H	H	H	H	H	NH <sub>2</sub>
2026-3240	H	H	H	H	H	F
2026-3246	H	H	H	H	H	Br
7761-0151	H	H	H	H	H	Cl
2026-3267	H	H	H	Cl	H	Cl
2026-3269	H	H	H	H	Cl	Cl
2026-3262	H	H	H	H	H	C(CH <sub>3</sub> )
2026-3255	H	H	H	H	H	O-CH <sub>3</sub>
2026-3258	H	H	H	H	H	NO <sub>2</sub>
1346-1290	H	H	H	H	H	C(=O)-O-CH <sub>3</sub>
2026-3395	H	CH <sub>3</sub>	H	H	H	O-CH <sub>3</sub>
2026-3407	H	CH <sub>3</sub>	H	Cl	H	Cl
2026-3380	H	CH <sub>3</sub>	H	H	H	F
2026-3383	H	CH <sub>3</sub>	H	H	H	Cl
2026-3392	H	CH <sub>3</sub>	H	H	H	CH <sub>3</sub>
2026-3431	H	CH <sub>2</sub> -CH <sub>3</sub>	H	H	H	O-CH <sub>2</sub> -CH <sub>3</sub>
2026-3989	CH <sub>3</sub>	CH <sub>3</sub>	H	H	H	I
2026-4002	CH <sub>3</sub>	CH <sub>3</sub>	H	H	H	O-CH <sub>3</sub>
2026-3981	CH <sub>3</sub>	CH <sub>3</sub>	H	H	H	F
2026-3984	CH <sub>3</sub>	CH <sub>3</sub>	H	H	H	Cl
8503-0076	H	H	CH <sub>3</sub>	H	H	F
8503-0073	H	H	CH <sub>3</sub>	H	H	O-CH <sub>3</sub>

**Figure 3.12.** D1 parent scaffold and analogs

Most D1 compound analogs show significant toxicity at 100 uM (Table 3.2 and Figure 3.13). Halogenation caused increased toxicity at position R<sub>6</sub>. The chloro, bromo, and iodo substitutions are very toxic, while the fluoro substitution seems to be less toxic (except for the case of compound 2026-3981, where the combination of two methyl substitutions and a fluorine substitution make the compound severely toxic).

The rescue ability of analogs at 100 uM are shown in, Table 3.2 and Figure 3.14. The three compounds that were statistically significant at rescue were: 2026-3258, 2026-3383, and 8503-0076. The analogs differ by the following: 2026-3258 has one change from D1: a NO<sub>2</sub> group at position R<sub>6</sub>; 2026-3383 has two changes: methyl at position R<sub>2</sub>, and a chlorine at R<sub>6</sub>; and 8502-0076 also has two changes: methyl at position R<sub>3</sub>, and a fluorine at position R<sub>6</sub>. There were no obvious trends identified to increase viability among the D1 analogs at 100 uM.

Rescue ability of the analogs improved at 50 uM, as shown in Table 3.2, and Figure 3.15. At 50 uM compound concentrations, 13 out of the 21 analogs were statistically significant at rescue. At 50 uM concentration, D1 treated cells had the highest ability to rescue, with 95% viability, with untreated AB PC12 cells having a viability of 47%. The three D1 analogs identified in the 100 uM concentration test were also identified as able to rescue at the 50 uM concentration. In addition, several compounds that were not significant at rescue at 100 uM concentration were able to significantly rescue the toxicity of AB42.

**Table 3.2.** Summary of D1 analog toxicity and rescue ability summary. Green indicate statistically significant rescue ability by compounds in both 50 and 100 uM concentrations

							100 uM	significance	50 uM	significance	100 uM
							20 uM AB42		20 uM AB42		No AB42
ChemDiv	R <sub>1</sub>	R <sub>2</sub>	R <sub>3</sub>	R <sub>4</sub>	R <sub>5</sub>	R <sub>6</sub>	PC12 viability w/ compound		PC12 viability w/ compound		Compound toxicity
1602-1352 (D1)	H	H	H	H	H	NH <sub>2</sub>	64	yes	95	yes	65
2026-3240	H	H	H	H	H	F	49	no	63	yes	64
2026-3246	H	H	H	H	H	Br	32	no	56	yes	30
7761-0151	H	H	H	H	H	Cl	30	no	50	no	26
2026-3267	H	H	H	Cl	H	Cl	24	no	43	no	25
2026-3269	H	H	H	H	Cl	Cl	22	no	38	no*	22
2026-3262	H	H	H	H	H	C(CH <sub>3</sub> ) <sub>3</sub>	38	no	61	yes	77
2026-3255	H	H	H	H	H	O-CH <sub>3</sub>	38	no	53	yes	38
2026-3258	H	H	H	H	H	NO <sub>2</sub>	51	yes	48	no	42
1346-1290	H	H	H	H	H	C(=O)-O-CH <sub>3</sub>	39	no	42	no	47
2026-3395	H	CH <sub>3</sub>	H	H	H	O-CH <sub>3</sub>	43	no	62	yes	48
2026-3407	H	CH <sub>3</sub>	H	Cl	H	Cl	49	no	62	yes	48
2026-3380	H	CH <sub>3</sub>	H	H	H	F	41	no	49	no	46
2026-3383	H	CH <sub>3</sub>	H	H	H	Cl	59	yes	63	yes	50
2026-3392	H	CH <sub>3</sub>	H	H	H	CH <sub>3</sub>	37	no	61	yes	33
2026-3431	H	CH <sub>2</sub> -CH <sub>3</sub>	H	H	H	O-CH <sub>2</sub> -CH <sub>3</sub>	44	no	66	yes	55
2026-3989	CH <sub>3</sub>	CH <sub>3</sub>	H	H	H	I	22	no	55	yes	22
2026-4002	CH <sub>3</sub>	CH <sub>3</sub>	H	H	H	O-CH <sub>3</sub>	48	no	69	yes	38
2026-3981	CH <sub>3</sub>	CH <sub>3</sub>	H	H	H	F	18	no	45	no	14
2026-3984	CH <sub>3</sub>	CH <sub>3</sub>	H	H	H	Cl	37	no	47	no	29
8503-0076	H	H	CH <sub>3</sub>	H	H	F	68	yes	58	yes	50
8503-0073	H	H	CH <sub>3</sub>	H	H	O-CH <sub>3</sub>	47	no	55	yes	39
PC12 w/AB							43		47		38

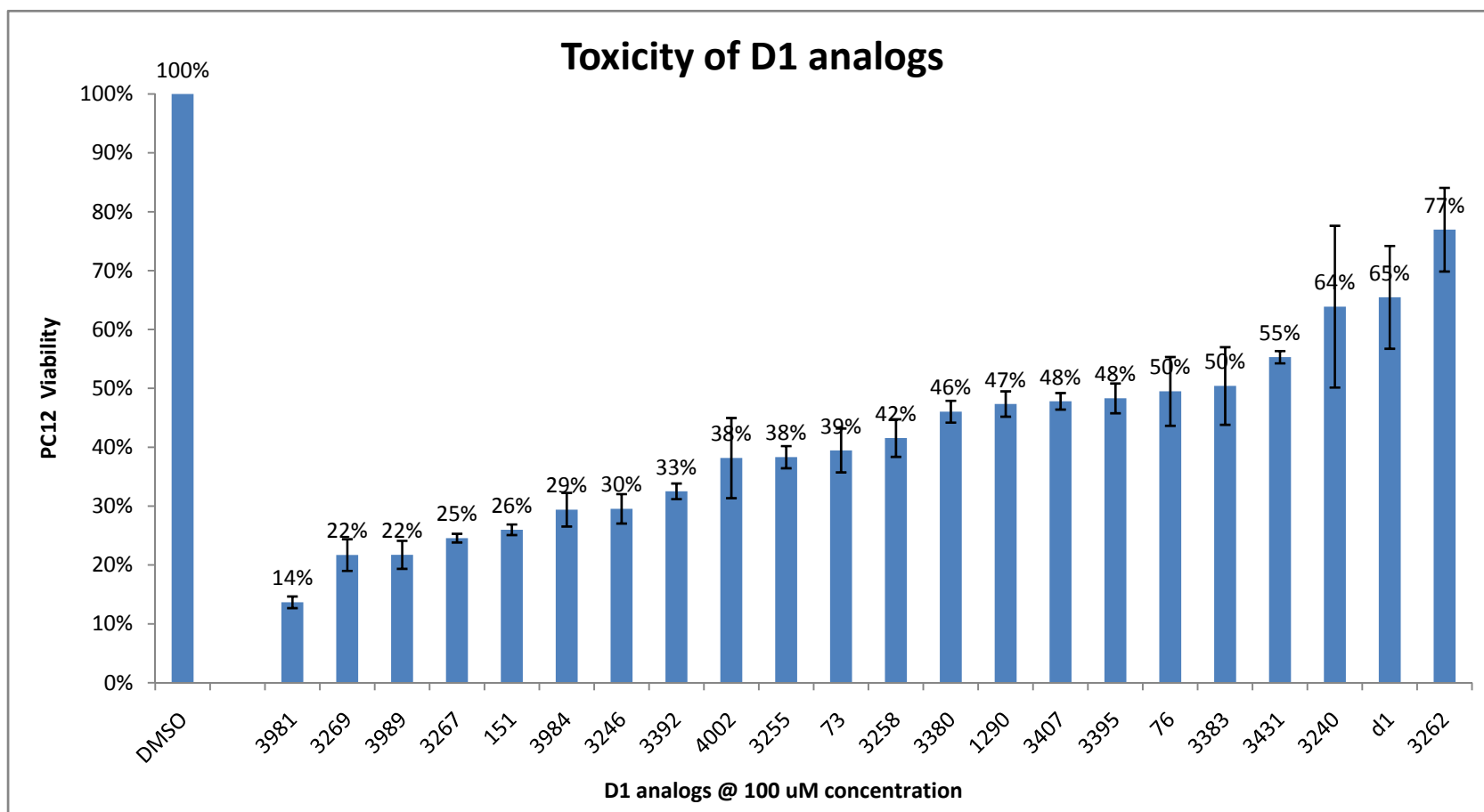


**Figure 3.13.** Toxicity of D1 analogs. PC12 cells treated with 100 uM of compound analogs. Values reported are the average viability scores of three wells. Cells were incubated for 24 hours.

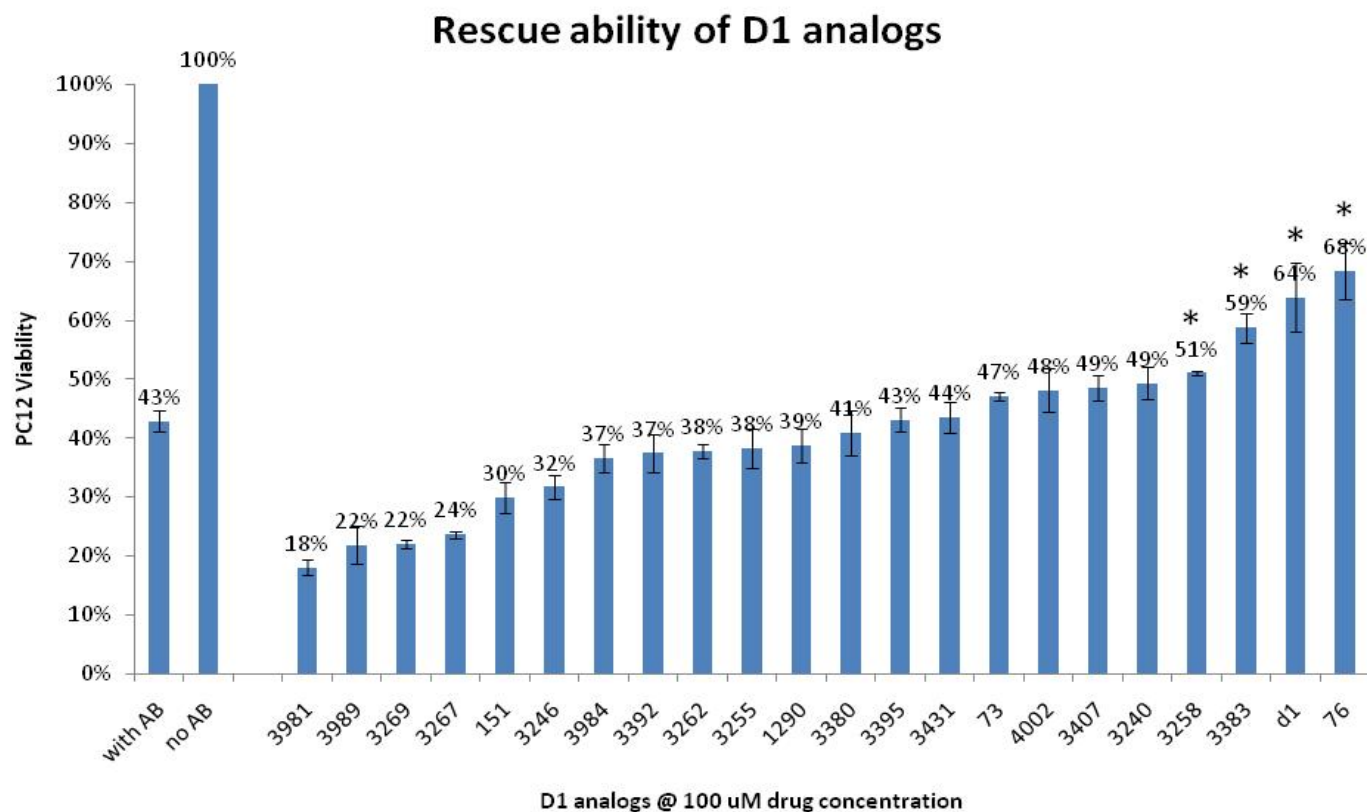


**Figure 3.14.** Rescue ability of D1 analogs at 100 uM. AB42 was used at a concentration of 20 uM, with 100 uM of compound analogs. Values reported are the average viability scores of three wells. Cells were incubated for 24 hours with AB42 and compound analog. \* indicated statistical significance as determined the two tailed Student's T-test ( $p < 0.05$ )

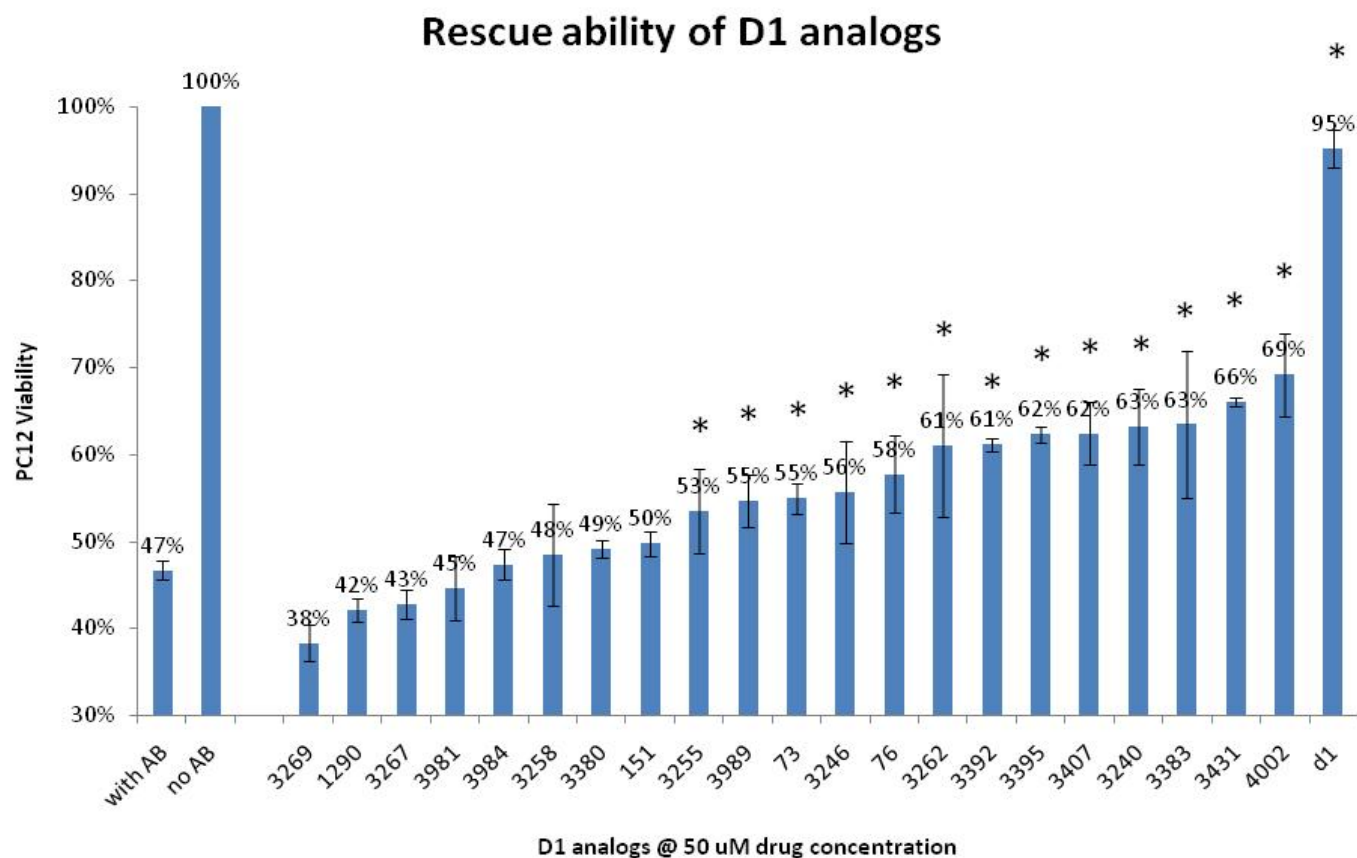


**Figure 3.15.** Rescue ability of D1 analogs at 50 uM. AB42 was used at a concentration of 20 uM, with 50 uM of compound analogs. Values reported are the average viability scores of three wells. Cells were incubated for 24 hours with AB42 and compound analog. \* indicated statistical significance as determined the two tailed Student's T-test ( $p < 0.05$ )

#### **3.2.4.5. Does D1 reduce aggregation of AB?**

I wanted to identify if compound D1 reduced AB aggregation. In order to determine if D1 was reducing AB aggregation, the standard thioflavin T assay was accomplished. Thioflavin T is a diagnostic dye that shifts its fluorescence on binding to the  $\beta$  sheet structure of amyloid fibrils. Less thioflavin T fluorescence indicates reduced AB aggregation.

The thioflavin T timecourse is shown in Figure 3.16. Fluorescence was measured at 0, 5, and 26 hours. Control wells of buffer only and buffer with D1 were also measured at the initial timepoint to identify if D1 was fluorescently active at the thioflavin T wavelengths. The buffer with D1 sample shows moderate fluorescence suggesting that D1 is fluorescent at the same wavelengths as thioflavin T. Surprisingly, the initial reading (time 0) of AB42 with D1 revealed an incredibly high fluorescence when compared to the sample with AB only, which suggests that the addition of D1 to AB causes the increase in fluorescence. Equally surprising was the decrease in fluorescence values from the initial time reading to the 5 hour time reading.

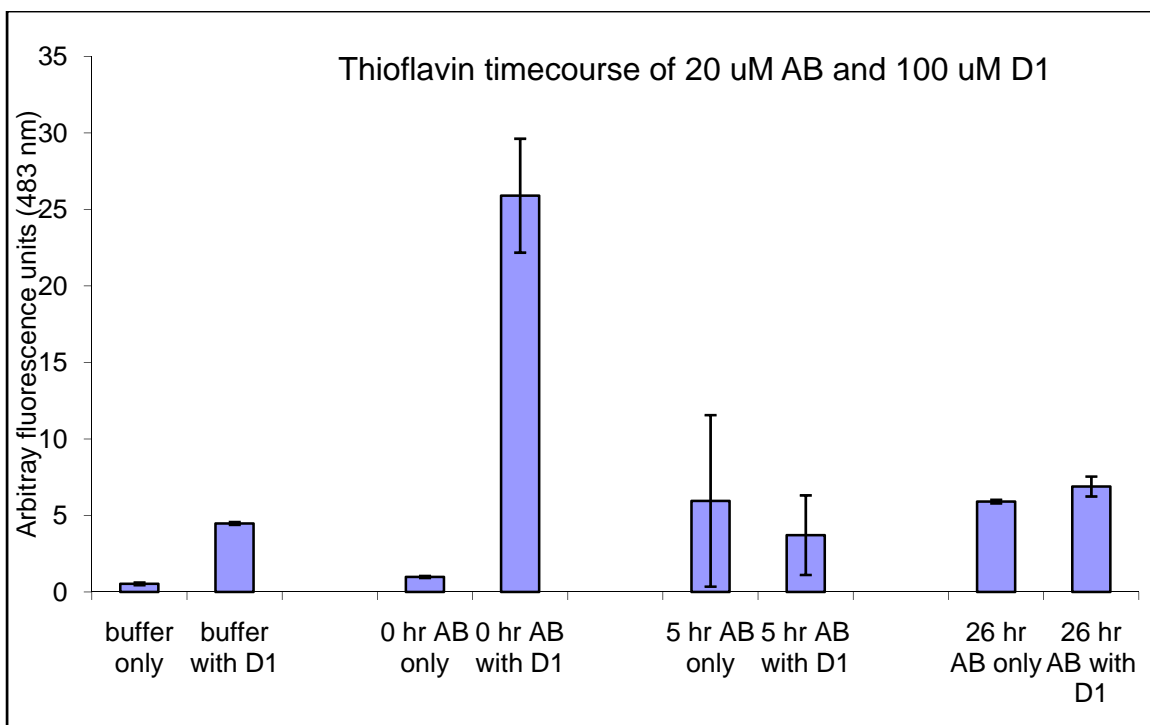


**Figure 3.16.** Thioflavin T timecourse of AB42 with and without compound D1. Values are averages of three different samples. 5 and 26 hour timepoints were incubated at 37 deg C.

The high levels of thioflavin T fluorescence from the AB with compound D1 suggest increased AB aggregation. To identify if this was occurring, EM images were taken at the initial timepoint. As shown in Figure 3.17, the EM image shows a very large amount of non-specific amorphous protein aggregation, as compared to the AB42 alone.

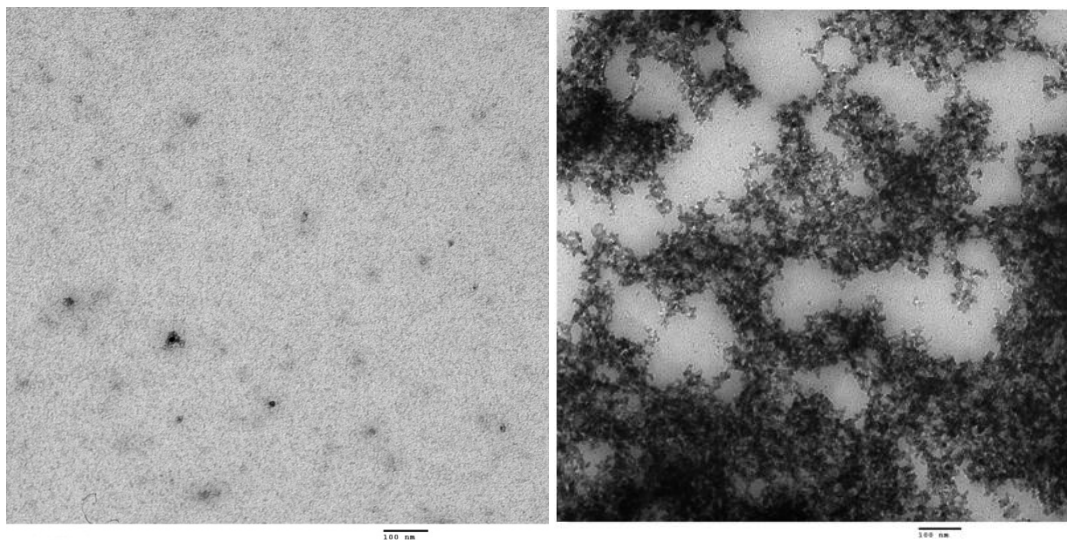


**Figure 3.17.** EM images of AB42 and AB42 with D1. Left: Image of AB42 sample at 0 hour. No AB42 aggregation can be detected. Right: Image of AB42 with D1 sample at 0 hour. Large amounts of non-fibrillar aggregation can be seen. Scale bar on both images: 100 nm, 25,000 x magnification.

### 3.3. Discussion

Research has indicated that soluble oligomeric species are better correlated with Alzheimer's disease than the presence of plaques (11, 12). In light of the recent report on dimer toxicity, screens that can identify monomeric binding to AB are important to discover compounds that can have the potential to become therapeutics.

#### 3.3.1. SMM screening effectiveness

Compound binding is a critical step for any enzymatic action or inhibition. As shown in Figure 3.4, Figure 3.6 and Figure 3.7, the SMM screen is effective at identifying compounds that bind to fluorescently labeled AB40. Figure 3.7 indicates that the binding assay is reliable and consistent at identifying compounds that bind to AB40, and not to control compound spots. Due to the large number of compounds printed onto each slide, the SMM screen is very effective at reducing numbers of compounds to test in subsequent experiments. In our example, the SMM screen looked at approximately 20,000 compounds and identified 79 for follow on testing.

Compound D1 was identified by the SMM binding screen. As shown in Figure 3.9, D1 has structural similarities to thioflavin T, which is known to bind to AB fibrils with nanomolar affinity (27, 28). Thioflavin T has a benzothiazole component attached to an aromatic ring. In D1, the benzothiazole is replaced by a benzoxazole; the only change is that sulfur is replaced with oxygen. Interestingly, another compound identified by the SMM screen, compound 1216, also shares a similar motif to D1 and thioflavin T. The structure of compound 1216 is shown in Figure 3.18 and has two benzimidazole functional group attached to an aromatic ring. Compound 1216 was also able to rescue

AB induced toxicity (Figure 3.8). In the initial toxicity study, PC12 cells treated with AB and 1216 had 93% viability, in contrast to the PC12 treated with AB and no compound.

The benzothiazole, benoxazole, and benzimidazole motif seems to be important in AB binding. Frentizole, an antiviral and immunosuppressive agent used in rheumatoid arthritis, binds to AB and has a benzothiazole motif (29, 30). Frentizole was identified in a screen to inhibit binding of AB to an alcohol dehydrogenase (31). Xie *et al* created analogs to frentizole and identified micromolar inhibitors to the AB-alcohol dehydrogenase interaction (31). It is encouraging that the SMM screen was able to identify compounds with similar motifs to compounds known to bind to AB. These results suggest the SMM screen is effective at identifying compounds that bind to AB.

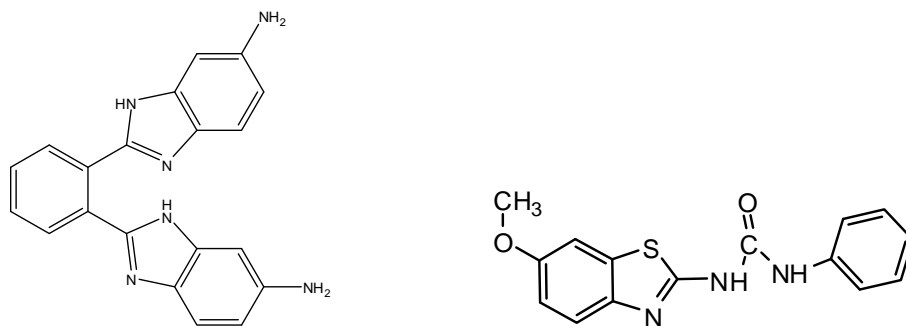


**Figure 3.18.** Structure of compound 1216 (left) and frentizole (right).

### 3.3.2. Rescue ability of D1

After identifying compounds that bound to AB, I wanted to know if they could reduce AB induced toxicity in cultured rat neuronal cells, or PC12 cells. Initial toxicity tests of the 79 SMM selected compounds identified 15 compounds that were able to rescue above 80% (Figure 3.8 and Table 3.1). As discussed above, D1 was able to

significantly reduce AB42 induced toxicity. As shown in Figure 3.10, there is a dose dependence increase in viability in cells when treated with increasing amounts of D1. PC12 cells treated with 50 uM of D1 had the highest cell viability, which suggests an optimal compound to AB binding ratio. In the toxicity experiments with the highest D1 rescue ability, AB42 was at a concentration of 20 uM, and compound D1 was at a concentration of 50 uM, which suggests an optimum ratio of 2 D1 molecules binding per molecule of AB. D1 concentrations below this of 2:1 ratio would not bind all of the AB, and remaining AB could aggregate to the toxic species, resulting in decreased viability. However, D1 concentrations higher than the 2:1 ratio would bind all the AB, but would leave excess D1 available. As shown in Figure 3.11, high concentrations (50 uM and 100 uM) of D1 are toxic. A binding ratio of 2 molecules of D1 to 1 molecule of AB may explain why both the treated cells with 25 uM and 100 uM both had less viability than 50 uM concentrations.

### **3.3.3. Does D1 cause aggregation of AB?**

When comparing the initial (0 hour) thioflavin T fluorescence values of D1 with AB42 to D1 in buffer (Figure 3.16), it is clear that the difference in fluorescence can only be attributed to the addition of AB peptide. This suggests that D1 is immediately nucleating/aggregating AB42 into a thioflavin T active species. EM images confirmed the aggregation of AB with D1, as shown in Figure 3.17. These data also suggests that D1 causes the immediate, non-fibrillar aggregation of AB42. An interesting note is that compound D1 would not have been identified as a hit in the thioflavin T based anti-aggregation screen. This screen selects for *reduced* fluorescence after an incubation

period. D1 treated samples had fluorescence readings equal to or higher than their AB only samples, which would have indicated that the compound did not inhibit AB aggregation.

#### **3.3.4. Possible mechanisms of D1 rescue**

The SMM screen identified D1 as a compound that binds to AB40, and toxicity experiments indicate that D1 can rescue AB42 induced toxicity. Both the thioflavin T data and EM images show that thioflavin active AB aggregates form immediately when incubated with D1. How does D1 prevent AB induced toxicity?

There are three possible mechanisms whereby D1 can reduce AB toxicity.

Mechanism 1: D1 binds to AB and prevents AB aggregation to the toxic species:

In this case, D1 binds to a specific location on AB, and stabilizes a specific form (possibly monomeric?) or a secondary structure ( $\alpha$  helix or  $\beta$  sheet) which prevents the further aggregation to the toxic species. However, stabilization of a specific form or structure would not explain the increased amount of thioflavin T fluorescence, or the presence of large amounts of aggregates in the EM images.

Mechanism 2: D1 is a neuroprotective compound:

In this case, D1 is an inhibitor of the mechanism of toxicity. The main hypothesis on AB toxicity is that AB oligomers form channels in neuronal membranes that make them unable to regulate internal ion concentration, such as calcium, resulting in cell death (32-34). If D1 was neuroprotective, it could block the calcium channels formed by the toxic AB oligomer. However, this mechanism also does not explain the large aggregates or dramatic increase in thioflavin T fluorescence.

Mechanism 3: D1 nucleates non-specific AB aggregation into a non-toxic aggregate:

This is the most likely mechanism. The thioflavin T timecourse and EM data show that D1 causes non-specific aggregation of AB42. Toxicity data show that these aggregates are not toxic. This suggests that D1 prevents AB induced toxicity of PC12 cells by nucleating the formation of a non-specific, non-toxic AB aggregate, and shifting the normal toxic aggregation pathway to one that is non-toxic.

### **3.3.5. D1 SAR study**

In the SAR study of D1 analogs at 50  $\mu$ M, positions R<sub>6</sub> seems to be significant in rescue. D1's R<sub>6</sub> amine group can form a maximum of three hydrogen bonds: 2 donating, and 1 accepting. The compounds that had the second (compound 4002) and third (compound 3431) highest viability scores also have a hydrogen bond accepting oxygen at the R<sub>6</sub> position. The oxygen can accept two hydrogen bonds from the peptide backbone or side chain. In the case of position R<sub>6</sub>, it is likely that the amine group in D1 or oxygen in 3431 and 4002 analogs forms a critical hydrogen bond to the AB peptide backbone or side chain residue. Position R<sub>6</sub> may also be in a solvent exposed area as well.

### **3.3.6. SMM screening questions**

A final question of screen effectiveness must be discussed: If the SMM screen identifies compounds that bind at the early stage of aggregation, why are not all the compounds effective at rescuing AB induced toxicity in PC12 cells? As reported by the initial toxicity screen in Figure 3.8 and Table 3.1, 35 of the 79 compounds had no effect

on viability (did not increase viability above 69%) or had viability below cells treated with only AB. Reasons for this include:

- 1) Compounds are toxic by themselves.

- 2) The SMM screen may have identified a false positive, either a promiscuous compound or a compound that bound to the fluorescent tag. These false positives would not be expected to inhibit AB toxicity. However, these false positive compounds would be removed based on the results of follow on assays.

- 3) The compound bound to a region of AB that does is not necessary for the aggregation process. An example can be a compound that binds anywhere on the first ten residues of AB40/42. These residues of AB have been shown to be flexible in models derived from solid state NMR data (35). So, the location where the compound binds to AB is absolutely critical in the ability of the compound to rescue toxicity. Compounds that bind to the central hydrophobic cluster (residues 17 – 21) may have a better chance at preventing aggregation. Cairo, *et al* demonstrated this with their study that charged peptide fragments of up to 12 amino acids with the central LVFF fragment were able to rescue toxicity (36).

- 4) A final possibility for why these compounds do not rescue toxicity is that the compound may stabilize the toxic species. An example can be seen with D1 analog compound 3262. Drug toxicity studies indicate that at 100 uM concentration, it is somewhat toxic, with PC 12 cells having 77% viability (Table 3.2). However, with the addition of AB42 and 3262, the viability of the PC12 cells significantly decreases to 38%, (where cells treated with AB42 without drug is 43% viable). It may be possible that compound 3262 is stabilizing the toxic species, resulting in increased cell death.

These compounds that bind to AB but do not inhibit toxicity are not likely therapeutic candidates, but they can still be useful for their binding ability to AB. If the compounds are found to specifically bind to residues 1 – 10, then these compounds may become very useful as tags for AB. One well known example is the amyloid labeling agent , Pittsburgh B, (PIB). PIB is based on the structure of thioflavin T and is one of very few *in vivo* amyloid imaging agents (37-39). Another use for specific binders is to create a “Trojan horse” inhibitor. Gestwicki *et al* modified the amyloid dye Congo red to include a chaperon binding site. When Congo red bound AB with the chaperon attached, the resulting steric bulk of the chaperon prevented aggregation of AB (40).

### 3.4. Summary

In this chapter I described the design and implementation of a binding screen to identify compounds that bind to monomeric or low molecular weight AB oligomers. The SMM screen was able to identify compounds that have similar motifs to known compounds that bound to AB. Several SMM compounds were shown to rescue AB induced toxicity, and D1 was shown to be an effective inhibitor of toxicity. D1 increases aggregation of AB42, and we suggest that it nucleates a non-toxic aggregate on a different aggregation pathway. SAR studies accomplished on analogs of D1 suggest that this may be a good scaffold for elucidating the motifs responsible for binding and toxicity.

### 3.5. Materials and methods:

**Fluorescent peptide.** Fluorescently tagged N-terminal labeled Hylite 647 AB40 or Hylite 488 AB42 peptide was purchased from Anaspec (San Jose, CA), and used without additional purification. HPLC purity from Anaspec was reported at greater than 95%.

**Peptide purification.** Non fluorescent crude peptides from FMOC synthesis were purchased from the Keck Institute at Yale University, and purified using a C4 reverse phase column. Solvent gradients were run at 65°C using solvent A (95% water, 5% acetonitrile, 0.1% TFA); and Solvent B (50% acetonitrile, 50% water, 0.1% TFA).

**SMM microarray preparation.** SMM slides were generously provided by Angela Kohler (Broad Institute of Harvard and MIT, Cambridge, MA). SMM assay slides were prepared as described by Bradner *et al* (41) .

**Small molecule microarray experiment.** N-terminal HiLyte Fluorophore 647-AB40 (Anaspec, CA) was diluted to a stock concentration 9.35  $\mu$ M in 8 mM NaOH. The stock solution was diluted to a final concentration of 185 nM in 1 x PBS-T (0.1% Tween 20). SMM slides (in triplicate) were incubated for 30 minutes at room temperature (25°C) in 5 mL of diluted AB40, with a slow circular orbit. Following incubation, SMM slides were rinsed for two minutes with PBS-T, PBS, and deionized water. SMM slides were then spun dry for 30 seconds (Labnet slide spinner) and then scanned on a GenePix 4100A microarray scanner (Molecular Devices) with excitation wavelength 532 nm (green emission filter 557 – 592 nm) and excitation wavelength 635 nm (red emission filter 650 – 690 nm). Experiment was accomplished at the Broad Institute of Harvard and

MIT. Analysis of the SMM data was completed by the Data Analysis Group at the Broad Institute of Harvard and MIT.

**Compounds.** Additional compounds were purchased from ChemDiv (San Diego, CA).

**Thioflavin T Assay.** Peptides were dissolved in 300  $\mu$ L DMSO and diluted with 5 mL of 8 mM NaOH for a final peptide concentration of 20  $\mu$ M. Concentrated PBS buffer was added to the solution to adjust the pH (final concentration: 50 mM  $\text{NaH}_2\text{PO}_4$ , 100 mM NaCl, pH 7.10 – 7.20). Samples were incubated with and without compound at 37°C under quiescent conditions for the indicated time period. At various timepoints, 100  $\mu$ L aliquot of peptide sample was mixed with 100  $\mu$ L of a solution of thioflavin T (7  $\mu$ M ThT, 50 mM glycerol-NaOH, pH 7.10) and fluorescence was measured at 483 nm (excitation at 450 nm) on a Varioskan Plate reader (Thermo).

**Electron microscopy.** Solutions were prepared as described above at peptide concentrations of 20  $\mu$ M. Samples were incubated at 37°C under quiescent conditions for the indicated time period. Following incubation, glow discharged formvar carbon coated grids were floated on a drop of each sample for 2 minutes, washed twice with distilled water, and then stained for 20 minutes with 1% uranyl acetate. Samples were imaged using a Zeiss 912ab Electron Microscope at Princeton University. Peggy Bisher assisted with machine operation and image capture.

**Toxicity experiments.** Rat pheochromocytoma (PC12) cells (ATCC, Rockville, MD) were grown on collagen coated ,tissue treated petrie dishes (Falcon) in complete growth media (82.5% F12K 15% horse serum, 2.5% fetal bovine serum, ATCC Rockville, MD) in a humidified incubator at 37°C and 5%  $\text{CO}_2$  (Herra, Thermo

Scientific). Cells were grown to confluence, harvested by spraying through an 18.5 gauge needle, resuspended in fresh complete media and plated onto tissue treated flat bottom 96 well plates (Costar) at a density of 10 000 cells per well (100 uL/well). Plates were incubated at 37°C for 24 hours to allow cells to attach. Lyophilized AB42 (1 mg) was dissolved in 100 uL of cell culture grade DMSO (ATCC), sonicated and then diluted with 1.0 mL of sterile 1 x PBS buffer (Invitrogen) for a final stock concentration of 200 uM. 10 uL of the final AB42 peptide solution was added to each well (100 uL) for a final peptide concentration of 20 uM. 1 uL of 10 mM inhibitor compound dissolved in DMSO was added to each well (in triplicate) for a final drug concentration of 100 uM. Plates with AB peptide and inhibitor compound were incubated for 24 hours. Cell viability was determined with the MTT assay (Roche (42, 43)). Briefly, 10 uL of MTT was added to each well. After incubation for 4 hr at 37°C, 100 uL of solubilization solution (10% SDS in 0.01 M HCl) was added and incubated overnight at 37°C. The absorbance at 570 nm was measured using a microplate reader (Thermo Varioskan), with background subtraction (670 nm). Statistical significance was calculated with the two tailed (uncorrelated) TTEST function in Excel.

### 3.6. References

1. Hoshino, M., Katou, H., Hagihara, Y., Hasegawa, K., Naiki, H., and Goto, Y. (2002) Mapping the core of the beta 2-microglobulin amyloid fibril by H/D exchange, *Nat Struct Mol Biol* 9, 332-336.
2. Kelly, J. W. (2002) Towards an understanding of amyloidogenesis, *Nat Struct Mol Biol* 9, 323-325.
3. Hardy, J., and Selkoe, D. J. (2002) The Amyloid Hypothesis of Alzheimer's Disease: Progress and Problems on the Road to Therapeutics, *Science* 297, 353-356.
4. Hardy, J. A., and Higgins, G. A. (1992) Alzheimer's disease: the amyloid cascade hypothesis, *Science* 256, 184-185.
5. Kuo, Y.-M., Emmerling, M. R., Vigo-Pelfrey, C., Kasunic, T. C., Kirkpatrick, J. B., Murdoch, G. H., Ball, M. J., and Roher, A. E. (1996) Water-soluble Amyloid beta (N-40, N-42) Oligomers in Normal and Alzheimer Disease Brains, *J. Biol. Chem.* 271, 4077-4081.
6. Lue, L.-F., Kuo, Y.-M., Roher, A. E., Brachova, L., Shen, Y., Sue, L., Beach, T., Kurth, J. H., Rydel, R. E., and Rogers, J. (1999) Soluble Amyloid Beta Peptide Concentration as a Predictor of Synaptic Change in Alzheimer's Disease, *Am J Pathol* 155, 853-862.
7. Mucke, L., Masliah, E., Yu, G.-Q., Mallory, M., Rockenstein, E. M., Tatsuno, G., Hu, K., Kholodenko, D., Johnson-Wood, K., and McConlogue, L. (2000) High-Level Neuronal Expression of Amyloid beta 1-42 in Wild-Type Human Amyloid Protein Precursor Transgenic Mice: Synaptotoxicity without Plaque Formation, *J. Neurosci.* 20, 4050-4058.
8. Roher, A. E., Chaney, M. O., Kuo, Y.-M., Webster, S. D., Stine, W. B., Haverkamp, L. J., Woods, A. S., Cotter, R. J., Tuohy, J. M., Krafft, G. A., Bonnell, B. S., and Emmerling, M. R. (1996) Morphology and Toxicity of Amyloid Beta -(1-42) Dimer Derived from Neuritic and Vascular Amyloid Deposits of Alzheimer's Disease, *J. Biol. Chem.* 271, 20631-20635.
9. Dahlgren, K. N., Manelli, A. M., Stine, W. B., Jr., Baker, L. K., Krafft, G. A., and LaDu, M. J. (2002) Oligomeric and Fibrillar Species of Amyloid-beta Peptides Differentially Affect Neuronal Viability, *J. Biol. Chem.* 277, 32046-32053.
10. Kaye, R., Head, E., Thompson, J. L., McIntire, T. M., Milton, S. C., Cotman, C. W., and Glabe, C. G. (2003) Common Structure of Soluble Amyloid Oligomers Implies Common Mechanism of Pathogenesis, *Science* 300, 486-489.
11. Lesne, S., Koh, M. T., Kotilinek, L., Kaye, R., Glabe, C. G., Yang, A., Gallagher, M., and Ashe, K. H. (2006) A specific amyloid-beta protein assembly in the brain impairs memory, *Nature* 440, 352-357.
12. Shankar, G. M., Li, S., Mehta, T. H., Garcia-Munoz, A., Shepardson, N. E., Smith, I., Brett, F. M., Farrell, M. A., Rowan, M. J., Lemere, C. A., Regan, C. M., Walsh, D. M., Sabatini, B. L., and Selkoe, D. J. (2008) Amyloid-Beta protein dimers isolated directly from Alzheimer's brains impair synaptic plasticity and memory, *Nat Med advanced online publication*.

13. Vegas, A. J., Fuller, J. H., and Koehler, A. N. (2008) Small-molecule microarrays as tools in ligand discovery, *Chem Soc Rev* 37, 1385-1394.
14. Vegas, A. J., Bradner, J. E., Tang, W., McPherson, O. M., Greenberg, E. F., Koehler, A. N., and Schreiber, S. L. (2007) Fluorous-Based Small-Molecule Microarrays for the Discovery of Histone Deacetylase Inhibitors, *Angewandte Chemie International Edition* 46, 7960-7964.
15. Bradner, J. E., McPherson, O. M., Mazitschek, R., Barnes-Seeman, D., Shen, J. P., Dhaliwal, J., Stevenson, K. E., Duffner, J. L., Park, S. B., Neubergh, D. S., Nghiem, P., Schreiber, S. L., and Koehler, A. N. (2006) A Robust Small-Molecule Microarray Platform for Screening Cell Lysates, *Chemistry & Biology* 13, 493-504.
16. Barnes-Seeman, D., Park, S. B., Koehler, A. N., and Schreiber, S. L. (2003) Expanding the Functional Group Compatibility of Small-Molecule Microarrays: Discovery of Novel Calmodulin Ligands, *Angewandte Chemie International Edition* 42, 2376-2379.
17. Koehler, A. N., Shamji, A. F., and Schreiber, S. L. (2003) Discovery of an Inhibitor of a Transcription Factor Using Small Molecule Microarrays and Diversity-Oriented Synthesis, *J. Am. Chem. Soc.* 125, 8420-8421.
18. Kuruvilla, F. G., Shamji, A. F., Sternson, S. M., Hergenrother, P. J., and Schreiber, S. L. (2002) Dissecting glucose signalling with diversity-oriented synthesis and small-molecule microarrays, *Nature* 416, 653-657.
19. Schmitz, K., Haggarty, S. J., McPherson, O. M., Clardy, J., and Koehler, A. N. (2007) Detecting Binding Interactions Using Microarrays of Natural Product Extracts, *J. Am. Chem. Soc.* 129, 11346-11347.
20. Uttamchandani, M., Walsh, D. P., Khersonsky, S. M., Huang, X., Yao, S. Q., and Chang, Y. T. (2004) Microarrays of Tagged Combinatorial Triazine Libraries in the Discovery of Small-Molecule Ligands of Human IgG, *J. Comb. Chem* 6, 862-868.
21. Gravina, S. A., Ho, L., Eckman, C. B., Long, K. E., Otvos, L., Jr., Younkin, L. H., Suzuki, N., and Younkin, S. G. (1995) Amyloid beta protein (A beta) in Alzheimer's disease brain. Biochemical and immunocytochemical analysis with antibodies specific for forms ending at A beta 40 or A beta 42(43), *J Biol Chem* 270, 7013-7016.
22. Soreghan, B., Kosmoski, J., and Glabe, C. (1994) Surfactant properties of Alzheimer's Amyloid beta peptides and the mechanism of amyloid aggregation, *J. Biol. Chem.* 269, 28551-28554.
23. Christopeit, T., Hortschansky, P., Schroeckh, V., Guhrs, K., Zandomenighi, G., and Fandrich, M. (2005) Mutagenic analysis of the nucleation propensity of oxidized Alzheimer's beta-amyloid peptide, *Protein Sci* 14, 2125-2131.
24. McPherson, O. M., and Koehler, A. N. personal communication.
25. Seiler, K. P., George, G. A., Happ, M. P., Bodycombe, N. E., Carrinski, H. A., Norton, S., Brudz, S., Sullivan, J. P., Muhlich, J., Serrano, M., Ferraiolo, P., Tolliday, N. J., Schreiber, S. L., and Clemons, P. A. (2008) ChemBank: a small-molecule screening and cheminformatics resource database, *Nucl. Acids Res.* 36, D351-359.

26. Duffner, J. L., Clemons, P. A., and Koehler, A. N. (2007) A pipeline for ligand discovery using small-molecule microarrays, *Current Opinion in Chemical Biology* 11, 74-82.
27. Lockhart, A., Ye, L., Judd, D. B., Merritt, A. T., Lowe, P. N., Morgenstern, J. L., Hong, G., Gee, A. D., and Brown, J. (2005) Evidence for the Presence of Three Distinct Binding Sites for the Thioflavin T Class of Alzheimer's Disease PET Imaging Agents on beta-Amyloid Peptide Fibrils, *J. Biol. Chem.* 280, 7677-7684.
28. LeVine, I., H. (1995) Thioflavine T Interaction with Amyloid Beta-Sheet Structures., *Amyloid: The International Journal of Experimental and Clinical Investigation* 2, 1-6.
29. Scheetz, M. E., Carlson, D. G., and Schinitzky, M. R. (1977) Frentizole, a novel immunosuppressive, and azathioprine: their comparative effects on host resistance to *Pseudomonas aeruginosa*, *Candida albicans*, herpes simplex virus, and influenza (Ann Arbor) virus, *Infect. Immun.* 15, 145-148.
30. Rooth, W., and Srikrishnan, T. (1999) Crystal structure and conformation of frentizole, [1-(6-methoxy-2-benzothiazolyl)-3-phenylurea, an antiviral agent and an immunosuppressive drug, *Journal of Chemical Crystallography* 29, 1187-1191.
31. Xie, Y., Deng, S., Chen, Z., Yan, S., and Landry, D. W. (2006) Identification of small-molecule inhibitors of the Amyloid Beta-ABAD interaction, *Bioorganic & Medicinal Chemistry Letters* 16, 4657-4660.
32. Arispe, N., Diaz, J. C., and Simakova, O. (2007) Amyloid beta ion channels. Prospects for treating Alzheimer's disease with Amyloid beta channel blockers, *Biochimica et Biophysica Acta (BBA) - Biomembranes* 1768, 1952-1965.
33. Ho, R., Ortiz, D., and Shea, T. B. (2001) Amyloid-beta promotes calcium influx and neurodegeneration via stimulation of L voltage-sensitive calcium channels rather than NMDA channels in cultured neurons *Journal of Alzheimer's Disease* 3, 479-483.
34. Marx, J. (2007) Alzheimer's Disease: Fresh Evidence Points to an Old Suspect: Calcium, *Science* 318, 384-385.
35. Petkova, A. T., Ishii, Y., Balbach, J. J., Antzutkin, O. N., Leapman, R. D., Delaglio, F., and Tycko, R. (2002) A structural model for Alzheimer's beta-amyloid fibrils based on experimental constraints from solid state NMR, *Proceedings of the National Academy of Sciences of the United States of America* 99, 16742-16747.
36. Cairo, C. W., Strzelec, A., Murphy, R. M., and Kiessling, L. L. (2002) Affinity-Based Inhibition of beta-Amyloid Toxicity, *Biochemistry* 41, 8620-8629.
37. Jack, C. R., Jr., Lowe, V. J., Selkoe, D. J., Weigand, S. D., Kemp, B. J., Shiung, M. M., Knopman, D. S., Boeve, B. F., Klunk, W. E., Mathis, C. A., and Petersen, R. C. (2008) <sup>11</sup>C PiB and structural MRI provide complementary information in imaging of Alzheimer's disease and amnesic mild cognitive impairment, *Brain* 131, 665-680.
38. Klunk, W. E., Engler, H., Nordberg, A., Wang, Y., Blomqvist, G., Holt, D. P., Bergström, M., Savitcheva, I., Huang, G.-F., Estrada, S., Ausén, B., Debnath, M. L., Barletta, J., Price, J. C., Sandell, J., Lopresti, B. J., Wall, A., Koivisto, P., Antoni, G., Mathis, C. A., and Långström, B. (2004) Imaging brain amyloid in

- Alzheimer's disease with Pittsburgh Compound-B, *Annals of Neurology* 55, 306-319.
39. Mathis, C. A., Wang, Y., Holt, D. P., Huang, G. F., Debnath, M. L., and Klunk, W. E. (2003) Synthesis and Evaluation of <sup>11</sup>C-Labeled 6-Substituted 2-Arylbenzothiazoles as Amyloid Imaging Agents, *J. Med. Chem.* 46, 2740-2754.
  40. Gestwicki, J. E., Crabtree, G. R., and Graef, I. A. (2004) Harnessing Chaperones to Generate Small-Molecule Inhibitors of Amyloid Beta Aggregation, *Science* 306, 865-869.
  41. Bradner, J. E., McPherson, O. M., and Koehler, A. N. (2006) A method for the covalent capture and screening of diverse small molecules in a microarray format, *Nat. Protocols* 1, 2344-2352.
  42. Maehara, Y., Anai, H., Tamada, R., and Sugimachi, K. (1987) The ATP assay is more sensitive than the succinate dehydrogenase inhibition test for predicting cell viability, *European Journal of Cancer and Clinical Oncology* 23, 273-276.
  43. Vistica, D. T., Skehan, P., Scudiero, D., Monks, A., Pittman, A., and Boyd, M. R. (1991) Tetrazolium-based assays for cellular viability: a critical examination of selected parameters affecting formazan production, *Cancer Res* 51, 2515-2520.

## **Chapter 4. Identifying the role of aromaticity in AB aggregation, fibrilization, toxicity, and aggregation inhibition**

### **4.1. Introduction to aromatic interactions**

In this chapter, I will discuss the role of aromaticity in amyloid beta peptide aggregation. First, I will introduce aromatic interactions and  $\pi$ -stacking, and discuss the hypothesis that  $\pi$ -stacking is critical to AB aggregation, and the related hypothesis that disturbing the  $\pi$ -stacking interaction is the mechanism for aggregation inhibition for aromatic compounds. I will then dispute these hypotheses by presenting evidence found with AB peptide mutants (where aromatic residues are mutated to non-aromatic residues) and show that aromatic residues are not required for aggregation or fibrilization. Also, I will show that mutants without aromatic residues can be inhibited by aromatic compounds. Finally, I show that these AB mutants are even more toxic than the original wild type peptide.

Aromatic-aromatic interactions are non-covalent, attractive interactions between two planar aromatic rings, known as  $\pi$ -stacking. These  $\pi$ -stacking interactions minimize the energy of a given system and stabilize both DNA and protein structures (*1*). As shown in Figure 4.1, there are four different low energy structures that can occur: parallel displaced, T-shaped, parallel staggered, or herringbone (*1, 2*). In proteins, the parallel displaced structure is most common.

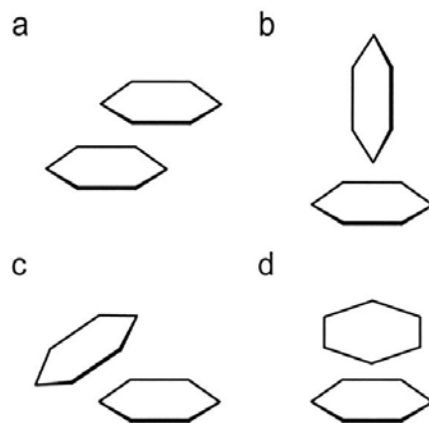


**Figure 4.1.** Illustration of  $\pi$ -stacking structures. a) parallel displaced; b) T-shaped; c) parallel staggered; d) herringbone. Figure from Gazit (2).

It has been suggested that the  $\pi$ -stacking of aromatic residues is important in the process of amyloid formation. Gazit noted that aromatic residues are very common in amyloidogenic peptide fragments that can form fibrils, as shown in Table 4.1 (2). According to the statistics compiled by Gazit, the frequency of aromatic residues incorporation into proteins is relatively low, with tryptophan at 1.32%, tyrosine at 3.25% and phenylalanine at 3.91% (2). The high occurrence of aromatic residues found in amyloid fragments, combined with the fact that aromatic residues are not commonly incorporated into proteins suggests that aromatic residues may have a significant role in amyloid formation (2-4).

**Table 4.1.** Functional amyloid related sequences that contain aromatic residues, adapted from Gazit (2).

Disease or condition	parent peptide	active sequence with aromatic residue
Alzheimer's disease	amyloid beta peptide	KLV <b>FF</b> AE
Creutzfeldt-Jakob disease	PrP	PHGGG <b>W</b> GQ
Yeast prion protein	Sup35p	PQGG <b>Y</b> QQ <b>Y</b> N GNNQQN <b>Y</b>
Type II diabetes	islet amyloid polypeptide/amylin	<b>F</b> GAIL TNVGSNT <b>Y</b> QRLAN <b>FL</b> VH

Gazit has also suggested that disturbing the  $\pi$ -stacking process in amyloid formation can be an effective mechanism to prevent aggregation (2, 5, 6). This may also explain why many aggregation inhibitors are aromatic, as discussed in Chapter 1. If the  $\pi$ -stacking interactions are significant in amyloid formation, disturbing this interaction may potentially inhibit the aggregation process, as shown Figure 4.2.

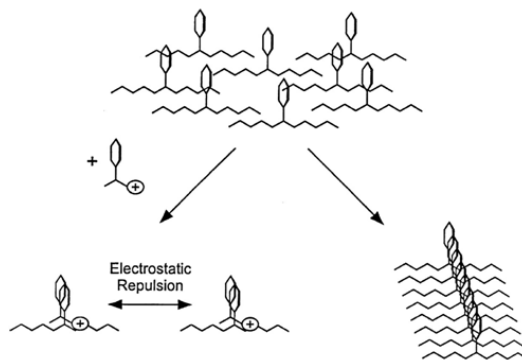


**Figure 4.2.** Potential mechanism for aggregation inhibition by disturbing aromatic  $\pi$  interactions. A charged aromatic inhibitor can interact with the aromatic residue of the peptide. Subsequent aggregation is prevented because of the electrostatic repulsion. Figure from Gazit (2).

## 4.2. Investigating the role of aromatic residues and $\pi$ -stacking in Alzheimer's disease

Alzheimer's disease is caused by the aggregation of the amyloid beta (AB) peptide. In the sequence of the 42 residue peptide, there are three phenylalanine (Phe, F) residues at positions 4, 19, and 20, and one tyrosine (Tyr, Y), at position 10. The sequence for AB is shown below with aromatic residues highlighted in red, using the one letter abbreviations for amino acids.

DAE **F** RHDSG **Y**<sup>10</sup> EVHHQKLV **F F**<sup>20</sup> AEDVGSNKG A<sup>30</sup> IIGLMVGGVV<sup>40</sup> IA<sup>42</sup>

The first 10 to 14 residues in AB have been reported to be flexible (7, 8). This suggests that both the Phe residue at position 4 and the Tyr at position 10 are not involved in significant  $\pi$ -stacking. Proline scanning mutagenesis of AB has shown that residues 15 – 21 are in an area that is highly sensitive to proline replacement, which includes residues Phe 19 and Phe 20 (7, 9) and is known as the central hydrophobic cluster. Structural models of the AB40 (residues 10 to 40) derived from solid state NMR studies show the parallel displaced motif of  $\pi$ -stacking for Phe residues 19 and 20 (Figure 4.3).

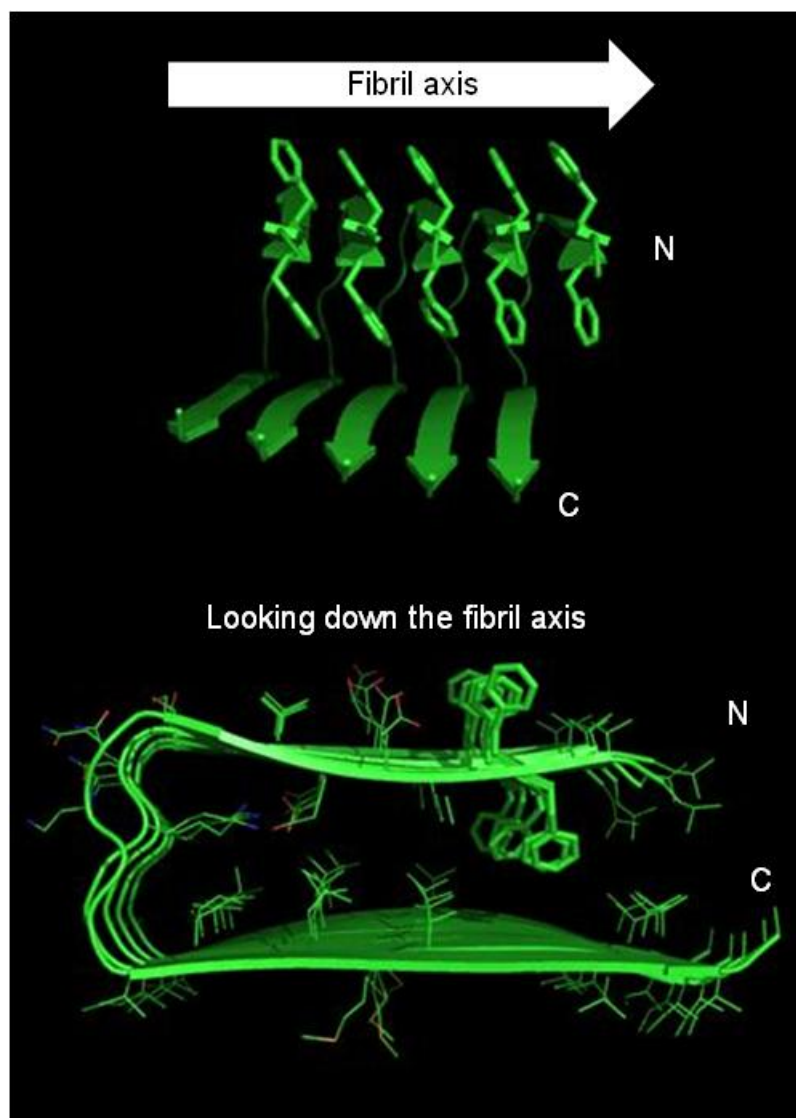


**Figure 4.3.** Model structure of AB 10 – 40 fibril based on solid state NMR studies.

Different views show the  $\pi$ -stacking interaction of Phe 19 (interior) and Phe 20 (exterior).

Figure created with Pymol. Coordinates provided by Dr. Robert Tycko (8).

Recent reports have questioned the role of aromatic-aromatic interactions in amyloidogenic peptides. Kim *et al* suggest that aryl-aryl contacts may not be as important in the kinetic and thermodynamic aspect of protein folding. In a study designed to investigate aromatic interactions between aromatic and alkyl groups, they

show that the electrostatic potential of the aromatic ring is not a dominant aspect of the aryl-aryl interaction and suggest that C-H contacts in CH- $\pi$  interactions may be more important (10). In addition, mutations in amylin, the amyloidogenic peptide responsible for type II diabetes, indicate that aromatic residues in the sequence are not required for fibril formation. Tracez *et al* show that amylin fragments with the aromatic Phe residues replaced by Leu residues were still able to form amyloid (11). Furthermore, Marek *et al* reported that an amylin triple mutant, where all three aromatic residues were mutated to Leu (F15L/F23L/Y37L), readily formed fibrils (12).

I wanted to determine if aromatic residues were necessary for AB aggregation and fibrilization. To investigate this, Phe residues in the central hydrophobic cluster (position 19 and 20) were mutated to Ile (AB42 F19I/F20I, referred to as 42 Ile Ile) and Leu (AB42 L19L/F20L, referred to as 42 Leu Leu) and were tested for their aggregation propensity. The same mutations were made to the 40 length peptide, AB40 F19I/F20I (40 Ile Ile) and AB40 F19L/F20L (40 Leu Leu).

I also wanted to investigate the mechanism of aggregation inhibition by aromatic and non-aromatic compounds. To test whether disruption of the  $\pi$ -stacking is the mechanism of inhibition by aromatic inhibitors, aromatic aggregation inhibitors were added to both 42 Ile Ile and 40 Ile Ile mutants. To test if non-aromatic inhibitors could inhibit wild type AB, non-aromatic inhibitors were also added to wild type AB42, as well as 42 Ile Ile and 40 Ile Ile mutants.

### 4.3. Results

#### 4.3.1. Aggregation and fibrilization propensity of AB mutant peptides lacking Phe 19 and Phe 20

In order to determine the aggregation and fibrilization propensity of AB mutants without aromatic residues Phe 19 and Phe 20, both of these Phe residues were mutated to the same non-aromatic residue. Ile and Leu residues were chosen to replace Phe because they are similar in charge, hydrophobicity and  $\beta$  sheet propensity when compared to Phe (Table 4.2). In addition, comparing Ile and Leu mutations also provided information on how physical structural differences affect aggregation. A soluble AB42 peptide double mutant (AB42 F19S/L34P, known as GM6) was used as a non-aggregation control (13). All AB mutant sequences that were investigated for aggregation propensity are shown in Figure 4.4.

**Table 4.2.** Hydrophobicity and  $\beta$  sheet propensity of Phe, Ile and Leu. Hydrophobicity values from (14) (measured by partition coefficient between water and octanol) and beta sheet propensity from (15)

amino acid residue	hydrophobicity	$\beta$ sheet propensity
Phe	-1.79	-0.56
Ile	-1.80	-0.55
Leu	-1.70	-0.48

AB mutants		1	2	3	4	5	6	7	8	9	10	11	12	13	14	15	16	17	18	19	20	21	22	23	24	25	26	27	28	29	30	31	32	33	34	35	36	37	38	39	40	41	42
AB40	WT40	D	A	E	F	R	H	D	S	G	Y	E	V	H	H	Q	K	L	V	F	F	A	E	D	V	G	S	N	K	G	A	I	I	G	L	M	V	G	G	V	V		
AB42	WT42	D	A	E	F	R	H	D	S	G	Y	E	V	H	H	Q	K	L	V	F	F	A	E	D	V	G	S	N	K	G	A	I	I	G	L	M	V	G	G	V	V	I	A
AB40 F19I/F20I	40 Ile Ile	D	A	E	F	R	H	D	S	G	Y	E	V	H	H	Q	K	L	V	I	I	A	E	D	V	G	S	N	K	G	A	I	I	G	L	M	V	G	G	V	V		
AB40 F19I/F20I	40 Leu Leu	D	A	E	F	R	H	D	S	G	Y	E	V	H	H	Q	K	L	V	L	L	A	E	D	V	G	S	N	K	G	A	I	I	G	L	M	V	G	G	V	V		
AB40 F19I/F20I	42 Ile Ile	D	A	E	F	R	H	D	S	G	Y	E	V	H	H	Q	K	L	V	L	L	A	E	D	V	G	S	N	K	G	A	I	I	G	L	M	V	G	G	V	V	I	A
AB40 F19I/F20I	42 Leu Leu	D	A	E	F	R	H	D	S	G	Y	E	V	H	H	Q	K	L	V	I	I	A	E	D	V	G	S	N	K	G	A	I	I	G	L	M	V	G	G	V	V	I	A
AB42 F19S/L34P	GM6	D	A	E	F	R	H	D	S	G	Y	E	V	H	H	Q	K	L	V	S	F	A	E	D	V	G	S	N	K	G	A	I	I	G	P	M	V	G	G	V	V	I	A

**Figure 4.4.** Amino acid sequences of AB42 and mutants used in this study. Amino acid sequences are shown using the single letter code with non-polar residues in yellow, polar residues in red, and glycine in blue. Mutations are boxed.

The aggregation profile for AB42 and mutants was determined by measuring thioflavin T fluorescence. Thioflavin T is a dye that exhibits negligible fluorescence in solution but experiences a significant increase in fluorescence intensity after binding to amyloid fibrils (16). Higher thioflavin T fluorescence indicates increased aggregation and fibrilization. The aggregation profile of AB42 is shown in green in Figure 4.5. The typical aggregation profile of AB42 has a short lag phase, followed by an assembly and growth phase. The soluble mutant, GM6 (in purple), does not show any significant thioflavin T fluorescence when compared to AB42, indicating less aggregation. Surprisingly, the mutant with the highest aggregation profile is the 42 Ile Ile mutant (in blue). The 42 Ile Ile mutant has virtually no lag time before significant thioflavin T fluorescence is seen. Also, the 42 Ile Ile mutant is much faster at aggregation when compared to the wild type AB42 and 42 Leu Leu (in red) mutants. After 7 hours, the 42 Ile Ile mutant has already reached 70% of its total fluorescence. The 42 Leu Leu aggregation profile, as shown in red, has a more pronounced lag time before entering the assembly/growth phase. The fluorescence intensity of the 42 Leu Leu mutant was less than AB42 until approximately 30 hours, where the 42 Leu Leu mutant starts to aggregate very quickly.

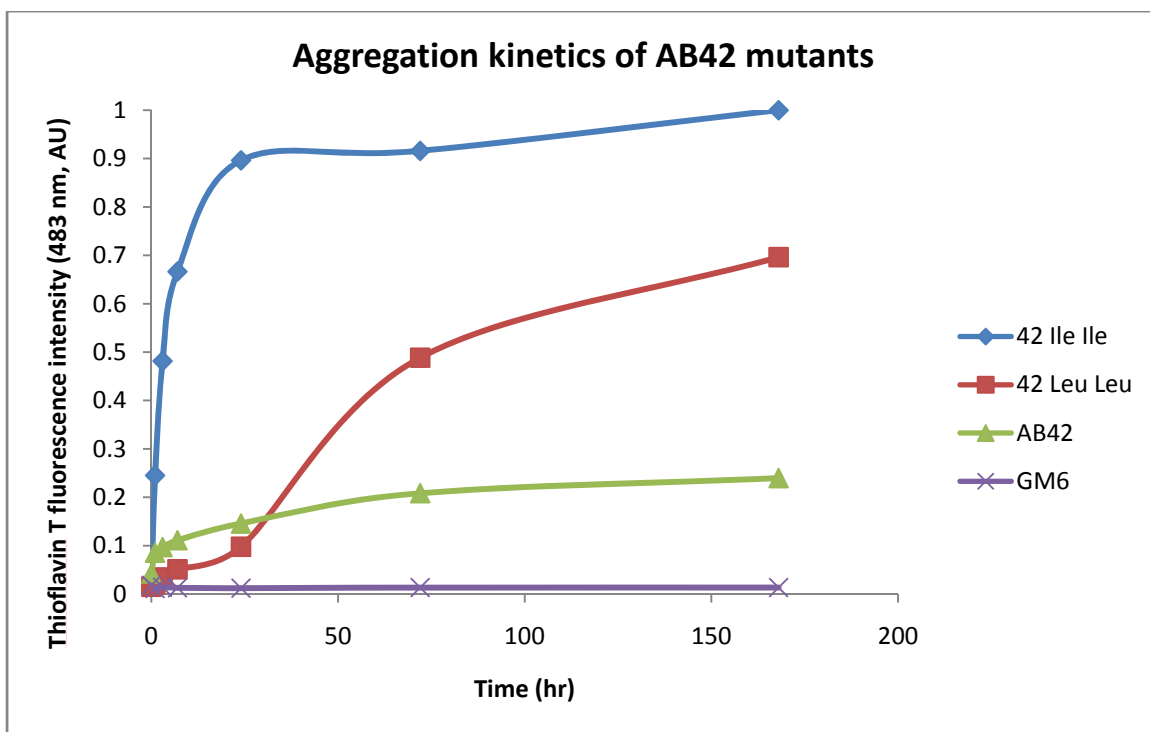


**Figure 4.5.** Aggregation profile in hours of AB42 and mutants as determined by thioflavin T fluorescence. Each peptide is at a concentration of 20  $\mu$ M, incubated at 37°C under quiescent conditions. Measurements are an average of two readings.

In Figure 4.5, the slope of the 42 Leu Leu aggregation profile indicates that it is still increasing at the end of 7 days. A longer aggregation profile was taken with AB42, 42 Ile Ile, and 42 Leu Leu as shown in Figure 4.6. As shown in Figure 4.6, the 42 Ile Ile mutant again has the fastest aggregation profile. Interestingly, the fluorescence of the 42 Leu Leu mutant continued to increase and was higher than the 42 Ile Ile mutant when the aggregation timecourse ended. However, the 42 Leu Leu mutant did not show the same lag time as the first aggregation profile.

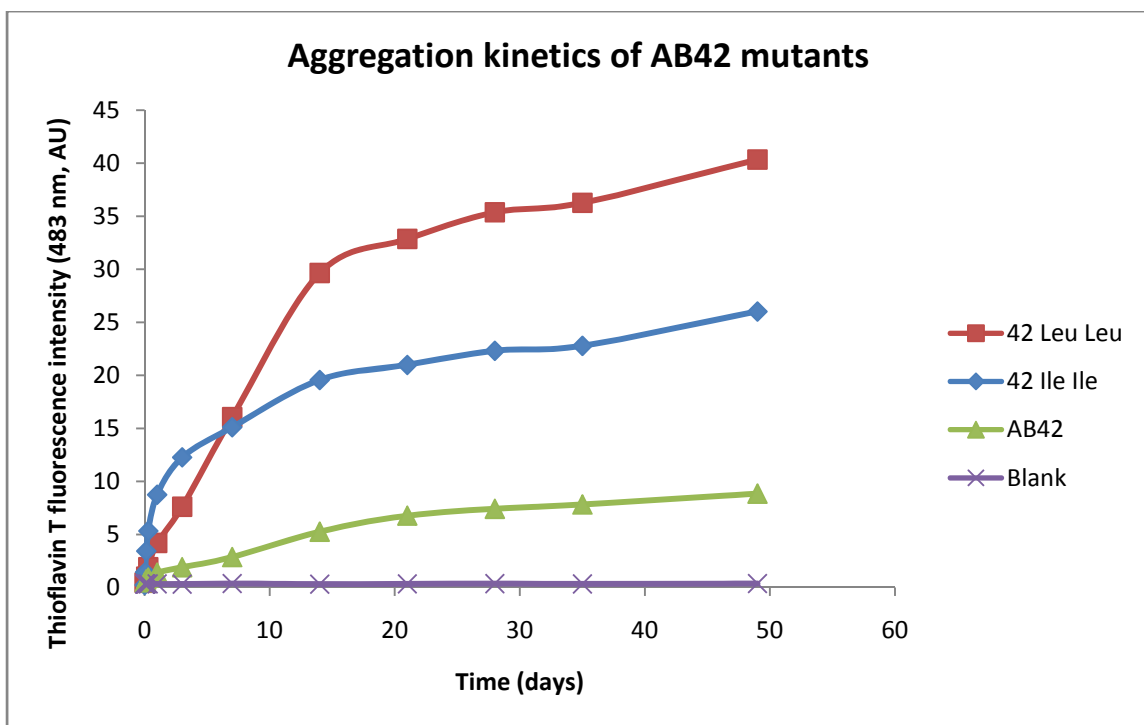


**Figure 4.6.** Aggregation profile in days of AB42 and mutants as determined by thioflavin T fluorescence. Each peptide is at a concentration of 20  $\mu$ M, incubated at 37°C under quiescent conditions. Measurements are an average of three readings.

I also wanted to identify the effect on the aggregation profiles for the 40 residue peptide mutants. AB40 is two residues shorter than AB42, more abundantly found, and is less amyloidogenic (17). Figure 4.7 shows the aggregation kinetics of the 40 Ile Ile and 40 Leu Leu mutants when compared to wild type AB42 and AB40. The AB40 Ile Ile aggregation profile (in blue) is much faster than the wild type AB40 profile (in purple). Interestingly, the aggregation profile of 40 Ile Ile is almost equal to the aggregation profile of wild type AB42 (in green). As discussed in Chapter 1, AB40 is missing two C-terminal amino acids, (Ile 41 and Ala 42) and is known to aggregate slower than AB42. Thus, it is striking that the Phe to Ile double mutant in the context of the 40 residue

peptide is similar to the wild type AB42 aggregation profile, as the hydrophobicities of the Phe and Ile peptides are similar (Table 4.2).

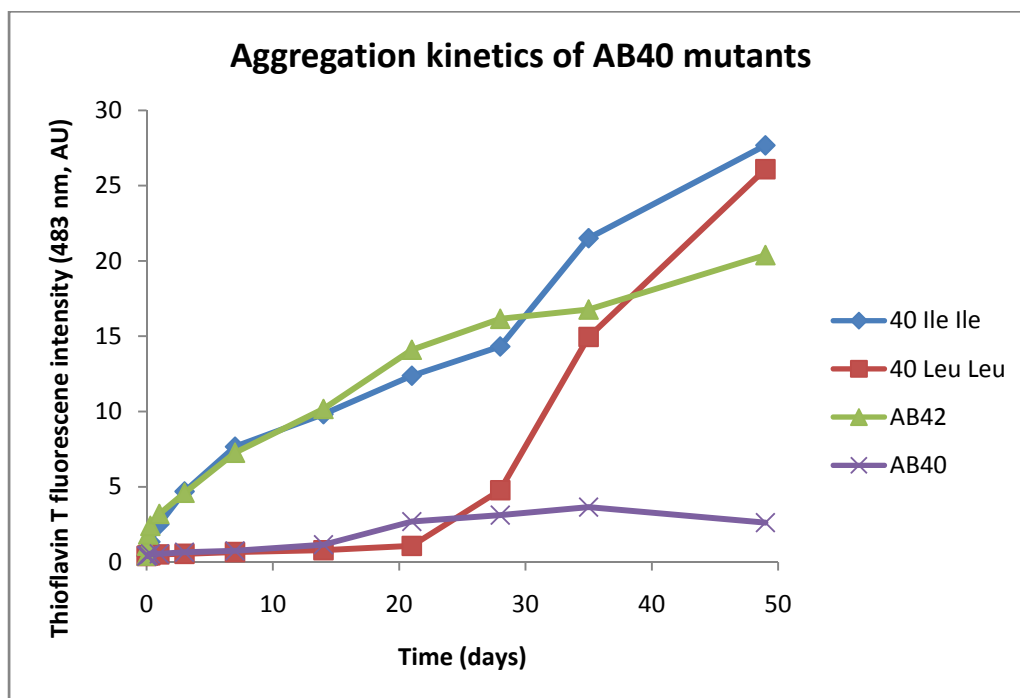


**Figure 4.7.** Aggregation profile in days of AB40 and mutants as determined by thioflavin T fluorescence. Each AB peptide is at a concentration of 20  $\mu$ M, incubated at 37°C under quiescent conditions. Measurements are an average of three readings.

These thioflavin T aggregation profiles show the same trend in both mutant AB 42 and 40 peptides with both Phe 19 and 20 mutated to Ile. The Ile Ile mutation has the fastest aggregation profile in both the 42 and 40 length mutants, while the Leu Leu mutant has a pronounced lag time before a very rapid increase in fluorescence in both peptide lengths. As shown by the thioflavin T fluorescence kinetic profiles of both AB40 and AB42 peptide mutants, these results clearly demonstrate that aromatic residues in AB are not required or necessary for AB aggregation and fibrilization.

#### **4.3.2. Electron microscopy images of 42 Ile Ile and 42 Leu Leu mutant AB peptides**

In order to determine if these mutants were able to form fibrils, EM images of the mutants were taken to identify fibril formation, and to compare fibril morphologies of the peptide mutants. The EM images of mutant fibrils are shown in Figure 4.8. AB42 fibrils are abundant, with the morphology of the fibrils being straight, long and unbranched. 42 Ile Ile fibrils are also very abundant, straight, long and unbranched. AB42 Leu Leu fibrils are less abundant than the AB42 Ile Ile mutant, but otherwise similarly long and unbranched. The EM images clearly show that both 42 Ile Ile and 42 Leu Leu mutants can form fibrils.

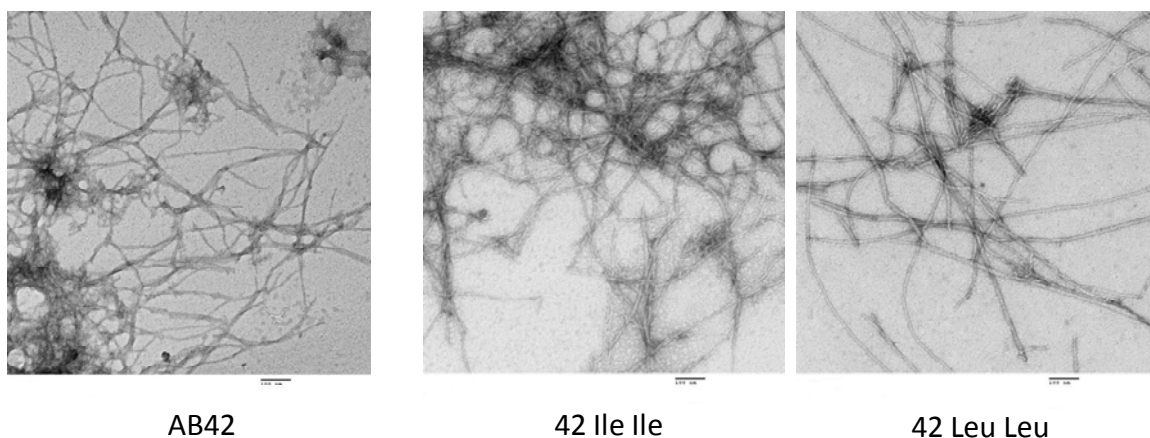


**Figure 4.8.** Electron microscopy images of AB42, 42 Ile Ile, and 42 Leu Leu mutants. Fibrils imaged after 7 days of quiescent incubation at 37°C. Scale bar: 100 nm.

#### 4.3.3. Inhibiting AB Ile Ile and Leu Leu mutants with aromatic inhibitors

Since the EM images of the Ile Ile and Leu Leu mutants showed distinct fibril formation, I wanted to know if aromatic drugs could inhibit the aggregation of these mutants. As discussed in Chapter 1, many AB aggregation inhibitors are aromatic. The exact aggregation inhibition mechanism is unknown, but Gazit has suggested that aromatic compounds disturb and destabilize the AB  $\pi$ -stacking process in aggregation, as shown in Figure 4.2. If this is indeed the mechanism of inhibition, aromatic compounds should be more effective at inhibiting the wild type AB42 peptide than either the 42 Ile Ile, or 42 Leu Leu mutants. I also investigated whether or not non-aromatic compound inhibitors would also be more effective at inhibiting the Ile Ile and Leu Leu mutants than the wild type AB42 peptide.

Three aromatic AB aggregation inhibitors and one non-aromatic aggregation inhibitor were selected for testing in wild type AB42 and both 42 and 40 Ile Ile mutants.

Congo Red is an amyloid staining agent and has been shown to inhibit aggregation (19). Resveratrol is sirtuin activator that extends the lifespan in *S. cerevisiae*, and has been shown to promote intracellular degradation of AB, but has not been shown to inhibit AB peptide aggregation (20, 21). Curcumin is a spice found in yellow curry, and shown to inhibit AB oligomerization and fibrilization (22). Myristyltrimethylammonium bromide (MTMA), a detergent like compound, was shown to inhibit AB aggregation and selected as the non-aromatic inhibitor (23).

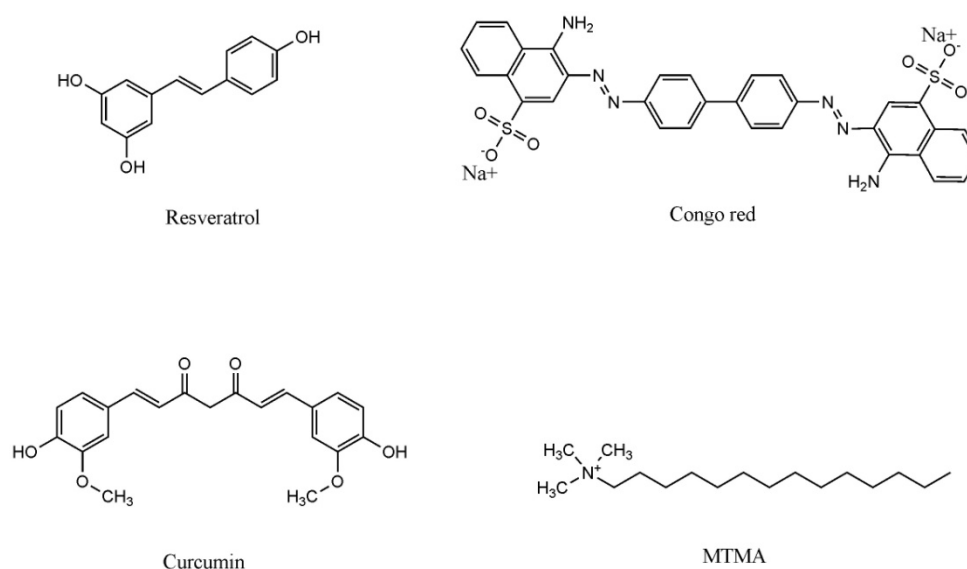


**Figure 4.9.** Structure of aromatic and non-aromatic inhibitors

As shown in Figure 4.10, the aromatic drugs resveratrol, curcumin, and Congo Red are effective at reducing aggregation in AB42 (shown in blue). However, all three aromatic drugs also are equally effective at inhibiting aggregation in both 42 and 40 length Ile Ile mutants (shown in red and green, respectively). The inhibition levels for wild type AB and Ile Ile mutants are very similar for all three compounds. Congo Red is especially effective, completely preventing any thioflavin T fluorescence, suggesting

total aggregation inhibition in both wild type AB and Ile Ile mutants. These results show that aromatic compounds are equally effective at inhibiting AB aggregation, and do not favor AB peptide with aromatic residues. Because aromatic compounds equally inhibit AB42 and both Ile Ile mutants, this suggests that the mechanism for aggregation inhibition by aromatic compounds is not due to the disruption of  $\pi$ -stacking.

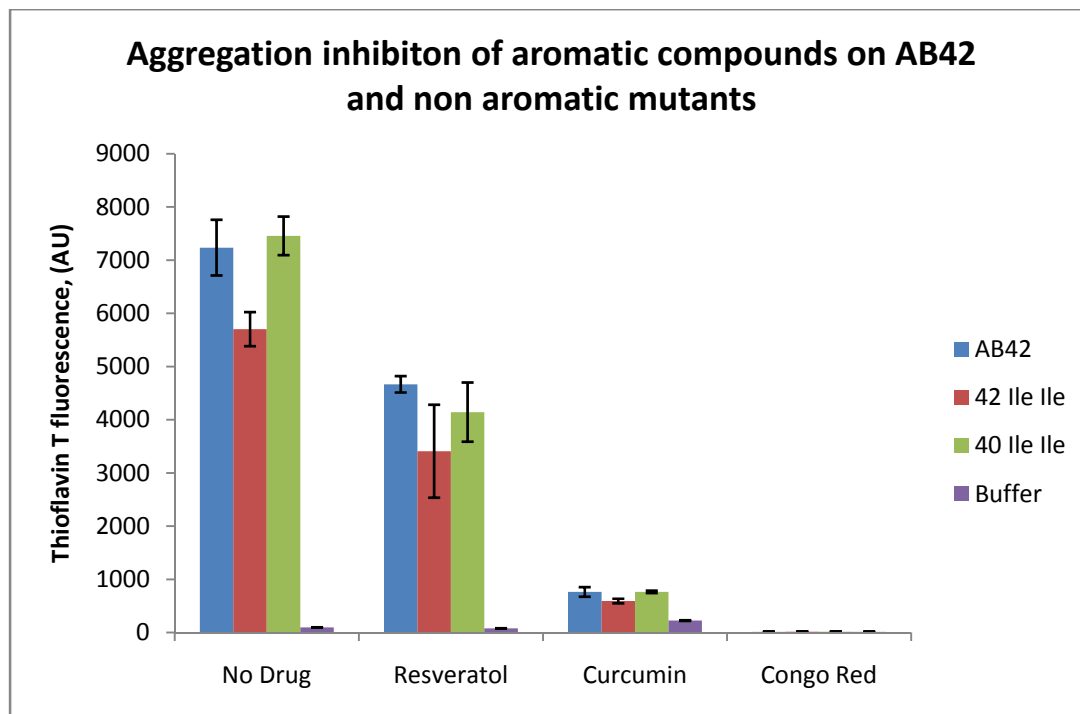


**Figure 4.10.** Aggregation reduction by aromatic compounds of AB42 and Ile Ile mutants, as measured by thioflavin T fluorescence. Lower numbers indicate aggregation inhibition. 20  $\mu$ M AB concentration, 100  $\mu$ M drug concentration, 5 hour incubation at 37°C, triplicate samples. Standard error reported.

Since aromatic compounds were equally effective at inhibiting both Ile Ile AB mutants, I also wanted to see if a non-aromatic aggregation inhibitor was more effective at inhibiting aggregation on the Ile Ile mutants than on wild type AB42. As shown in

Figure 4.11, MTMA is equally effective at reducing aggregation in wild type AB42 and in both 42 and 40 length Ile Ile mutants.

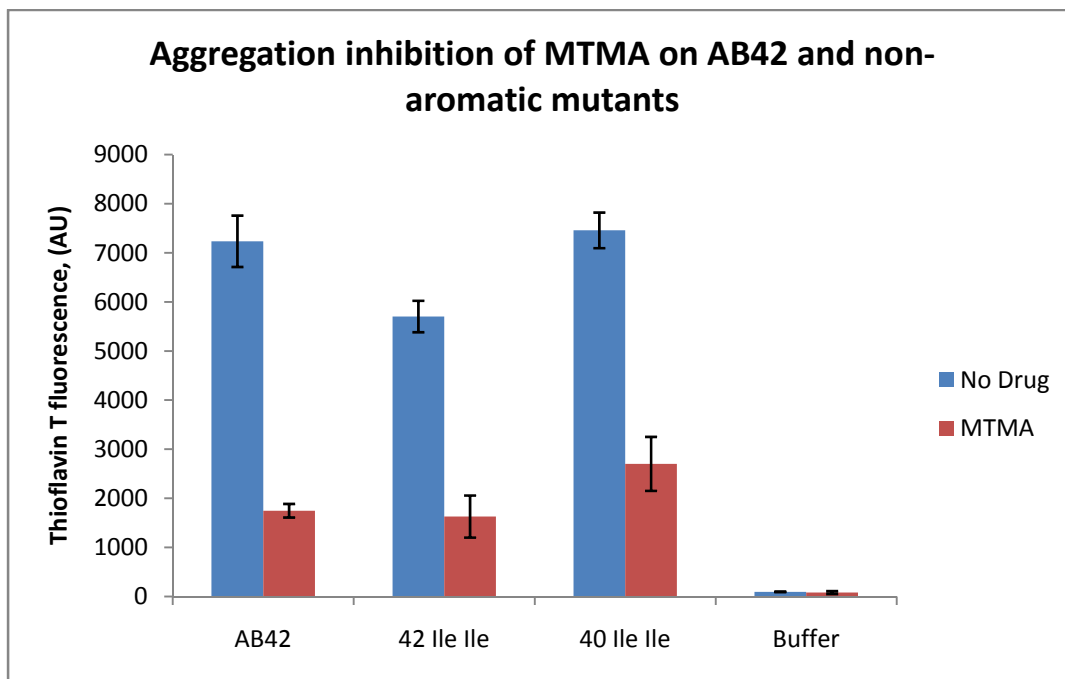


**Figure 4.11.** Aggregation reduction by non-aromatic MTMA of AB42 and Ile Ile mutants, as measured by thioflavin T fluorescence. Lower numbers indicate aggregation inhibition. 20  $\mu$ M AB concentration, 100  $\mu$ M drug concentration, 5 hour incubation at 37°C, triplicate samples. Standard error reported.

#### 4.3.4. Toxicity of AB Ile Ile and Leu Leu mutants

Since the Ile Ile mutants have very high aggregation rates, I wanted to identify if there was a correlation between the AB aggregation rate and toxicity. I hypothesized that the faster aggregating mutants might be less toxic because the toxic oligomer would not exist for an extended period of time.

For the toxicity assays, I studied two incubation times for the mutant peptides, fresh and aged. The fresh condition consisted of AB peptide solution immediately added to PC12 cells and incubated for 24 hour with PC12 cells. The aged condition consisted of AB peptide solution incubated for 72 hours at 37°C, followed by a 24 hour incubation with PC12 cells. PC12 cell viability of AB and mutants 40 Ile Ile and 40 Leu Leu are shown Figure 4.12. The PC12 cells incubated with fresh and aged AB40 were not toxic, while the AB42 samples show a similar toxicity in both fresh and aged conditions. The fresh 40 Ile Ile mutant sample is slightly toxic, while the aged 40 Ile Ile sample is very toxic. The 40 Leu Leu mutant is not toxic under either condition. This viability study shows that mutations that increase aggregation are toxic, with the aged 40 Ile Ile condition being even *more* toxic than even aged wild type AB42.

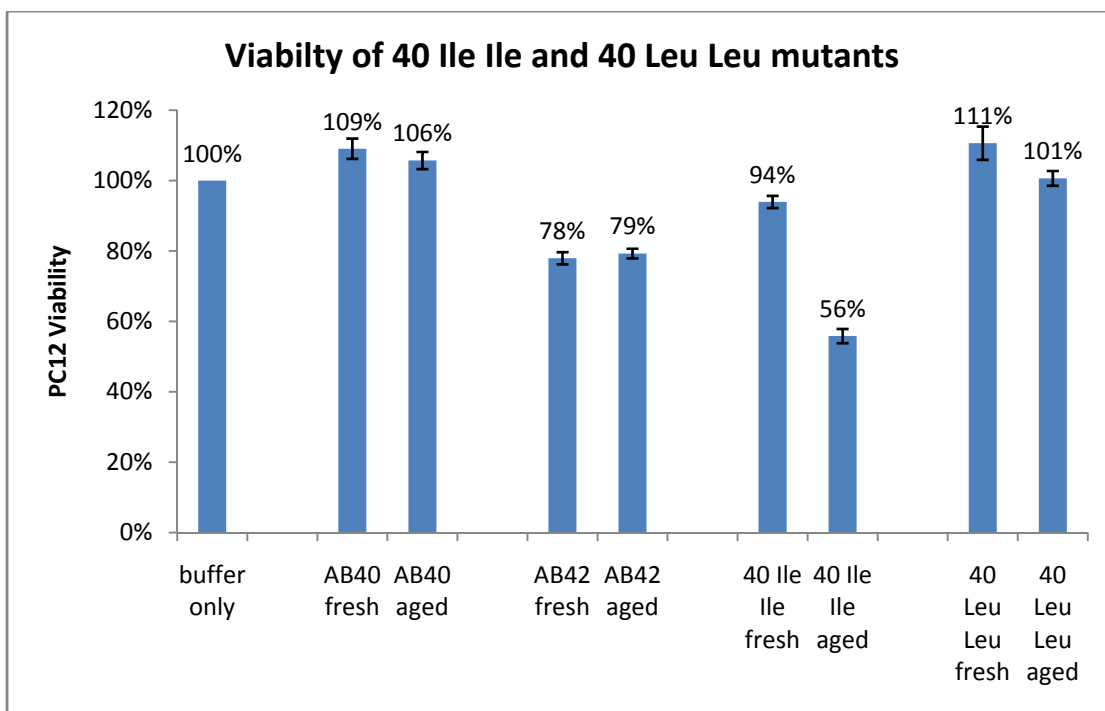


**Figure 4.12.** Viability of PC12 cells when treated with AB and mutants. PC12 cells with AB concentration of 20  $\mu$ M, and incubated for 24 hours. Samples measured in triplicate with standard error reported.

In Figure 4.13, the viability of the PC12 cells treated with AB double mutants 40 Ile Ile and 42 Ile Ile are compared. In the fresh condition, the 40 Ile Ile mutant is slightly toxic, while the fresh condition for the 42 Ile Ile mutant is very toxic. Both the 40 and 42 Ile Ile mutants are very toxic in the aged condition, and even more toxic than the aged wild type AB42 peptide. This data again suggests that the toxicity of AB peptides is correlated to aggregation propensity of the mutant peptide. The data from the 42 and 40 Ile Ile mutants and from 40 Leu Leu mutants suggests that aggregation rate can determine toxicity.

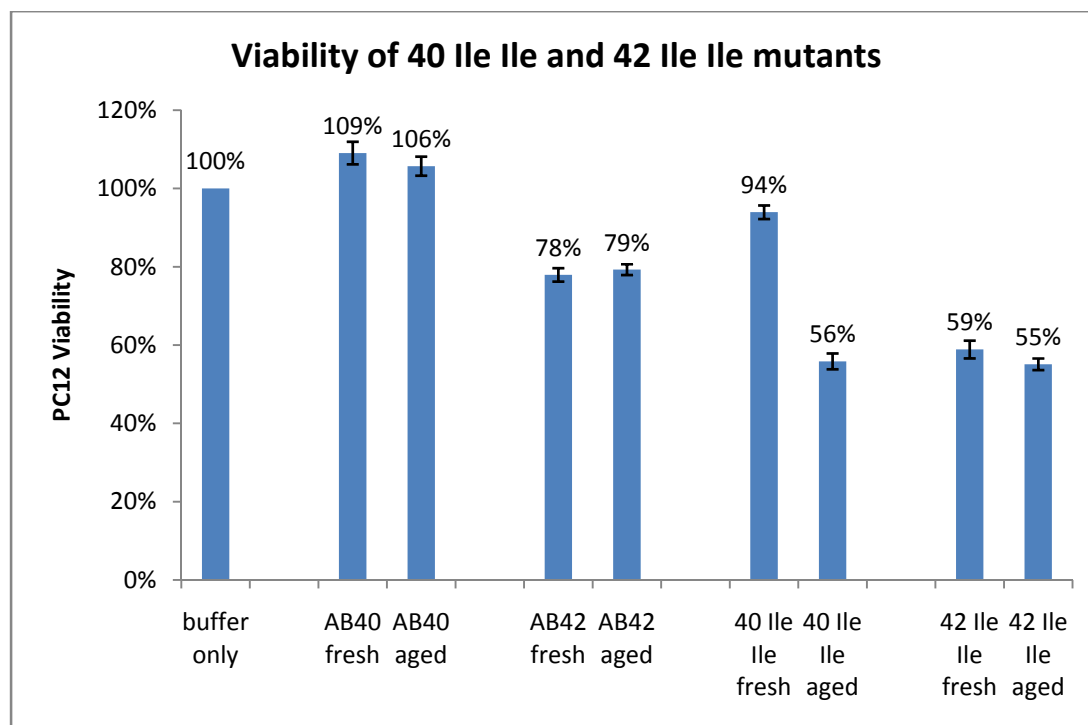


**Figure 4.13.** Viability of PC12 cells when treated with 40 Ile Ile and 42 Ile Ile. PC12 cells with concentration of 20  $\mu$ M, and incubated for 24 hours. Samples measured in triplicate with standard error reported.

#### 4.4. Discussion

It has been proposed that aromatic-aromatic interactions play an important role in the aggregation of amyloid fibrils, and that disrupting the  $\pi$ -stacking in amyloid fibrils is a mechanism for inhibition (2). However, recent reports have questioned the role of aromatic  $\pi$ -stacking in amyloid aggregation (11, 12). As shown by the thioflavin T aggregation profiles and EM images of fibrils from both 42 Ile Ile and 42 Leu Leu mutants described in this chapter, it is clear that aromatic residues are **not** required or necessary for aggregation or fibril formation. In fact, the mutant with the fastest

aggregation profile is the 42 Ile Ile mutant, which does not include any aromatic residues in the central hydrophobic cluster of AB.

Distinct amyloid fibrils were seen in the EM images of the 42 Ile Ile mutant. A second mutant that was able to form fibrils was the 42 Leu Leu mutant. The 42 Leu Leu mutant was also able to aggregate and form fibrils, but at a rate much slower than the 42 Ile Ile mutant. The EM images, in addition to the thioflavin T aggregation data, clearly show that aromatic residues are not required or necessary for aggregation or fibrilization.

The increase in aggregation was seen in the 40 length double mutants. The 40 Ile Ile mutant's aggregation profile was much faster than the profile for the 40 Leu Leu mutant. The 40 Ile Ile mutant's aggregation profile was similar to that of wild type AB42, which is striking, since AB40 is known to aggregate much more slowly than AB42. It is interesting to note that changing two residues within the central hydrophobic cluster can modify the aggregation rate from the wild type AB40 to AB42. Kim and Hecht identified that hydrophobicity of the residues at position 41 and 42 were a major contributor to the increased aggregation (18). The data in this chapter suggests that the hydrophobicity of the residues in the central hydrophobic cluster are as important for aggregation propensity as they are in positions 41 and 42. Another trend identified was that the 40 Leu Leu mutant also had a very long lag before significant aggregation, similar to that seen in the 42 Leu Leu mutant.

The increase in lag time (nucleation) with Leu Leu mutants in 40 and 42 length peptides was similar to the results that Marek *et al* describe in their study of non-aromatic amylin mutants. In their experiment, they mutated the three aromatic residues to Leu (F15L/F23L/Y37L). This amylin triple mutant was able to form fibrils, but at a slower

rate than wild type amylin. They concluded that aromatic residues were not necessary for fibril formation, but that aromatic residues influence the aggregation rate as specific residue have a propensity for aggregation (12). It would be interesting to know if the triple amylin Ile mutation would aggregate faster than the wild type amylin peptide.

A recent analysis of the aggregation propensity of all natural amino acids by Dobson and co-workers suggested that Trp and Phe residues are significantly more amyloidogenic than aliphatic amino acids; about 3 and 6 times higher than that of Ile and Val (24). These experimental results differed from their analysis. Their analysis would suggest that wild type AB42, with two Phe residues at 19 and 20, would aggregate *faster* than the 42 Ile Ile mutant. It is clear that a factor other than aromaticity must be favoring the aggregation of the 42 Ile Ile mutant over wild type AB42. This mutant provides clear evidence that aromatic residues are not critical for AB aggregation and fibrilization. As shown in Table 4.2, the Ile residue is similar in hydrophobicity and  $\beta$  sheet propensity to both the Leu and Phe residues. As mutations in the sequence of AB determine the aggregation pathway, the Ile Ile mutant is likely to nucleate faster, leading to increased fibril formation, or pack better in the core, leading to a lower energy structure than wild type AB42. Another possible explanation is that  $\pi$ -stacking may actually slow the nucleation and aggregation process. As shown in Figure 4.1, there are four possible  $\pi$ -stacking structures that can be formed from two aromatic moieties. This means that each of the three Phe residues in the AB sequence can form multiple “incorrect”  $\pi$ -stacking interactions with other Phe residues from other AB peptides until it reaches the final, global low energy form. Since each  $\pi$ -stacking interaction is a favorable interaction, it will take an increased amount of time to find the lowest energy state.

The data on the 40 and 42 Leu Leu mutants is in agreement with the amylin mutations found by Tracz *et al* and Marek *et al*. Both studies found that the Phe to Leu mutant peptides were able to form fibrils, but the mutation decreased the rate of fibril formation. The same trend was seen in both of our 40 and 42 length Leu Leu AB mutants. Both of these mutants were able to aggregate and form fibrils, but they had an extended lag time before increased aggregation. However, after the extended lag time, the aggregation rate dramatically increased, as determined by the increase in thioflavin T fluorescence. In contrast, the 42 Ile Ile mutants had virtually no lag time whatsoever, and was also able to form fibrils. (The comparable Ile mutations in amylin were not reported.) The difference between the two amino acids leucine and isoleucine is the branching of a methyl group. In isoleucine, the methyl group branches from the  $\alpha$  carbon, and in leucine, it branches from the  $\beta$  carbon. This small change completely changes the aggregation kinetics of AB. The reason for this can be explained by better packing in the core packing of AB (Figure 4.3), or increased nucleation, as discussed previously.

Since the Ile Ile mutants were capable of aggregating and forming fibrils, I wanted to test if aromatic compounds were capable of inhibiting these AB mutants. The data shows that the aromatic aggregation inhibitors resveratrol, curcumin, and Congo Red are equally effective at inhibiting wild type AB (with aromatic residues F19 F20) and mutant peptides aggregation (without aromatic peptides at position 19 and 20). Because these aromatic compounds inhibited Ile Ile mutant peptide aggregation, this suggests that disruption of the  $\pi$ -stacking process is **not** the major inhibition mechanism by aromatic compounds. In addition, the non-aromatic compound inhibitor MTMA was able to

equally inhibit wild type AB42 and the 40 and 42 Ile Ile mutants. It is interesting to note that both aromatic and non-aromatic aggregation inhibitors were equally effective at inhibiting wild type and mutant AB peptides; aromatic inhibitors were not more effective at inhibiting wild type AB, and non-aromatic inhibitors were not more effective at inhibiting the Ile Ile mutants. These data are also consistent with the suggestion that disruption of  $\pi$ -stacking is not the primary mechanism for aggregation inhibition by aromatic compounds. Hydrophobic interactions are likely to have a larger role in aggregation inhibition than the disruption of the aromatic-aromatic interactions.

Finally, the toxicity of AB mutants lacking aromatic residues in the central hydrophobic cluster was also studied. The faster aggregating mutants seemed to be more toxic than the slower aggregating mutants. The AB42 Ile Ile mutant was significantly more toxic than AB42, and the 40 Ile Ile mutant was more toxic than the 40 Leu Leu in both fresh and aged conditions. In both examples, the faster aggregating mutant was more toxic. This suggests that peptide toxicity is correlated to aggregation propensity.

## **4.5. Summary**

I have demonstrated that aromatic residues are not required for AB aggregation and fibrilization. Surprisingly, the AB42 Ile Ile is significantly faster at aggregation compared to wild type AB42. I have also shown that aromatic aggregation inhibitors can also inhibit aggregation mutants without aromatic residues in the central hydrophobic cluster with the same effectiveness, suggesting that aromatic compounds do not inhibit aggregation by disturbing the  $\pi$ -stacking interaction. Finally, I show that the both the 40

and 42 Ile Ile mutations are toxic, and in some cases, even more toxic than wild type AB42.

## 4.6. Materials and methods

**Peptide purification.** Crude peptides from solid phase synthesis were purchased from the Keck Institute at Yale University, and purified using a C4 reverse phase column. Solvent gradients were run at 65°C using solvent A (95% water, 5% acetonitrile, 0.1% TFA); and Solvent B (50% acetonitrile, 50% water, 0.1% TFA).

**Thioflavin T Assay.** Peptides were dissolved in 300 uL DMSO and diluted with 5 mL of 8 mM NaOH for a final peptide concentration of 20 uM. Concentrated PBS buffer was added to the solution to adjust the pH (final concentration: 50 mM NaH<sub>2</sub>PO<sub>4</sub>, 100 mM NaCl, pH 7.10 – 7.20). Samples were incubated with and without compound at 37°C under quiescent conditions for the indicated time period. At various timepoints, 100 uL aliquot of peptide sample was mixed with 100 uL of a solution of thioflavin T (7 uM ThT, 50 mM glycine-NaOH, pH 7.10) and fluorescence was measured at 483 nm (excitation at 450 nm) on a Varioskan Plate reader (Thermo). Some samples were measured on a Yyon Fluoromax 3 Spectrofluorimeter. A 500 uL aliquot of sample was added to 2.7 mL of 7 uM ThT into a 4 sided fluorescence cuvette. Excitation was at 450, and the emission wavelength was scanned from 470 – 490 nm. The data at 483 nm was selected for data analysis.

**Electron Microscopy.** Solutions were prepared as described above at peptide concentrations of 20 uM. Samples were incubated at 37°C under quiescent conditions for the indicated time period. Following incubation, glow discharged formvar carbon coated grids were floated on a drop of each sample for 2 minutes, washed twice with distilled water, and then stained for 20 minutes with 1% uranyl acetate. Samples were imaged using a Zeiss 912ab Electron Microscope.

**Toxicity experiments.** Rat pheochromocytoma (PC12) cells (ATCC, Rockville, MD) were grown on collagen coated ,tissue treated petrie dishes (Falcon) in complete growth media (82.5% F12K 15% horse serum, 2.5% fetal bovine serum, ATCC Rockville, MD) in a humidified incubator at 37oC and 5% CO<sub>2</sub> (Herra, Thermo Scientific). Cells were grown to confluence, harvested by spraying through an 18.5 gauge needle, resuspended in fresh media and plated onto tissue treated flat bottom 96 well plates (Costar) at a density of 10 000 cells per well (100 uL/well). Plates were incubated at 37°C for 24 hours to allow cells to attach. Lyophilized AB42 (1 mg) was dissolved in 100 uL of cell culture grade DMSO (ATCC), briefly sonicated and then diluted with 1.0 mL of sterile 1 x PBS buffer (Invitrogen) for a final stock concentration of 200 uM. 10 uL of the final AB42 peptide solution was added to each well (100 uL) for a final peptide concentration of 20 uM. Plates with AB peptide were incubated for 24 hours. Cell viability was determined with the MTT assay (Roche, Nutley, NJ). Briefly, 10 uL of MTT was added to each well. After incubation for 4 hr at 37°C, 100 uL of solubilization solution (10% SDS in 0.01 M HCl) was added and incubated overnight at 37oC. The absorbance at 570 nm was measured using a microplate reader (Thermo Varioskan), with background subtraction (670 nm). Statistical significance was calculated with the two tailed (uncorrelated) TTEST function in Excel.

## 4.7. References

1. McGaughey, G. B., Gagne, M., and Rappe, A. K. (1998)  $\pi$ -Stacking Interactions. Alive and well in proteins, *J. Biol. Chem.* 273, 15458-15463.
2. Gazit, E. (2002) A possible role for  $\pi$ -stacking in the self-assembly of amyloid fibrils, *FAESB J* 16, 77-83.
3. Bemporad, F., Taddei, N., Stefani, M., and Chiti, F. (2006) Assessing the role of aromatic residues in the amyloid aggregation of human muscle acylphosphatase, *Protein Sci* 15, 862-870.
4. Tartaglia, G. G., Cavalli, A., Pellarin, R., and Caflisch, A. (2004) The role of aromaticity, exposed surface, and dipole moment in determining protein aggregation rates, *Protein Sci* 13, 1939-1941.
5. Porat, Y., Abramowitz, A., and Gazit, E. (2006) Inhibition of Amyloid Fibril Formation by Polyphenols: Structural Similarity and Aromatic Interactions as a Common Inhibition Mechanism, *Chemical Biology & Drug Design* 67, 27-37.
6. Shoval, H., Lichtenberg, D., and Gazit, E. (2007) The molecular mechanisms of the anti-amyloid effects of phenols, *Amyloid* 14, 73 - 87.
7. Williams, A. D., Portelius, E., Kheterpal, I., Guo, J.-t., Cook, K. D., Xu, Y., and Wetzel, R. (2004) Mapping Beta Amyloid Fibril Secondary Structure Using Scanning Proline Mutagenesis, *Journal of Molecular Biology* 335, 833-842.
8. Petkova, A. T., Ishii, Y., Balbach, J. J., Antzutkin, O. N., Leapman, R. D., Delaglio, F., and Tycko, R. (2002) A structural model for Alzheimer's beta - amyloid fibrils based on experimental constraints from solid state NMR, *Proc Natl Acad Sci U S A* 99, 16742-16747.
9. Tjernberg, L. O., Callaway, D. J. E., Tjernberg, A., Hahne, S., Lilliehook, C., Terenius, L., Thyberg, J., and Nordstedt, C. (1999) A Molecular Model of Alzheimer Amyloid beta -Peptide Fibril Formation, *J. Biol. Chem.* 274, 12619-12625.
10. Kim, E. I., Paliwal, S., and Wilcox, C. S. (1998) Measurements of Molecular Electrostatic Field Effects in Edge-to-Face Aromatic Interactions and CH- $\pi$ ; Interactions with Implications for Protein Folding and Molecular Recognition, *J. Am. Chem. Soc.* 120, 11192-11193.
11. Tracz, S. M., Abedini, A., Driscoll, M., and Raleigh, D. P. (2004) Role of Aromatic Interactions in Amyloid Formation by Peptides Derived from Human Amylin, *Biochemistry* 43, 15901-15908.
12. Marek, P., Abedini, A., Song, B., Kanungo, M., Johnson, M. E., Gupta, R., Zaman, W., Wong, S. S., and Raleigh, D. P. (2007) Aromatic Interactions Are Not Required for Amyloid Fibril Formation by Islet Amyloid Polypeptide but Do Influence the Rate of Fibril Formation and Fibril Morphology, *Biochemistry* 46, 3255-3261.
13. Wurth, C., Guimard, N. K., and Hecht, M. H. (2002) Mutations that reduce aggregation of the Alzheimer's Amyloid beta 42 peptide: an unbiased search for the sequence determinants of Amyloid beta amyloidogenesis, *J Mol Biol* 319, 1279-1290.

14. Fauchere, J., and Pliska, V. (1983) Hydrophobic parameters of amino-acid side chains from the partitioning of N-acetyl-amino-acid amides, *Eur. J. Med. Chem.* 18, 369-375.
15. Kim, C. A., and Berg, J. M. (1993) Thermodynamic beta-sheet propensities measured using a zinc-finger host peptide, *Nature* 362, 267-270.
16. Naiki, H., Higuchi, K., Hosokawa, M., and Takeda, T. (1989) Fluorometric determination of amyloid fibrils in vitro using the fluorescent dye, thioflavin T1, *Anal Biochem* 177, 244-249.
17. Jarrett, J. T., Berger, E. P., and Lansbury, P. T., Jr. (1993) The carboxy terminus of the beta amyloid protein is critical for the seeding of amyloid formation: implications for the pathogenesis of Alzheimer's disease, *Biochemistry* 32, 4693-4697.
18. Kim, W., and Hecht, M. H. (2005) Sequence Determinants of Enhanced Amyloidogenicity of Alzheimer Amyloid Beta 42 Peptide Relative to Amyloid Beta 40, *J. Biol. Chem.* 280, 35069-35076.
19. Lorenzo, A., and Yankner, B. A. (1994) Beta-amyloid neurotoxicity requires fibril formation and is inhibited by congo red, *Proceedings of the National Academy of Sciences of the United States of America* 91, 12243-12247.
20. Marambaud, P., Zhao, H., and Davies, P. (2005) Resveratrol Promotes Clearance of Alzheimer's Disease Amyloid Beta Peptides, *J. Biol. Chem.* 280, 37377-37382.
21. Howitz, K. T., Bitterman, K. J., Cohen, H. Y., Lamming, D. W., Lavu, S., Wood, J. G., Zipkin, R. E., Chung, P., Kisielewski, A., Zhang, L.-L., Scherer, B., and Sinclair, D. A. (2003) Small molecule activators of sirtuins extend *Saccharomyces cerevisiae* lifespan, *Nature* 425, 191-196.
22. Yang, F., Lim, G. P., Begum, A. N., Ubeda, O. J., Simmons, M. R., Ambegaokar, S. S., Chen, P. P., Kaye, R., Glabe, C. G., Frautschy, S. A., and Cole, G. M. (2005) Curcumin Inhibits Formation of Amyloid Beta Oligomers and Fibrils, Binds Plaques, and Reduces Amyloid in Vivo, *J. Biol. Chem.* 280, 5892-5901.
23. Wood, S. J., MacKenzie, L., Maleeff, B., Hurle, M. R., and Wetzel, R. (1996) Selective inhibition of amyloid beta fibril formation, *J Biol Chem* 271, 4086-4092.
24. Pawar, A. P., DuBay, K. F., Zurdo, J., Chiti, F., Vendruscolo, M., and Dobson, C. M. (2005) Prediction of "Aggregation-prone" and "Aggregation-susceptible" Regions in Proteins Associated with Neurodegenerative Diseases, *Journal of Molecular Biology* 350, 379-392.